DEVELOPMENT OF POLY (VINYL ALCOHOL)/SILK FIBROIN INJECTABLE HYDROGELS BY PHOTO CROSSLINKING FOR MENISCUS TISSUE ENGINEERING

JIRAPORN SINNA

A Thesis Submitted in Partial Fulfillment of the Requirements for the

Degree of Master of Engineering in Materials Engineering

Suranaree University of Technology

Academic Year 2022

การพัฒนาไฮโดรเจลแบบฉีดจากพอลิไวนิลแอลกอฮอล์และไหมไฟโบรอินโดยใช้แสงเพื่อให้เกิดโครงสร้างร่างแหสำหรับใช้ในวิศวกรรมเนื้อเยื่อหมอนรองเข่า

นางสาวจิราภรณ์ สินนา

มหาวิทยาลัยเทคโนโลยีสุรนารี

วิทยานิพนธ์นี้เป็นส่วนหนึ่งของการศึกษาตามหลักสูตรปริญญาวิศวกรรมศาสตรมหาบัณฑิต

สาขาวิชาวิศวกรรมวัสดุ

มหาวิทยาลัยเทคโนโลยีสุรนารี

ปีการศึกษา 2565

DEVELOPMENT OF POLY (VINYL ALCOHOL)/SILK FIBROIN INJECTABLE HYDROGELS BY PHOTO CROSSLINKING FOR MENISCUS TISSUE ENGINEERING

Suranaree University of Technology has approved this thesis submitted in partial fulfillment of the requirements for a Master's Degree.

Thesis Examining Committee

.....

(Assoc. Prof. Dr. Wimonlak Sutapun)
Chairperson

.....

(Assoc. Prof. Dr. Yupaporn Ruksakulpiwat)
Member (Thesis Advisor)

.....

(Assoc. Prof. Dr. Chaiwat Ruksakulpiwat)
Member (Thesis Co-advisor)

.....

(Asst. Prof. Dr. Piya-on Numpaisal)
Member (Thesis Co-advisor)

.....

(Prof. Dr. Hathaikarn Manuspiya)
Member

.....

(Assoc. Prof. Dr. Pranee Chumsamrong)
Member

.....

(Asst. Prof. Dr.Nitinat Suppakarn)
Member

.....

(Assoc. Prof. Dr. Chatchai Jothityangkoon)
Vice Rector for Academic Affairs and Quality Assurance

.....

(Assoc. Prof. Dr. Pornsiri Jongkol)
Dean of Institute of Engineering

มหาวิทยาลัยเทคโนโลยีสุรนารี

จิราภรณ์ สินนา : การพัฒนาไฮโดรเจลแบบฉีดจากพอลิไวนิลแอลกอฮอล์และไหมไฟโบรอินโดยใช้แสงเพื่อให้เกิดโครงสร้างร่างแหสำหรับใช้ในวิศวกรรมเนื้อเยื่อหมอนรองเข่า (DEVELOPMENT OF POLY (VINYL ALCOHOL)/ SILK FIBROIN INJECTABLE HYDROGELS BY PHOTO CROSSLINKING FOR MENISCUS TISSUE ENGINEERING). อาจารย์ที่ปรึกษา : รองศาสตราจารย์ ดร.ยุพาพร รักสกุลพิวัฒน์ , 88 หน้า

คำสำคัญ : พอลิไวนิลแอลกอฮอล์ ไหมไฟโบรอิน ไฮโดรเจลแบบฉีด วิศวกรรมเนื้อเยื่อหมอนรองเข่า

จุดมุ่งหมายในการศึกษานี้คือ การพัฒนาไฮโดรเจลแบบฉีดโดยใช้แสงยูวีทำให้เกิดการเชื่อมขวางแบบร่างแหโดยสารจะเปลี่ยนสถานะจากของเหลวกลายเป็นของแข็งคล้ายเจลโดยใช้วัสดุจากพอลิไวนิลแอลกอฮอล์และไหมไฟโบรอินเพื่อใช้เป็นโครงร่างเลี้ยงเซลล์ในหมอนรองเข่า ซึ่งจะนำไปประยุกต์ใช้ในการผ่าตัดแบบส่องกล้องในข้อเข่า (Arthroscopic Surgery) และศึกษาสมบัติทางกายภาพ สมบัติทางกลของวัสดุและทดสอบความเป็นพิษต่อเซลล์ เพื่อนำไปใช้เป็นไฮโดรเจลแบบฉีดรักษาส่วนที่ฉีกขาดในหมอนรองเข่าในอนาคต

พอลิไวนิลแอลกอฮอล์เป็นหนึ่งในวัสดุที่ใช้งานบ่อยที่สุดในวิศวกรรมเนื้อเยื่อ มีคุณสมบัติเชิงกลสูง ไม่เป็นพิษ มีความเข้ากันได้ทางชีวภาพที่ดี และย่อยสลายได้ในทางชีวภาพ แต่มีข้อด้อยคือเซลล์ไม่สามารถยึดติดได้ ส่วนไหมไฟโบรอินมีความเข้ากันได้ของเซลล์ที่ดีเยี่ยม เช่น การยึดเกาะเซลล์ได้ดีและการเพิ่มจำนวนเซลล์ที่ดี รวมถึงสมบัติทางกลและการย่อยสลายได้ในชีวภาพ วัสดุทั้งสองนี้จึงถูกนำมาใช้กันอย่างแพร่หลายในฐานะโครงร่างเลี้ยงเซลล์สำหรับวิศวกรรมเนื้อเยื่อ ถึงแม้วิศวกรรมเนื้อเยื่อจะได้ผลที่ดีในการทดลองในหลอดทดลอง แต่ยังไม่สามารถใช้งานในทางคลินิกได้ จึงขอเสนอโครงร่างเลี้ยงเซลล์แบบการขึ้นรูปสองเฟส (Biphasic) ที่สามารถฉีดผ่านการผ่าตัดแบบส่องกล้องเข้าไปในหมอนรองเข่า ซึ่งสามารถเปลี่ยนจากของเหลวให้กลายเป็นของแข็งคล้ายเจลโดยใช้แสงยูวี ไฮโดรเจลจึงเป็นวัสดุที่ถูกเลือกนำมาพัฒนาเป็นไฮโดรเจลแบบฉีดได้ เพื่อปรับปรุงคุณสมบัติของวัสดุให้มีการยึดเกาะเซลล์ที่ดีขึ้น รวมทั้งความเข้ากันได้กับสภาพแวดล้อมทางชีวภาพในร่างกายของพอลิไวนิลแอลกอฮอล์และไหมไฟโบรอิน โดยไหมไฟโบรอินถูกเตรียมด้วยกระบวนการละลายโดยใช้ไมโครเวฟเป็นตัวช่วยให้สามารถลดเวลาในการเตรียม รวมทั้งได้น้ำหนักโมเลกุลที่สูง การกราฟต์ด้วยไกลซิดิลเมทาคริเลท ลงบนสายโซ่ของพอลิไวนิลแอลกอฮอล์ (PVA-g-GMA) ผ่านปฏิกิริยาทรานส์เอสเทอริฟิเคชัน และไหมไฟโบรอิน (SF-g-GMA) ผ่านปฏิกิริยาการเปิดวงแหวนของอีพอก เพื่อปรับปรุงหมู่ฟังก์ชันที่สามารถเกิดกระบวนการพอลิเมอไรเซชันด้วยแสงยูวีได้ (Photopolymerization) สภาวะที่ดีที่สุดของ PVA-g-GMA ถูกเตรียมที่ความเข้มข้น 10 เปอร์เซ็นน้ำหนักโดยปริมาตร และ SF-

g-GMA ถูกเตรียมที่ความเข้มข้น 50 เปอร์เซ็นน้ำหนักโดยปริมาตร นำทั้งสองมาผสมที่สัดส่วนต่างกัน PVA-g-GMA ต่อ SF-g-GMA 100:0, 75:25, 50:50, 25:75 และ 0:100 สัดส่วนน้ำหนักโดยน้ำหนัก จากนั้นใช้ตัวริเริ่มปฏิกิริยาทางแสง คือ Lithium phenyl-2,4,6-trimethylbenzoylphosphinate (LAP) ผสมเข้ากับสารละลายผสมแล้วขึ้นรูปเป็นไฮโดรเจลด้วยการฉีดเข้าแม่พิมพ์แล้วให้ไฮโดรเจลคงรูปด้วยแสงยูวี ที่ความยาวคลื่นแสง 365 นาโนเมตร ความเข้มแสง 6 มิลลิวัตต์ต่อตารางเซนติเมตร เป็นเวลา 10 นาที

จากการศึกษาสัดส่วนที่ต่างกันในการขึ้นรูปไฮโดรเจลโดยการผสมระหว่าง PVA-g-GMA และ SF-g-GMA พบว่า ทุกสัดส่วนสามารถขึ้นรูปเป็นไฮโดรเจลแบบฉีดได้ ไหมไฟโบรอินเปลี่ยนแปลงโครงสร้างทางเคมีจากโครงสร้างแบบสุ่มเป็นโครงสร้างการจัดเรียงตัวเป็นแผ่นชีต ซึ่งส่งผลต่อสมบัติเชิงกล ให้ค่ามอดุลัสการกดอัดใกล้เคียงกับหมอนรองเข่าของมนุษย์ และมีขนาดรูปพรุน 27-155 ไมโครเมตร ใกล้เคียงกับขนาดของเซลล์คอนโดรไซต์ของมนุษย์รวมทั้งการผสมระหว่าง PVA-g-GMA และ SF-g-GMA มีสมบัติการย่อยสลายที่ดีกว่า PVA-g-GMA และ SF-g-GMA ที่ไม่ผสมกัน นอกจากนี้ยังได้ทำการศึกษาการห่อหุ้มเซลล์ด้วยไฮโดรเจล โดยการผสมเซลล์คอนโดรไซต์ของมนุษย์ลงในสารละลายผสมระหว่าง PVA-g-GMA และ SF-g-GMA แล้วฉีดขึ้นรูปเป็น Biphasic ไฮโดรเจล เมื่อเพิ่มปริมาณสัดส่วน SF-g-GMA มากขึ้นช่วยส่งเสริมการรอดของเซลล์คอนโดรไซต์ของมนุษย์มากขึ้น โดยส่งเสริมการมีชีวิตอยู่ของเซลล์คอนโดรไซต์ของมนุษย์ ดังนั้น เมื่อศึกษาคุณสมบัติต่างๆ แล้วพบว่า biphasic ไฮโดรเจลแบบฉีด โดยใช้สารละลาย PVA-g-GMA และ SF-g-GMA ที่อัตราส่วน 75 ต่อ 25 เปอร์เซ็นต์น้ำหนักโดยน้ำหนัก มีความสามารถในการพัฒนาเพื่อเป็นbiphasic ไฮโดรเจลแบบฉีดที่มีเซลล์เป็นองค์ประกอบเพื่อรักษาการฉีกขาดของหมอนรองเข่าที่สามารถขึ้นรูปได้ด้วยแสงยูวีและใช้เทคนิคการผ่าตัดแบบส่องกล้องได้

มหาวิทยาลัยเทคโนโลยีสุรนารี

ลายมือชื่อนักศึกษา.....วิราภรณ์ สินนา.....

ลายมือชื่ออาจารย์ที่ปรึกษา.....

สาขาวิชาวิศวกรรมพอลิเมอร์ ลายมือชื่ออาจารย์ที่ปรึกษาร่วม.....

ปีการศึกษา 2565 ลายมือชื่ออาจารย์ที่ปรึกษาร่วม.....

JIRAPORN SINNA : DEVELOPMENT OF POLY (VINYL ALCOHOL)/SILK FIBROIN INJECTABLE HYDROGELS BY PHOTO CROSSLINKING FOR MENISCUS TISSUE ENGINEERING THESIS ADVISOR : ASSOC. PROF. YUPAPORN RUKSAKULPIWAT, Ph.D., 88 PP.

Keyword: Poly (vinyl alcohol) Silk Fibroin Injectable Hydrogel Meniscus Tissue Engineering

The aim of this research is to develop photocrosslinking of a biphasic injectable hydrogel material that can be injected into the human body as liquids and cure to form an in situ solid hydrogel. A biphasic injectable hydrogel material with a modified chemical structure derived from poly (vinyl alcohol) (PVA) and silk fibroin (SF) for meniscus tissue engineering that is applicable to arthroscopic surgery.

PVA is one of the most commonly used materials in tissue engineering because of its high mechanical properties, non-toxic nature, good biocompatibility, and biodegradability. But the disadvantage is that the cells cannot adhere. As for SF, it has excellent cell compatibility, such as cell adhesion and cell proliferation, as well as mechanical properties and biodegradability. Thus, these two materials have been frequently used as cytoskeletons in tissue engineering. Although tissue engineering works well in in vitro experiments, it is not yet clinically viable. We therefore propose a biphasic scaffold that could be injected via an arthroscope portal during the liquid phase and become solid after injection into the meniscus and can be injected into the human body as liquids and cure to form an in situ solid hydrogel. To improve the properties of the material to have better cell adhesion as well as the biocompatibility of polyvinyl alcohol and silk fibroin. The silk fibroin was prepared by a microwave-assisted dissolve process to reduce the preparation time and obtain a high molecular weight. Grafting glycidyl methacrylate (GMA) onto PVA (PVA-g-GMA) chains via transesterification reaction and SF (SF-g-GMA) via epoxy ring opening reaction to improve functional groups capable of polymerization with UV light. The best condition of PVA-g-GMA was prepared at a concentration of 10% w/v and concentrated at 50%

w/v. The PVA-g-GMA and SF-g-GMA were mixed in different proportions: 100:0, 75:25, 50:50, 25:75, and 0:100% w/w, and then the photoinitiator, lithium phenyl-2,4,6-trimethylbenzoylphosphinate (LAP), was mixed with the mixture and formed into a hydrogel by injecting it into a mold, and then the hydrogel was stabilized by UV light. (wavelength 365 nm, light intensity 6 mW/cm^2) for 10 minutes.

The different proportions in hydrogel formation by mixing PVA-g-GMA and SF-g-GMA were studied. Relate found that all proportions can be molded into injectable hydrogels. SF changes its chemical structure from random to β-sheet conformation, which affects its mechanical properties. The compressive modulus was similar to that of the human meniscus. It has a porous size of 27–155 μm, similar to that of human chondrocyte cells. PVA-g-GMA and SF-g-GMA have better degradation properties than unmixed PVA-g-GMA and SF-g-GMA.

Hydrogel encapsulation of cells was also studied. Human chondrocytes were mixed in a mixture of PVA-g-GMA and SF-g-GMA and then injected into a biphasic hydrogel under UV light. Live and dead cells were tested for cytotoxicity properties and gene expression. PVA-g-GMA/SF-g-GMA biphasic injectable hydrogels, increasing the ratio of SF-g-GMA promoted the viability of human chondrocytes with the in vitro cell test. The PVA-g-GMA/SF-g-GMA 75:25 biphasic injectable hydrogel has the potential to be used as a rapidly photocurable biphasic injectable hydrogel for cell-encapsulated augmentation based on mechanical properties, live and dead cells, cell viability, gene expression, and in vitro degradation for meniscus repair by using arthroscopic surgery.

มหาวิทยาลัยเทคโนโลยีสุรนารี

Student's Signature.....Jiraporn Sinna.....
Advisor's Signature.....
Co-Advisor's Signature.....
Co-Advisor's Signature.....

School of Polymer Engineering
Academic Year 2022

ACKNOWLEDGEMENT

Firstly, I gratefully acknowledge Suranaree University of Technology and the Center of Excellence on Petrochemical and Materials Technology (PETROMAT) for their financial support. I would like to express my sincere gratitude to my advisor, Assoc. Prof. Yupaporn Ruksakulpiwat, and my co-advisors, Assoc. Prof. Chaiwat Ruksakulpiwat and Asst. Prof. Piya-on Numpisal, for the support of my master's study and research, for their guidance, patience, knowledge, enthusiastic encouragement, and useful critiques of this research work.

I am also grateful to Assoc. Prof. Dr. Wimonlak Sutapun, Prof. Dr. Hathaikan Manuspiya, Assoc. Prof. Dr.Pranee Chumsamrong, and Asst. Prof. Dr. Nitinat Suppakarn for their valuable suggestions as committee members. I especially would like to thank Assoc. Prof. Dr. Tulyapruek Tawonsawatruk and Mr.Narongrit Srikaew for human chondrocyte cells and cell culture studies.

I would like to offer my special thanks to my friends of the School of Polymer Engineering, research team, and staff for creating a fun, comfortable, and inviting research environment. The long hours in the lab would not have been the same without all of you.

Finally, I would like to thank my family and my partner for their support, food support, and encouragement throughout my study at Suranaree University of Technology.

JIRAPORN SINNA

TABLE OF CONTENT

Page

ABSTRACT (THAI) I
ABSTRACT (ENGLISH) III
ACKNOWLEDGEMENT V
TABLE OF CONTENTS VI
LIST OF TABLES X
LIST OF FIGURES XI
CHAPTER
I. INTRODUCTION 1
1.1 Background 1
1.2 Research objectives 4
1.3 Scope of research 4
II. LITERATURE REVIEWS 6
2.1 Meniscus 6
2.1.1 Anatomy and cellular components 6
2.1.2 Meniscus repair 8
2.1.2.1 Open surgery 8
2.1.2.2 Minimally invasive surgery 8
2.2 Tissue engineering 8
2.2.1 Cell 9
2.2.2 Bioactive molecule 10
2.2.3 Scaffold 10
2.3 Hydrogel 10
2.3.1 Natural hydrogel 11
2.3.2 Synthetics hydrogel 11

TABLE OF CONTENTS (Continued)

Page

2.4 Injectable hydrogel system 11
2.4.1 Injectable hydrogel via physical crosslinking 12
2.4.1.1 Temperature-Induced 12
2.4.1.2 pH-Induced 13
2.4.1.3 Ion-Induced 13
2.4.2 Injectable hydrogel via chemical crosslinking 14
2.4.2.1 Crosslinking Agents 14
2.4.2.2 Click Chemistry 14
2.4.2.3 Photopolymerization 14
2.5 Silk fibroin 15
2.5.1 Silk fibroin extraction 18
2.5.1.1 Silk fibroin fiber degumming 18
2.5.1.2 Silk fibroin dissolving 19
2.6 Poly (vinyl alcohol) 20
2.7 Poly (vinyl alcohol) modified base hydrogel by Photocrosslinking 21
2.8 Silk fibroin modified base hydrogel by photocrosslinking 23
2.9 Poly (vinyl alcohol) blend with silk fibroin base hydrogel by photocrosslinking 26
III. RESEARCH METHODOLOGY 29
3.1 Materials 29
3.2 Experimental 29
3.2.1 Preparation of glycidyl methacrylate (GMA) grafted onto silk fibroin (SF-g-GMA) 29
3.2.2 Preparation of glycidyl methacrylate grafted onto PVA (PVA-g-GMA) 30

TABLE OF CONTENTS (Continued)

Page

3.2.3 Characterization for SF-g-GMA and PVA-g-GMA 31
3.2.3.1 Nuclear Magnetic Resonance (^{1}H-NMR) 31
3.2.3.2 Fourier Transform Infrared Spectroscopy (FTIR) 32
3.2.3.3 Determination of Molecular weight (MW) 32
3.2.4 Preparation of PVA-g-GMA/SF-g-GMA injectable hydrogel 32
3.2.5 Characterization for PVA-g-GMA/SF-g-GMA injectable hydrogel 33
3.2.5.1 Gel fraction and Swelling ratio 33
3.2.5.2 Compression test 33
3.2.5.3 Rheological and viscosity measurements 34
3.2.5.4 Morphological structure measurement 34
3.2.5.5 In vitro degradation 34
3.2.5.6 Cell viability and Live/Dead cell in 3D cell culture 35
3.2.5.7 Quantitative analysis for gene expression 35
3.2.5.8 Statistical analysis 36
IV. RESULTS AND DISCUSSION 37
4.1 Weight average molecular weight (Mw) of SF unmodified and SF-g-GMA 37
4.2 Effect of the grafting conditions of GMA onto PVA (PVA-g-GMA) and SF (SF-g-GMA) 39
4.2.1 ^{1}H-NMR characteristic of PVA-g-GMA and SF-g-GMA 39
4.2.2 FTIR characteristic of PVA-g-GMA and SF-g-GMA 46
4.3 Effect of PVA-g-GMA/SF-g-GMA ratio on physical properties and mechanical properties of injectable hydrogel 49

TABLE OF CONTENTS (Continued)

Page

4.3.1 Gel fraction and swelling ratio of injectable hydrogel 49
4.3.2 The FTIR The FTIR spectra of PVA-g-GMA/SF-g-GMA injectable hydrogel 52
4.3.3 Rheological and viscosity measurements 54
4.3.4 Mechanical properties of PVA-g-GMA/SF-g-GMA injectable hydrogel 57
4.3.5 The morphology and pore size of biphasic injectable hydrogel 59
4.3.6 In vitro degradation of biphasic injectable hydrogel 62
4.3.7 Live and dead cell of biphasic injectable hydrogel 64
4.3.8 Quantitative analysis of gene expression of biphasic injectable hydrogel 66
V. CONCLUSION AND RECCOMENDATIONS 68
5.1 Conclusion 68
5.2 Recommendations 68
REFERENCES 70
APPENDIX A 81
BIOGRAPHY 87

LIST OF TABLES

Table **Page**

3.1 Sequences of primer sets for RT-qPCR 36

4.1 Degree of substitution, DS% of the PVA-g-GMA 39

4.2 Degree of methacrylate, DM% of the SF-g-GMA 42

4.3 Weight average molecular weight (Mw), number average molecular weight (Mn), and polymer dispersion index (PDI) of SF unmodified and SF-g-GMA at various grafting times 46

4.4 PVA-g-GMA/SF-g-GMA biphasic injectable hydrogel mechanical properties 59

มหาวิทยาลัยเทคโนโลยีสุรนารี

LIST OF FIGURES

Figure **Page**

2.1 Illustration of the medial and lateral menisci on the tibial plateau from above 6
2.2 Schematic illustration of approaches to make injectable hydrogels for cartilage and bone tissue-engineering applications 7
2.3 Schematic representation of methods of meniscus tissue engineering 9
2.4 The cross-section demonstrates injection of various biological materials into a meniscus defect 12
2.5 Schematic mechanism of hydrogel driven by (a.) changing temperature (b.) pH-inducing (c.) ionic interaction 13
2.6 Schematic mechanism of an enzymatic reaction with (a.) horseradish peroxidase and hydrogen peroxide as catalyst systems; (b.) photocrosslinking reaction of vinyl groups bearing polymers; and (c.) alkyne-azide click reaction with Cu(I) as catalyst 15
2.7 SEM image of (a.) raw silk fiber from silk cocoon and (b.) silk fibroin degummed from raw silk fiber 16
2.8 Schematic diagram of the silk structure. (a) heavy chain and light chain which linked by disulfide bonds. (b) silkworm thread, fibril overall structure and silk fibroin polypeptide chains 17
2.9 Chemical structures of the most reactive amino acids in silk fibroin 17
2.10 Silk is primarily composed of (Gly-Ala-Gly-Ala-Gly-Ser)$_6$ amino acid repeat units that selfassemble into an anti-parallel β-sheet structure 18
2.11 (a.) The structure of vinyl alcohol (b.) poly (vinyl alcohol) is synthesized by the hydrolysis of poly (vinyl acetate) 20

LIST OF FIGURES (Continued)

Figure **Page**

2.12 Chemical structure of poly (vinyl alcohol) (a) partially hydrolyzed; (b.) fully hydrolyzed 21
3.1 Scheme of protocols used to extraction the silk fibroin and GMA grafting onto SF 30
4.1 (a.) Raw silk cocoon consists of silk fibroin and silk sericin and (b.) silk fibroin degummed by Na2CO3 solution 37
4.2 SDS-page analysis of SF-g-GMA prepared with time various at 1, 2, and 3 h 38
4.3 Purpose of a mechanism for GMA grafting onto PVA: (1) by epoxy ring opening; (2) by transesterification 40
4.4 The ^{1}H-NMR spectra and molecular structure of (a.) GMA monomer, (b.) PVA unmodified, and (c.) PVA-g-GMA 100 mM 41
4.5 Comparison the ^{1}H-NMR spectra of GMA monomer, PVA unmodified and PVA-g-GMA 100 mM 42
4.6 The ^{1}H-NMR spectra of GMA monomer, PVA unmodified and PVA-g-GMA various GMA contents at 50, 100, 150, 200, 250, and 300 mM 43
4.7 Purpose of a mechanism for GMA grafting onto SF by epoxy ring opening 44
4.8 The ^{1}H-NMR spectra and molecular structure of (a.) GMA monomer, (b.) SF unmodified, and (c.) SF-g-GMA 490 mM 45
4.9 The ^{1}H-NMR spectra of GMA monomer, SF unmodified and SF-g-GMA various contents at 70, 210, 350, and 490 mM 46
4.10 Comparison of the FTIR spectra of GMA monomer, PVA-g-GMA 100 mM, and PVA unmodified 47
4.11 PVA-g-GMA 100 mM, and PVA unmodified (A), the FTIR spectra of GMA grafting contents at 50, 100, 150, 200, 250, and 300 mM on PVA 48
4.12 The FTIR spectra of SF unmodified, GMA various contents at 70, 210, 350, and 490 mM on SF 49

LIST OF FIGURES (Continued)

Figure **Page**

4.13 (a.) Gel fraction and (b.) swelling ratio of PVA-g-GMA at various irradiation times 50
4.14 (a.) Gel fraction and (b.) swelling ratio of SF-g-GMA at various SF-g-GMA concentration 51
4.15 (a.) Gel fraction and (b.) swelling ratio of PVA-g-GMA/SF-g-GMA injectable hydrogel at 10 min by photocrosslinked 51
4.16 FTIR spectra of PVA-g-GMA/SF-g-GMA biphasic injectable hydrogel 53
4.17 Mechanism of PVA-g-GMA/SF-g-GMA biphasic injectable hydrogel 53
4.18 The rheological properties of PVA-g-GMA/SF-g-GMA dynamic viscosity measurement of PVA-g-GMA/SF-g-GMA solution at different bending ratio 54
4.19 Comparison of dynamic loss modulus (G') and dynamic storage modulus (G'') of PVA-g-GMA/SF-g-GMA biphasic injectable hydrogel 55
4.20 (a.) The dynamic loss modulus (G') and (b.) dynamic storage modulus (G'') of PVA-g-GMA/SF-g-GMA biphasic injectable hydrogel 56
4.21 Stress-Strain curve of PVA-g-GMA/SF-g-GMA injectable hydrogel 57
4.22 Mechanical properties of PVA-g-GMA/SF-g-GMA injectable hydrogel. (a.) Compressive modulus, (b.) Compressive strength, and (c.) Compressive strain 58
4.23 The SEM images of PVA-g-GMA/SF-g-GMA hydrogels with different ratios: 100:0, 75:25, 50:50, 25:75, and 0:100. The scale bar measures 100 um 60
4.24 Compressive modulus and pore size of PVA-g-GMA/SF-g-GMA biphasic injectable hydrogel 61
4.25 Box plot of the pore size of PVA-g-GMA/SF-g-GMA biphasic injectable hydrogel 57
4.26 Histogram of the pore size distribution of PVA-g-GMA/SF-g-GMA injectable hydrogel 58

LIST OF FIGURES (Continued)

Figure **Page**

4.27 In vitro degradation of PVA-g-GMA/SF-g-GMA biphasic injectable hydrogel 59
4.28 Human chondrocyte cell line growth inside the PVA-g-GMA/SF-g-GMA biphasic injectable hydrogel after UV crosslinking. The morphologies of the chondrocytes inside the hydrogel were observed using live and dead staining at day 1, day 3, and day 7 61
4.29 The survival rates of human chondrocytes cell inside the PVA-g-GMA/SF-g-GMA biphasic injectable hydrogel 62
4.30 Gene expression of human chondrocyte cell inside the PVA-g-GMA/SF-g-GMA biphasic injectable hydrogel analyzed by qRT-PCR of COL1A1, COL2A1, and ACAN at days 7(a.), 14(b.), and 28(c.) 63

มหาวิทยาลัยเทคโนโลยีสุรนารี

CHAPTER I

INTRODUCTION

1.1 Background

The meniscus, a fibrocartilage tissue of the knee joint that aids in body weight distribution, lubrication, and nourishment for the knee joint, is a crucial crescent-shaped component of the knee joint. An injury to the meniscus can result from overuse, sports, mishaps, or aging. Surgery to remove the damaged meniscus in its entirety or in part is frequently the result of this. Increased stress on the joint cartilage, which might eventually result in osteoarthritis, is a typical issue when part of the meniscus is removed (fMakris, Hadidi, & Athanasiou, 2011). The meniscus consists of 3 zones: the outer zone (red-red zone), which contains 80% of collagen I; aggrecan and fibroblast-like cells are the component and vascular region; the middle zone (red-white zone); and the inner zone (white-white zone), which contains 60% of collagen II, aggrecan, avascular tissue, and fibrochondrocyte or chondrocyte-like cells. The meniscal tears of the inner zones cannot be repaired easily due to their avascular nature, and articular cartilage has a limited regenerative and self-healing capacity (Fox, Bedi, & Rodeo, 2012) (Numpaisal, Rothrauff, Gottardi, Chien, & Tuan, 2017).

Tissue engineering (TE) consists of three keys: scaffold, cells, and bioactive molecules (A. X. Sun et al., 2016). These approaches constitute the currently available option that meniscal repair is a biological augmentation, which is a method that helps the meniscus' excellent self-healing ability and decreases the need for meniscus surgery (Liu et al., 2017). Nowadays, meniscus surgery for athletes is minimally invasive; these are small wounds, but applying tissue engineering techniques must be done during surgery, and meniscal surgery is performed by opening the knee joint. To overcome these problems, surgery was performed once by cells rapidly digesting the meniscus but has not yet been completely replace with arthroscopic meniscus repair (Jinglei Wu et al., 2015).

Hydrogels 3-dimensiomnal (3D) polymer network in which the water swelling and porosity allows solvents and nutrients to diffuse homogeneously. Hydrogels can be fabricated in different forms depending on individual cell types (Pyarasani, Jayaramudu, & John, 2018). The hydrophilicity of hydrogels is primarily caused by the distribution of hydrophilic functional groups throughout the polymeric chain's backbone, including amide, carboxyl, amino, and hydroxyl groups (El-Sherbiny & Yacoub, 2013).

Poly (vinyl alcohol) (PVA) has gained popularity as a scaffold supporting material for tissue engineering applications due to its high mechanical properties, non-toxic nature, good biocompatibility, and biodegradability (Chocholata, Kulda, Dvorakova, Kolaja Dobra, & Babuska, 2020). However, it does not efficiently support cell adhesion on its surface owing to the hydrophilic moieties provided by the hydroxyl group (–OH) on its backbone. PVA has been applied to several advanced biomedical applications (Baker, Walsh, Schwartz, & Boyan, 2012)

Silk fibroin (SF) is a natural polymer that consists of two main parts: silk fibroin (SF) and silk sericin (SS). There is 66.5–73.5 %wt silk fibroin and 26.5–33.5 %wt sericin (H. Y. Wang, Zhang, & Wei, 2021). SF has high mechanical strength, flexibility, light weight, and excellent biocompatibility, such as adherence and proliferation of various cells. Arginine-Glycine-Aspartate (RGD) tripeptide, which is found in silk fibroin, can encourage cell attachment (W. Sun, Gregory, Tomeh, & Zhao, 2021). Recently, the application of silk fibroin in biomedical materials has received great attention, especially in the application of tissue engineering (Das et al., 2015).

These factors have led to a lot of interest in injectable hydrogel due to its tissue engineering capabilities for healing. These healing gels are injected into the body in liquid form, and upon physical or chemical crosslinking, they rapidly transform into a solid hydrogel. Because of configurational changes, the chemical covalent crosslinking is permanent and irreversible; yet, it is mechanically durable, and the rate of the polymer network's biodegradation is often under control (Chenga et al., 2021). Photocrosslinking has been used to prepare synthetic covalent hydrogels because polymer solutions easily undergo chemical crosslinking upon irradiation to create a hydrogel (Parhi, 2017). The radiation approach, also known as photocrosslinking, is an

effective pathway for the synthesis of polymer hydrogels. A good option to produce injectable hydrogels is photocrosslinking (Alonso, Andrade Del Olmo, Perez Gonzalez, & Saez-Martinez, 2021).

There are two basic methods for using scaffolds for tissue engineering: (i) seeding cells onto porous scaffolds that have already been constructed, or (ii) encapsulating cells within the scaffold while it is being formed (Nicodemus & Bryant, 2008).

A biphasic injectable hydrogel is a type of biomaterial that can be injected as a liquid and later transitions into a gel-like state once inside the body. This type of hydrogel has two distinct phases: a liquid phase for easy injection and a gel phase that provides a stable and biocompatible matrix (Liu et al., 2017) (Piantanida, Alonci, Bertucci, & De Cola, 2019). The injectable biphasic hydrogel has significant applications in regenerative medicine, tissue engineering, and drug delivery. When administered as a liquid, it can easily fill irregularly shaped defects or target specific areas within the body. After injection, it undergoes a gelation process, transforming into a semi-solid or gel-like substance that supports cell growth and tissue regeneration and provides mechanical stability (J. Wu et al., 2020). The ability to inject the hydrogel minimizes the need for invasive surgical procedures and allows for localized and targeted therapeutic applications (Ketabat, Khorshidi, & Karkhaneh, 2018). These properties make injectable biphasic hydrogels promising candidates for a wide range of medical applications, including wound healing, cartilage repair, and controlled drug release systems.

The requirements of this study were to (i) evaluate the effect of PVA-g-GMA/SF-g-GMA injectable hydrogel on the compressive properties compared with the human meniscal properties at compressive modulus 0.10-0.15 MPa (Sweigart et al., 2004) and (ii) determine the pore size diameter of PVA-g-GMA/SF-g-GMA injectable hydrogel so human chondrocyte cells can be seeded into the pore. The greatest diameter of the chondrocyte cells, which make up articular cartilage, ranges from around 10 μm. to about 30 μm. (Wehland et al., 2020).

Therefore, the study's goal is to develop a poly (vinyl alcohol)/silk fibroin biphasic injectable hydrogel that mimics the meniscus and evaluates its potential for use as a meniscus tissue engineering.

1.2 Research objectives

The main purpose of this research is to develop photocrosslinked biphasic injectable hydrogel from poly (vinyl alcohol) and silk fibroin and diagnose their potential use for meniscus tissue engineering and study the materials factors as followed.

1.2.1 To study the effect of the grafting conditions of GMA onto PVA (PVA-g-GMA) and SF (SF-g-GMA) and optimize the grafting reaction through the grafting conditions.

1.2.2 To study the physical and mechanical properties of PVA-g-GMA injectable hydrogel and SF-g-GMA injectable hydrogel

1.2.3 To study the effect of the ratio between PVA-g-GMA and SF-g-GMA on the physical and mechanical properties of biphasic injectable hydrogel

1.2.4 To study the potential use of photocrosslinked PVA-g-GMA/SF-g-GMA biphasic injectable hydrogels for meniscus tissue engineering scaffold.

1.3 Scope of research

Poly (vinyl alcohol) was synthesized by using glycidyl methacrylate (GMA) grafts at various GMA content levels of 50, 100, 150, 200, 250, and 300 mM, which is called PVA-g-GMA. 100 mM PVA-g-GMA was the optimal condition by degree of methacrylate substitution (DM%) using Nuclear Magnetic Resonance (NMR), and it was chosen to prepare PVA-g-GMA hydrogel at a 10% w/v concentration.

Silk fibroin (SF) was extracted from *Bombyx mori* silk cocoons by using microwave irradiation, and GMA was grafted onto SF at various GMA content levels of 70, 210, 350, and 490 mM, which is called SF-g-GMA. 490 mM SF-g-GMA had the highest degree of methacrylate substitution (DM%) of GMA by NMR and was used to prepare a 50% w/v concentration.

The PVA-g-GMA/SF-g-GMA biphasic injectable hydrogel was fabricated at different ratios of PVA-g-GMA to SF-g-GMA: 100/0, 75/25, 50/50, 25/75, and 0/100, by using Lithium phenyl (2,4,6- trimethylbenzoyl) phosphinate (LAP) as a free radical photoinitiator, for 10 minutes at low UV intensity (365 nm, 6 mW/cm^2).

The chemical interaction of PVA-g-GMA/SF-g-GMA biphasic injectable hydrogels was confirmed by FTIR. The PVA-g-GMA/SF-g-GMA biphasic injectable hydrogel morphology and pore size were observed by field emission scanning electron microscopy. The mechanical properties of PVA-g-GMA/SF-g-GMA biphasic injectable hydrogel were determined by a Texture analyzer machine. The degradation of PVA-g-GMA/SF-g-GMA biphasic injectable hydrogel was studied by immersing it in PBS solution, and the percentages of weight loss were calculated. The biocompatibility of PVA-g-GMA/SF-g-GMA biphasic injectable hydrogel was assessed by human chondrocyte cells seeded with the PVA-g-GMA/SF-g-GMA biphasic injectable hydrogel by photocrosslinking to assess cellular compatibility and cell growth and calculate chondrocyte cell survival.

มหาวิทยาลัยเทคโนโลยีสุรนารี

CHAPTER II

LITERATURE REVIEWS

2.1 Meniscus

2.1.1 Anatomy and cellular components

The knee consists of a meniscus structure. It consists of both the medial and lateral parts that lie between the femur and the tibia. Each is a complex, glossy white tissue composed of cells. Extracellular matrix (ECM) molecules, region-specific innervation, and blood vessels in both menisci are important components of a healthy knee. The main ligament is the medial ligament transverse tendon the ligaments of the femur and the anterior and posterior attachments (fMakris et al., 2011).

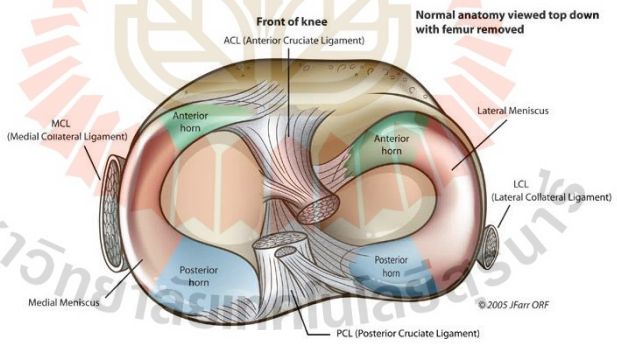

Figure 2.1 Illustration of the medial and lateral menisci on the tibial plateau from above (Svensson, 2019)

Normal human meniscal tissue consists primarily of water, extracellular matrix, and cells compose the majority (72%) of the meniscus. Collagen fibers comprise approximately 70% of the remaining dry material, followed by proteoglycans (17%), non-collagenous proteins (8%), deoxyribonucleic acid (DNA) (2%), and adhesion glycoproteins (1%)

The meniscus is made up of three zones: the outer zone (red-red zone), which contains 80% of collagen I and is composed of aggrecan and fibroblast-like cells, the middle zone (red-white zone), and the inner zone (white-white zone), which is 60% collagen II, aggrecan, avascular tissue, and fibrochondrocyte or chondrocyte-like cells. Due to their avascular character, the meniscal rips in the inner zones cannot be easily mended, and articular cartilage has a limited ability for regeneration and self-healing (Numpaisal et al., 2017).

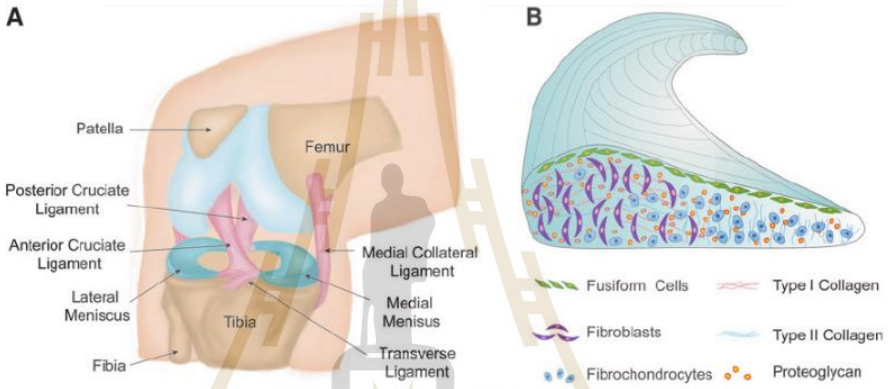

Figure 2.2 Schematic illustration of approaches to make injectable hydrogels for cartilage and bone tissue-engineering applications (H. Li et al., 2021).

The meniscus is resistant to several forces, including compression, and tension. In addition, it is crucial for the articular cartilage's nourishment, lubrication, shock absorption, load bearing, and load transfer. A specific form is necessary for these numerous and complicated activities. The wedge-shaped tissue excels at supporting the bent femoral condyle during articulation with the flat tibial plateau because of its form (H. Li et al., 2021).

The characteristics of human tissue have been characterized by several investigations. The tissue's tensile modulus, which ranges from 90 to 300 MPa for circumferentially, changes accordingly between the circumferential and radial directions (fMakris et al., 2011). With an aggregate modulus of 100–150 kPa (0.10-0.15 MPa), the meniscus resists axial compression (Chia & Hull, 2008).

2.1.2 Meniscus repair

If a meniscus tear is in a repairable region of the meniscus and meets certain criteria, the surgeon may choose to repair it using sutures or specialized devices. The torn edges are brought together and secured, promoting healing and restoration of the meniscus (de Albornoz & Forriol, 2012).

2.1.2.1 Open surgery

Open surgery for meniscus refers to a traditional surgical approach where a larger incision is made to directly access and repair or remove the damaged meniscus (Z. Wang et al., 2019). While open surgery may be necessary in certain cases, it generally has some disadvantages compared to minimally invasive arthroscopic surgery, such as a larger incision and increased trauma, prolonged healing and rehabilitation, and an increased risk of infection (Vaquero & Forriol, 2016).

2.1.2.2 Minimally invasive surgery

Arthroscopic surgery is a minimally invasive surgical procedure commonly used for the treatment of meniscus tears (Treuting, 2000). It involves the use of an arthroscope, which is a small, flexible tube with a camera and light attached to it. The surgeon makes small incisions near the knee joint and inserts the arthroscope to visualize the interior of the knee (Z. Wang et al., 2019).

One of the most promising approaches to treating meniscal damage in a clinical setting has arisen through the use of tissue engineering and meniscus scaffolds. An approach that could be minimally invasive is meniscal scaffolding by arthroscopic surgery.

2.2 Tissue engineering

Tissue engineering is a combination of several academic fields that aims to establish functional three-dimensional (3D) tissues. The three pillars of tissue engineering, which are cells, bioactive molecule, and scaffolds, are founded on knowledge of tissue structure and development. Chemicals, cell types, and biologically appropriate signaling structures are all utilized (A. X. Sun et al., 2016). Tissue

engineering's study of the interactions of cells with materials and their surface properties is to maintain, improve, or repair tissue function. It is also designed to repair organs or tissues that have been injured. (El-Sherbiny & Yacoub, 2013).

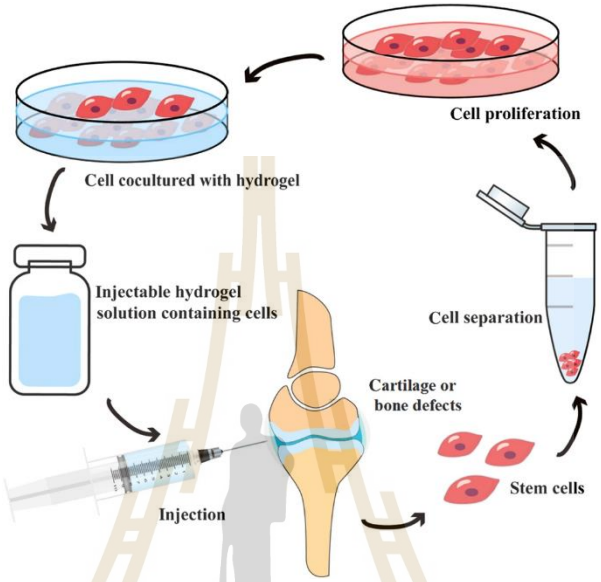

Figure 2.3 Schematic representation of methods of meniscus tissue engineering (Liu et al., 2017)

2.2.1 Cell

Cells need to be applied to populate matrices and create a matrix that matches characteristics of the natural tissue in order to develop an engineered tissue in vitro (Howard, Buttery, Shakesheff, & Roberts, 2008). The most significant developments in this field have been the creation of tissue for reimplantation using primary cells obtained from the patient and combined with scaffolds (Howard et al., 2008). The three main cell therapy approaches for healing patients' damaged or injured tissues are: implanting a construct composed of cells and scaffolds; implanting isolated cells; and allowing native cells to regenerate tissue in place (C. M. Murphy, O'Brien, Little, & Schindeler, 2013). Cells utilized in tissue engineering can come from a variety of sources, including autologous (from the patient), allogenic (from another human donor), and xenogeneic (from a donor of a different species) (Ikada, 2006).

2.2.2 Bioactive molecule

The potential for improving bone tissue production requires considerable attention to bioactive molecules like mechanical stimulation, ECM, and fluid flow. Through ECM-cell interactions, such signals can significantly modify the shape, activity, and gene expression of cells, which consequently controls cell migration, proliferation, and differentiation (Bonnans, Chou, & Werb, 2014). In addition, in the bioactive molecule, biophysical cues such as the mechanical forces that tissues and cells are exposed to are essential in regulating cellular behavior such as proliferation and differentiation and maintaining tissue and organ function over the course of organisms' lives (Y. Zhang & Habibovic, 2022).

2.2.3 Scaffold

The primary goal of tissue engineering is to develop scaffolds strategies for regenerating live, healthy, and useful tissues that may be used as tissue transplants or even organ substitutes. The overall strategy is to use three-dimensional (3D) scaffolds as support structures for cell proliferation and the formation of new tissues (Peretti et al., 2006). The scaffold may be designed to function only as a structural support, giving cells passive signals, or it may integrate biological cues to direct the development of cells and tissues. When using scaffolds for tissue engineering, there are two basic methods: (i) seeding cells onto porous scaffolds that have already been constructed, or (ii) encapsulating cells within the scaffold while it is being formed (Nicodemus & Bryant, 2008).

มหาวิทยาลัยเทคโนโลยีสุรนารี

2.3 Hydrogel

Three-dimensional (3D) crosslinked networks are composed of hydrogels that can take up a great deal of water or other biological fluids. The hydrophilic components included in the core polymer, such as carboxyl, hydroxyl ether, and amino groups, play a significant role in maintaining ownership of the 3D architecture (El-Sherbiny & Yacoub, 2013). Due to any adsorption, the hydrogel will continue to swell. Low surfaces due to fluidity, softness, and rubbery conflict with biological fluids, including water. The fact that swelling decreases the mechanical resistance between

the tissues of elastic flexibility in the implanted hydrogel in the case of the body's goals (Samadian, Maleki, Allahyari, & Jaymand, 2020).

2.3.1 Natural hydrogel

Natural hydrogel producing polymers have frequently been employed in tissue engineering applications because they are either components of or have macromolecular characteristics akin to natural ECMs. Collagen, gelatin, chitosan, hyaluronic acid, chondroitin sulfate, agarose, alginate, and fibrin are examples of natural polymers that are representative of nature (Awad, Wickham, Leddy, Gimble, & Guilak, 2004). Natural materials have the advantage of being biodegradable and having good compatibility with cells. Mimic the environment in which the cell is located. However, natural materials There is a limit to rapid degradation rates and poor mechanical properties. Because it is a substance that comes from nature. It is also difficult to control the chemical structure. (Kaith, Singh, Sharma, & Sud, 2021).

2.3.2 Synthetics hydrogel

Synthetic polymers are intriguing for hydrogel because of their often predictable and controlled chemical and physical characteristics. With appropriate molecular weights, block chain polymers, and degradable connections, synthetic polymers may be made repeatedly. Synthetic hydrogels provide better matrix design and chemical composition control than natural hydrogels, but they often have poorer cell adhesion, cell proliferation, and biological activity. Incorporating bioactive components for improved cellular bioactivity into synthetic hydrogels is one method for developing an optimal hydrogel for tissue engineering applications. Among the most often utilized synthetic polymers for hydrogels are poly (ethylene glycol), poly (vinyl alcohol), poly (propylene fumarate), PNIPAAm, Pluronic F-127, and polypeptides, all of which are synthetically generated materials. (Teh & Goh, 2017) (Ye, Wu, Su, Sun, & Guo, 2022).

2.4 Injectable hydrogel system

Injectable hydrogel has greater advantages than premade scaffolds in terms of

patient compliance and simplicity of clinical application for the treatment of geometrically difficult and big lesions using minimally invasive techniques as arthroscopy. Injectable hydrogel can be injected into the human body as liquids and cure to form an in situ solid hydrogel due to physical or chemical stimuli (Hou, De Bank, & Shakesheff, 2004) (Tan & Marra, 2010).

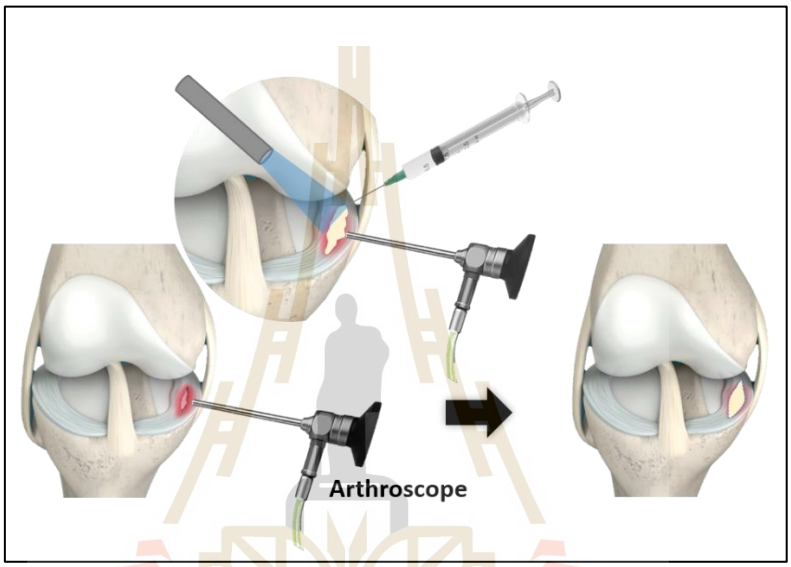

Figure 2.4 The cross-section demonstrates injection of various biological materials into a meniscus defect.

2.4.1 Injectable hydrogel via physical crosslinking

Physical crosslinking refers to the formation of temporary, reversible crosslinks within hydrogels without the involvement of chemical reactions. These physical interactions can be disrupted or reformed under certain conditions, allowing for changes in the gel's properties. Here are some common physical crosslinking methods used for hydrogels (Naeem et al., 2017):

2.4.1.1 Temperature-Induced

Temperature-Induced Injectable hydrogel: Some hydrogel systems exhibit a sol-gel transition based on temperature changes. Below a specific temperature, the hydrogel is in a liquid or sol state, but when the temperature is

increased, it undergoes gelation and forms a solid gel. This process is reversible, and the gel can revert to a sol state upon cooling (Xue et al., 2022).

2.4.1.2 pH-Induced

pH-sensitive hydrogels can undergo gelation or dissolution in response to changes in the surrounding pH. By adjusting the pH within a specific range, the gelation can be triggered or reversed, allowing for control over gel formation and dissolution (Naeem et al., 2017).

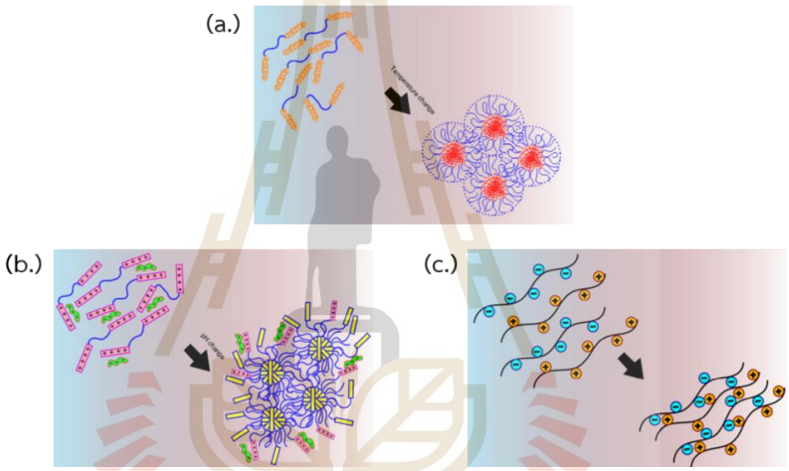

Figure 2.5 Schematic mechanism of hydrogel driven by (a.) changing temperature (b.) pH-inducing (c.) ionic interaction (Nguyen, Huynh, Park, & Lee, 2015)

2.4.1.3 Ion-Induced

Hydrogels that contain charged groups can form physical crosslinks through ionic interactions with oppositely charged ions. By altering the concentration or type of ions in the environment, the gelation properties of the hydrogel can be manipulated (Xue et al., 2022).

Physical crosslinking has benefitted such reversibility, reactivity to environmental factors, and the capacity to modify gel characteristics. In contrast to chemically crosslinked hydrogels, nevertheless, physical crosslinked hydrogels often show lower mechanical strength and stability (X. Li, Sun, Li, Kawazoe, & Chen, 2018).

2.4.2 Injectable hydrogel via chemical crosslinking

Chemical crosslinking is a method used to create stable, three-dimensional networks within hydrogels. It involves the formation of covalent bonds between polymer chains, which enhances the mechanical properties and stability of the hydrogel (Parhi, 2017). There are various chemical crosslinking methods used for hydrogels, including:

2.4.2.1 Crosslinking Agents

Chemical compounds, known as crosslinking agents or crosslinkers, are added to the hydrogel formulation. These agents have reactive functional groups that can form covalent bonds with the polymer chains, creating a network. Examples of crosslinking agents include glutaraldehyde, genipin, and carbodiimides like EDC (1-ethyl-3-(3-dimethylaminopropyl) carbodiimide) (Lim, 2022).

2.4.2.2 Click Chemistry

Click chemistry refers to a class of highly selective and efficient reactions used for crosslinking hydrogels. Examples include azide-alkyne cycloaddition reactions (CuAAC) and thiol-ene reactions. These reactions are known for their high reaction rates, biocompatibility, and specific chemistries (Bhattacharya & Shunmugam, 2020).

2.4.2.3 Photopolymerization

Photopolymerization: The primary idea behind this technique is to use chemical compounds, such as methacryloyl chloride, glycidyl methacrylate (GMA), and methacrylic anhydride, to introduce polymerizable vinyl groups onto the polymer (Balakrishnan & Banerjee, 2011). The photopolymerization method, that utilizes photoinitiators and light to initiate crosslinking. Photoinitiators, such as benzoin methyl ether or Irgacure, and Lithium Phenyl (2,4,6-Trimethylbenzoyl) Phosphinate (LAP) are incorporated into the hydrogel formulation. When exposed to specific wavelengths of light, the photoinitiator undergoes a reaction that generates free radicals. These free radicals then initiate the crosslinking reaction between polymer chains, creating a crosslinked hydrogel (for example, methacrylol chloride, glycidyl

methacrylate, methacrylic anhydride) (Nguyen et al., 2015).. Photopolymerization, which allows for the initiation of gelation precisely when and where it is needed, offers spatial control over hydrogel formation, and gelation can be precisely controlled in terms of timing (Pamplona et al., 2023).

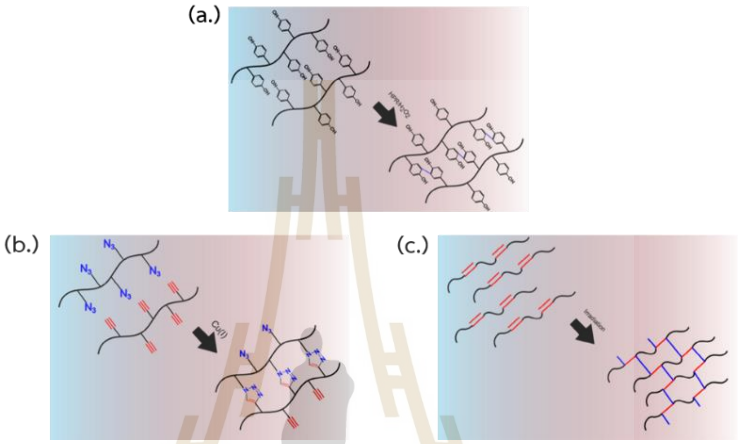

Figure 2.6 Schematic mechanism of an enzymatic reaction with (a.) horseradish peroxidase and hydrogen peroxide as catalyst systems; (b.) photocrosslinking reaction of vinyl groups bearing polymers; and (c.) alkyne-azide click reaction with Cu(I) as catalyst. (Nguyen et al., 2015)

2.5 Silk fibroin (SF)

Silk fibers produced by silkworms are widely used in our daily lives. While they have occupied an important niche in the textile industry for thousands of years, their potential as biomaterials has only been recognized and developed over the past decade. Silk fibroin (SF) derived from Bombyx mori is formed by the combination of a fibrillar protein, composed of about 66.5–73.5 %wt. fibroin as a core, and a glue-like protein, named silk sericin, which represents about 26.5–33.5 %wt. of the cocoon mass (H. Y. Wang et al., 2021).

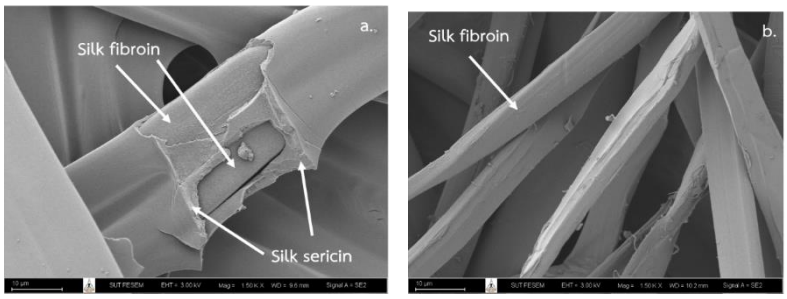

Figure 2.7 SEM image of (a.) raw silk fiber from silk cocoon and (b.) silk fibroin degummed from raw silk fiber

Silk fibroin is composed of three proteinaceous components: the heavy chain (350 kDa) fibroin (H-chain), the light chain (25 kDa) fibroin (L-chain) and P25 protein. The molar ratios of these three components are 6:6:1 respectively. The first one is hydrophobic and responsible of the formation of β-sheet structures, the second one is more hydrophilic and elastic and both of them are linked by a disulfide bond, meanwhile the P25 protein gives integrity to the complex (Szliszka et al., 2009).

Bombyx mori fibroin's primary amino acid components are Gly (43%), Ala (30%), and Ser (12%). The heavy chain is composed of up of 12 large hydrophobic domains that are connected by 11 smaller hydrophilic parts (Pham & Tiyaboonchai, 2020). It contains 46% Gly, 30% Ala, 12% Ser, 5.3% Tyr, etc. Gly-Ala-Gly-Ala-Gly-Ser is a repeating sequence found in each hydrophobic domain (Szliszka et al., 2009). The less numerous amino acids, such as serine (12.1%), tyrosine (5.3%), threonine (0.9%), aspartic acid (0.5%), and glutamic acid (0.6%), provide opportunities for chemical reactions and crosslinking (Mu, Sahoo, Cebe, & Kaplan, 2020).

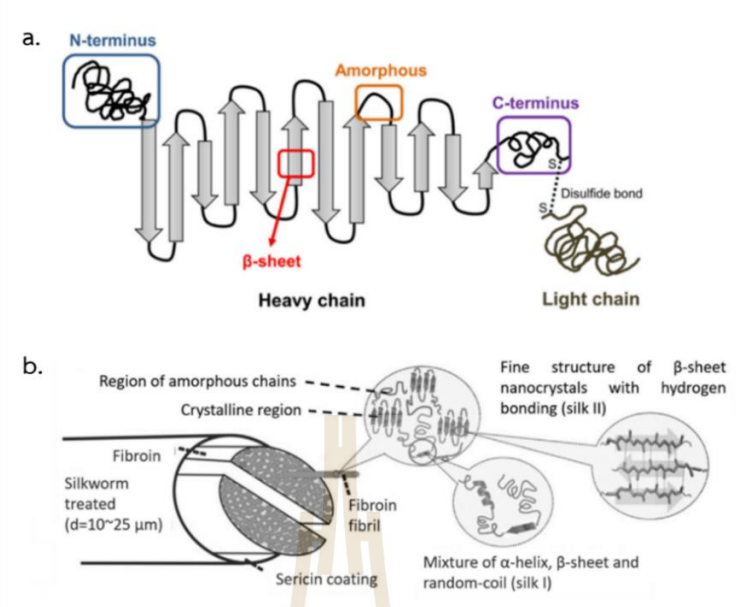

Figure 2.8 Schematic diagram of the silk structure. (a) heavy chain and light chain which linked by disulfide bonds. (b) silkworm thread, fibril overall structure and silk fibroin polypeptide chains. (W. Sun et al., 2021)

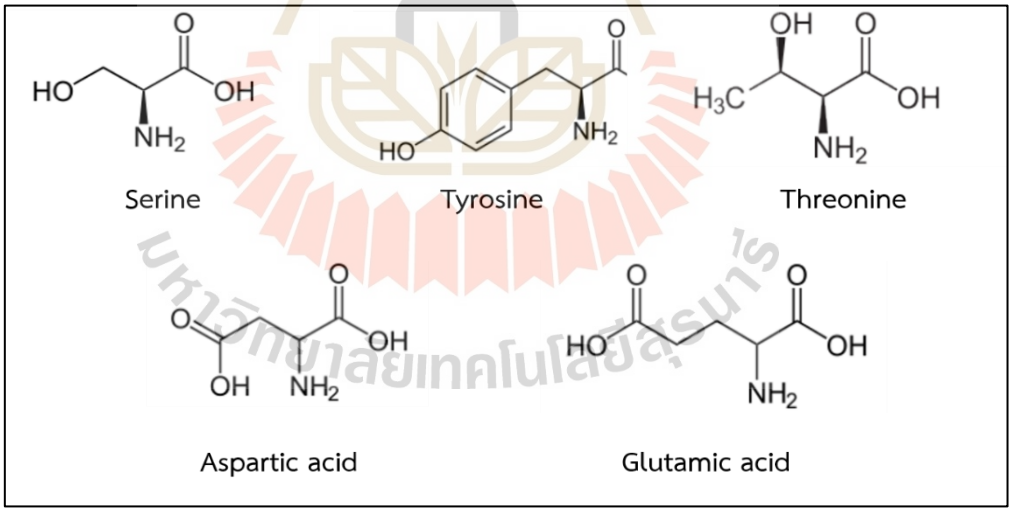

Figure 2.9 Chemical structures of the most reactive amino acids in silk fibroin

Silk fibroin has been demonstrated to contain silk I and silk II kinds of crystallinity (W. Sun et al., 2021). Silk I, which is mostly present in the silk glands of silkworms, has the least crystallinity and primarily consists of random coils and a-helices, which makes silk I thermodynamically unstable and water-soluble (W. Sun et

al., 2021). However, silk II, which is mostly present in silk fibers, has the highest crystallinity, is a member of the monoclinic crystal system, and is mainly composed of antiparallel β-sheet components. Silk II forms as the result of the hydrophobic interactions between hydrogen atoms and methyl groups, and it is thermodynamically stable. Silk II is stable, has excellent thermal and mechanical properties, and is not capable of dissolving in water (Xiufang Li, Fan, Zhang, Yan, & You, 2020).

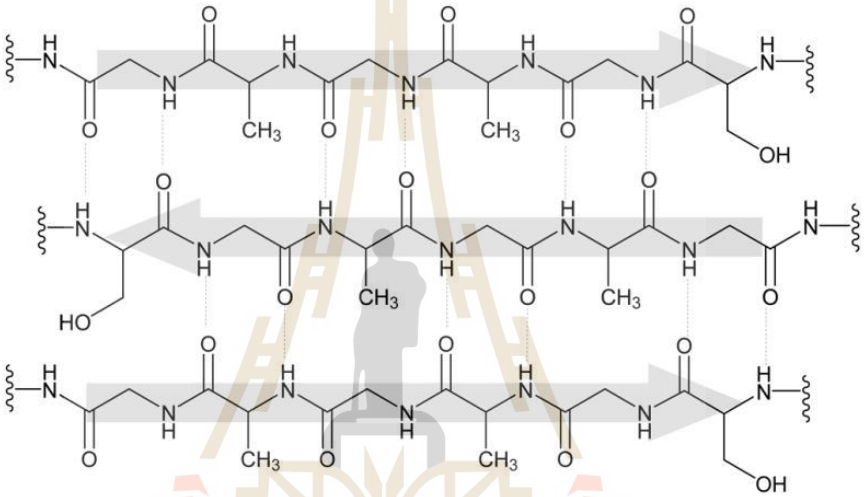

Figure 2.10 Silk is primarily composed of (Gly-Ala-Gly-Ala-Gly-Ser)$_6$ amino acid repeat units that selfassemble into an anti-parallel β-sheet structure (A. R. Murphy & Kaplan, 2009).

มหาวิทยาลัยเทคโนโลยีสุรนารี

2.5.1 Silk fibroin extraction

2.5.1.1 Silk fibroin fiber degumming

The degummed method is the first step in removing silk sericin from raw silk fiber using chemical agents, which is called degummed silk. The silk sericin is dissolved and denatured in a degummed agent. Degumming agents consist of alkaline and highly concentrated urea buffer and degumming agents such as sodium carbonate (Na_2CO_3), urea, and neutral soap, respectively.

Urea buffer was used with 6–8 M aqueous urea (pH 7) for 2-3 h at 80–90 °C. Urea buffer can break peptide chains less than Na_2CO_3. However, urea

buffer is a toxic reagent because β-mercaptoethanol makes urea agents unsuitable for degumming methods for medical applications (Zongqian Wang, Yang, Li, & Li, 2018).

Na_2CO_3 is a conventional degumming/standard method using 0.5–1% w/v Na_2CO_3 at a boiling temperature of 90–100 °C for 30–60 min and repeat 2-4 times that can successfully wash or remove silk sericin from silk fiber. Following degumming, the finished items were thoroughly washed with distilled water before being dried in an oven set at 40 °C (H. Yang, Wang, Wang, & Li, 2020).

2.5.1.2 Silk fibroin dissolving

Dissolving degummed silk fibers is the second step to creating a silk fibroin solution. The silk fibroin dissolving method is used to break the hydrogen bond of the b-sheet and transform the structure from silk I to silk II. The solubility of SF fibers in a variety of solvents, including as inorganic acids or alkalis, proteases, highly ionic aqueous or organic salt-containing systems, ionic liquids, and organic solvents, has been the object of several evaluations and studies (H. Y. Wang et al., 2021).

Degummed silk fibers were dissolved in $CaCl_2$: H_2O solution by stirring at 98 ± 2 °C for 1 h (Sinna, Numpaisal, Ruksakulpiwat, & Ruksakulpiwat, 2021). Ajisawa's ternary solvent consisting of calcium chloride/water/ethanol ($CaCl_2$/ CH_3CH_2OH/H_2O). Lithium salt solutions such as lithium bromide (LiBr-H_2O) and LiBr:CH_3CH_2OH: H_2O (45:44:11). 9.3 M LiBr-H_2O and 1:2:8 M $CaCl_2$/ CH_3CH_2OH/H_2O (Ajisawa's ternary solvent system) are the two most often applied solvent systems in the literature for dissolving silk fibroin fibers. Degummed silk fibers are dissolved in the initial process for 4 hours at 60 °C (Miyaguchi & Hu, 2005).

Additionally, it has been discovered that solutions of $Ca(NO_3)_2$:CH_3OH, $Ca(NO_3)_2$: CH_3CH_2OH:H_2O, and $CaCl_2$:CH_3CH_2OH:H_2O (Ajisawa's ternary solvent) may all be used to dissolve Bombyx mori silk. Despite the fact that silk dissolves in these systems, there are still certain issues. One big issue is that the traditional techniques of disintegration demand a lot of time and energy (X. Chen, Knight, Shao, & Vollrath, 2001).

The salt solution of silk fibroin must first be desalted in order to regenerate it afterwards. Dialyzing the very viscous silk fibroin salt solution against ultrapure water for 2–7 days is the most popular technique for removing salt ions (Woltje, Kolbel, Aibibu, & Cherif, 2021).

Microwave assisted method was developed for extraction silk fibroin with enhance dissolving rate. The degummed silk was dried overnight at room temperature and then dissolved in either $Ca(NO_3)_2$:CH_3CH_2OH:H_2O or $CaCl_2$:CH_3CH_2OH:H_2O (1:2:8) solutions. The benefits of this novel microwave-assisted technique, which include a substantial decrease in time and energy expenditures, have been demonstrated, and it currently represents a promising, cost-effective way to regenerate silk fibroin. The silk fibroin qualities obtained by the microwave-assisted method are comparable to those achieved by the traditional method and demonstrate a dissolving time of less than 30 minutes. (S. Li et al., 2018).

2.6 Poly (vinyl alcohol) (PVA)

In comparison to hydrogels produced from synthetic polymers, particularly made from polyvinyl alcohol (PVA), in particular, had greater properties. As shown in Figure 3, the synthetic polymer polyvinyl alcohol (PVA) is a water-soluble polymer that is produced as the result of partially or completely hydrolysis of polyvinyl acetate to remove the acetate groups.

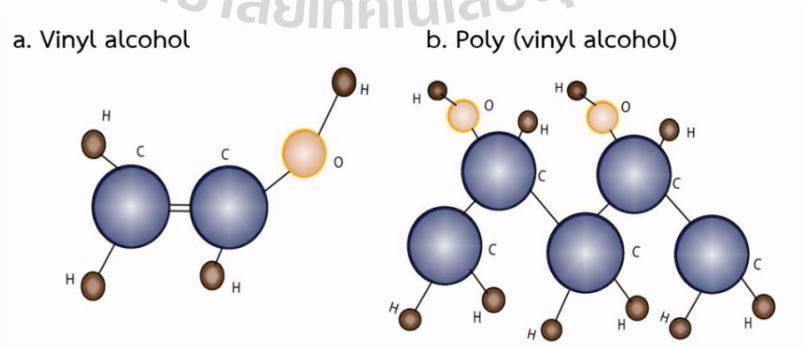

Figure 2.11 (a.) The structure of vinyl alcohol (b.) poly (vinyl alcohol) is synthesized by the hydrolysis of poly (vinyl acetate) (Baker et al., 2012)

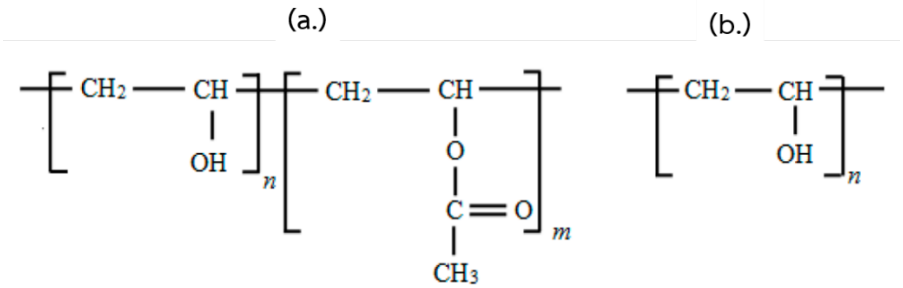

Figure 2.12 Chemical structure of poly (vinyl alcohol) (a) partially hydrolyzed; (b.) fully hydrolyzed

The hydrolysis of polyvinyl acetate produces the semi-crystalline polymer PVA hydrogel, which has strong solubility, biocompatibility, and biodegradability characteristics. It has a substantial swelling capability, which makes it a potential adsorbent. It has a high ability to absorb a large number of water molecules due to the electrostatic attraction between the hydrophilic functional groups, which contributes to its polymeric strength and is the basis for the development of the hydrogel connection system (Gaaz et al., 2015).

Polyvinyl alcohol (PVA), an FDA-approved material, has been widely used in a variety of biomedical applications, including implanted medical devices, contact lenses, artificial blood vessels, and osteochondral transplants. Due to its beneficial characteristics, which include biocompatibility, inertness, lack of biodegradability, minimal protein absorption, and readily modifiable mechanical properties (Baker et al., 2012)

2.7 Poly (vinyl alcohol) modified base hydrogel by photocrosslinking

(Crispim, Piai, Schüquel, Rubira, & Muniz, 2006) demonstrated the modification of PVA with glycidyl methacrylate (GMA) in DMSO under the catalysis of TEMED. Under bubbling N_2 at 30 °C, the solution was stirred for 24 hours. PVA that had been dissolved in DMSO was combined with GMA. The experimental settings were improved by the application of response surface approach. The ideal circumstances were 62 C and a 6-

hour response time. The reactions utilizing the molar ratios [-OH(PVA)/GMA] equal to 1/0.10, 1/0.25, 1/0.50, 1/0.75 and 1/1 were examined at these optimal circumstances. Both FTIR and NMR spectroscopies were used to analyze the process. Methacryloyl groups are inserted into PVA chains to cause transesterification, which results in the creation of glycidol as a byproduct. Methacryloyl groups are inserted into PVA chains to cause transesterification, which results in the creation of glycidol as a byproduct. The ratio between the averaged area due to the vinyl hydrogen from methacryloyl groups at 5.6 ppm and 6.0 ppm and the total area of the vinyl hydrogen and hydroxyl hydrogen of PVA was used to calculate the degree of substitution (DS), which represents the number of methacryloyl groups inserted.

(Martens & Anseth, 2000) studied acrylate-modified PVA macromers. PVA (10 g) was dissolved in DI water, and glycidyl acrylate was added along with HCl to attain a pH of approximately 1.5. The photoinitiator D2959 (0.05 wt%) was dissolved in the solution. The final solution was photopolymerized using an ultraviolet light source. The swelling behavior, where it can be noted that all of the gels rapidly reach their equilibrium swelling. In addition, the swelling ratio decreases slightly after reaching equilibrium, which is attributed to the relatively high sol fraction in these gels (35%), and this sol fraction does not appear to be dependent on the initial macromer concentration. The equilibrium degree of swelling, Q, decreases from 18 to 15 to 5.5 as the macromer solution concentration increases from 20 to 30 to 50 wt%. Since these gels underwent the same photoinitiation process and reacted to 100% conversion, the differences in swelling behavior were related to differences in the network structure.

(Kamoun, Omer, Khattab, Ahmed, & Elbardan, 2018) created and improved PVA-g-GMA hydrogels. DMSO was mixed with PVA to create a 5% (w/v) solution. To obtain the PVA/GMA molar ratios of (1/0.025), (1/0.05), (1/0.07), (1/0.09), (1/0.15), and (1/0.25), GMA was added to the PVA solution. The PVA-g-GMA solution combination had 1.0 mol% of TEMED added as a catalyst. In order to photocrosslink the PVA-g-GMA macromonomers, Irgacure 2959 (I2959) was used as a UV photoinitiator at 365 nm. The degree of swelling (%) of PVA-g-GMA hydrogels with various levels of macromonomer GMA It was discovered that when the GMA concentration increased, from 0.025 to

0.250 M, the swelling degree varied from 50 to 250 (wt%). These outcomes are brought about by the fact that hydrogels with low macromonomer contents (0.025, 0.050, and 0.070 M) of GMA have bigger pore diameters than those with high GMA concentrations. As a result, water is transported through hydrogel networks more quickly and with a greater swelling capacity. While PVA-g-GMA hydrogels with various GMA ratios exhibit a relatively smooth, uniform surface, compressed, and non-porous surface structure with few tiny cracks that clearly appear by increasing the content of GMA in hydrogels, the surface morphology of PVA hydrogels without GMA presents a rough, rugged, and heterogeneous surface structure. This may be explained by the fact that adding more GMA to PVA makes the hydrogel's surface more compact due to an increase in crosslinking density.

2.8 Silk fibroin modified base hydrogel by photocrosslinking

(S. H. Kim et al., 2018) studied biocompatible silk fibroin bioink for digital light processing 3D printing. Silkworm cocoon n (Jeonju, Korea) 40 g of sliced cocoons removed the sericin with 0.05 M Na_2CO_3 solution and dissolved degummed silk fibroin in 9.3 M lithium bromide (LiBr) solution at 60 °C for 1 h. Added GMA solutions 141, 282, 424, and 705 mM to the mixture after GMA and Sil-MA solution were filtered, dialyzed, and freeze-dried. Freeze-dried Sil-MA prepared with 424 mM of GMA dissolved in water at various concentrations of 10–30% w/v, and the LAP photoinitiator was added. Sil-Ma hydrogels were fabricated by DLP printing with 365 nm. UV-LED and UV light intensity of 3.5 mW cm^{-2} for 3 s. Identification of GMA-related peaks and SF-associated peaks and the degree of methacrylation by FTIR spectroscopy and ^{1}H-NMR spectroscopy, respectively. The methacrylation degree of Sil-MA was increased from 22.4% to 42.0% with increasing of GMA from 141 to 705 mM. According to the increase in Sil-MA concentration, both the compressive strain and the compressive stress at break increased. The compressive modulus at 50 % strain increase from 17.7 to 125.8 MPa with Sil-MA content from 10%w/v to 30%w/v. The compressive strength (910 MPa) and compressive modulus (125.8 MPa) of three-dimensionally printed silk-GMA (30 w/v%) were greater than those of either polycaprolactone (PCL)-blended gelatin hydrogels (75-94 kPa) or 30% Gelatin-MA (88 kPa). The 30% Sil-MA hydrogels were

strong enough to support the weight of about 7 kg and returned to their original shape immediately after the load was removed. In accordance with the various GMA concentrations, the resultant Sil-MA and Sil-MA hydrogel were each given a unique characterization. For the in vitro study using human chondrocyte cell concentrations of 1–2 x 10^7 cells/mL, that did not affect the integrity of the final construct. During the four weeks they observed, the 30% Sil-MA hydrogel degraded up to 50% and provided chondrocytes with a favorable environment.

(C. M. Yang et al., 2022) prepared a composite hydrogel consisting of SF modified by butyl glycidyl ether (BGE), tannic acid (TA), and ZnO nanoparticles for hemostatic activity applications. Degummed silk fibroin was dissolved in $CaCl_2$/EtOH/H_2O at ratios of 1:2:8 M at 70 °C for 1 h, then BGE (20 ml) was added to the SF solution. The mixing solution was stirred at 70 °C for 3 h. The SF-BGE solution was dialyzed, centrifuged, and freeze-dried at -80 °C for 7 days. The SF-BGE was verified using ^{1}H-NMR. The degree of substitution (DS%) of SF-BGE was invested using the proton peak of the aromatic ring of the tyrosine, and the DS% of SF-BGE was calculated as 31.6%. The 20% wt SF-BGE and 1.3% wt TA were mixed in distilled water with a ZnO:TA molar ratio of 10:2, and then the composite hydrogel was fabricated for 6 h. SF-BGE and SF-BGE/TA solutions and SF-BGE/TA/ZnO hydrogel were tested for cytocompatibility and cell viability using L929 cells (1x104 cells/well), and the tests were carried out with a LIVE/DEAD assay for imaging and CCK-8 for quantifying after incubation for 24 hours. According to the ISO 10993-5 standard, the SF-BGE/TA/ZnO hydrogel was shown to be non-toxic (grade 0). All samples had cell viability levels of 90–97% or higher.

(M. H. Kim & Park, 2016) synthesized of SF hydrogel via a chemical cross-linking reaction using gamma-ray irradiation. Degummed B. mori silk fiber (Jinju-si, Korea) is dissolved in a ternary solvent system composed of $CaCl_2$/EtOH/H_2O whose molar ratio is 1:2:8 at 85 C for 4 h. The solution was dialyzed for 72 h. to remove salt, centrifuged to remove silk aggregates. The final concentration was 2.3-7.9 %wt. SF C-gel was prepared by SF solutions of various doses of 15, 30, 45, 60, 75, and 90 kGy. concentrations poured into a petri dish and irradiated with gamma-rays from a Co-60 source at room temperature, which induced intermolecular cross-linking reactions. SF hydrogel started to develop right away after irradiation, and at doses more than 60 kGy, the hydrogel started to break. A 60 kGy absorption recommended dosage was appropriate for an SF solution. It was discovered that the SF C-gel in a deionized water

medium had a decreased swelling ratio and had quickly lost its stability, resulting in a swelling ratio below 0% because of the physical crosslinking. SEM images were used to describe the porous structure of the freeze-dried SF hydrogel. Pre-freezing temperatures of -20°C, -50°C, -80°C, and -196°C were used to create three-dimensional SF scaffolds, which were then freeze-dried. The hydrogel's porosity structure and the amount of SF, radiation exposure, and pre-freezing temperature were all closely associated. The SF C-gel had bigger pore diameters than the regular C-gel, which had consistent pore sizes and a porous network structure. The cytotoxicity of the SF hydrogel was investigated by an MTS assay using human mesenchymal stem cells (hMSCs). The SF hydrogel demonstrated no cytotoxicity with hMSCs. For the live and dead cells, most cells viability showed green fluorescence.

(Soon Hee Kim et al., 2020) reported SF modified by methacryloyl as a multipurpose medicinal glue that may be used as an adhesive, sealant, or hemostatic agent. Sil-MAS was synthesized by using Bombyx mori (B. mori) cocoons. Silk cocoons were degummed in 0.05 M Na_2CO_3 at 100 C for 30 min, the 20 g. silk degummed was dissolved in 9.3 M LiBr 100 ml at 60 C for 1 h. The 6 ml GMA solution was solely added to the silk solution with continued stir at 60 C for 3 h. The Sil-MAS solution was filtered, dialyzed, frozen, and freeze dried at -80 C for 48 h. ^{1}H-NMR spectroscopy was used to confirm that GMA modified SF. GMA reacted with SF by an epoxide ring opening reaction. The l-Sil-MAS (crosslinked material) was prepared by 25%w/v Sil-MAS dissolved in DI water, 0.3% w/v LAP (photoinitiator) was added into Sil-MAS solution. The l-Sil-MAS was fabricated to c-Sil-MAS (crosslinked material) by using UV spot-curing machine 365 nm., 6 mW/cm^2 intensity for 10–30 s at a distance of 5 cm. The viscosity of l-Sil-MAS was in the ideal ranges 30–1000 MPa.s for handling and permitted material penetration into the tissue locations. The mechanical properties of c-Sil-MAS make it an appropriate sealant for internal organs. Additionally, c-Sil-MAS exhibits excellent viscoelastic behavior and a high break elongation. 79% of the hydrophobic segments in SF are made up of amino acids with hydrophobic residues, whereas the hydrophilic segments in SF are made up of amino acids with polar side groups.

2.9 Poly (vinyl alcohol) blend with silk fibroin base hydrogel by photocrosslinking

(Parivatphun, Sangkert, Kokoo, Khangkhamano, & Meesane, 2022) presented mimicked biphasic scaffolds and assessed them to determine specific uses for oral and maxillofacial surgery. The SF cocoon (Thailand) was degummed and dissolved by Na_2CO_3 and 9.3 M LiBr, respectively. The SF solution was then dialyzed and centrifuged. The microbubble method was utilized to create biphasic scaffolds that were then freeze-thawed and freeze-dried using PVA and various concentrations of SF. The molecular organization was confirmed using FTIR. The interaction of the amide I, II, and III groups may be attributed to the SF molecules, but the mobility of the -OH group in the material was mostly caused by PVA molecules. The -OH, amide I, II, and III groups in the PVA/SF sponges demonstrated molecular mobility, indicating the sponges' loose structural development. The morphology was observed using scanning electron microscopy (SEM). The thin film layer and foam were two separate structures on the PVA/silk scaffolds. Without the intervention of any additional chemicals or organic solvents, the PVA solution proved stable. The scaffold constructs with varying pore diameters were created using various silk solution concentrations. PVA and SF pores range in size from 103 to 443 m on average. As the concentration of SF in the solution increased, the size of the sub-pores decreased while maintaining the same flow velocity. The use of the PrestoBlue reagent for osteoblast cell proliferation and fibroblast cell proliferation were assessed on days 1, 3, 5, and 7. From days 1 to 7, the overall trend for osteoblast and fibroblast cell growth was upward. As a result of the film layer's dense morphological structure and enough stability to promote cell adhesion, which in turn improved cell proliferation, the film layer displayed excellent fibroblast cell proliferation.

(Kundu, Poole-Warren, Martens, & Kundu, 2012) synthesized the SF/PVA system for macromolecular drugs. 10% w/v PVA was dissolved in DMSO at 80 °C and cooled to 60 °C. 2,6-di-tert-butyl-4-methylphenol, 2-ICEMA, was added, and the reaction was maintained at 60 °C in a N_2 atmosphere for 5 h. Toluene was used to precipitate the PVA solution. After being air dried, the precipitate was redissolved in deionized water and filtered. To create the finished product, freeze-drying is applied to the filtered PVA methacrylate. The final regenerated 6% (w/v) silk solution PVA/SF at ratios of 100/0,

90/10, 80/20, 70/30, 60/40, and 50/50 added 0.1 wt% photoinitiator Irgacure. SF powder was made by extraction with LiBr. UV light at 365 nm was used to polymerize all gels for 15 minutes at a 10 mW/cm^2 intensity. After fabrication, the hydrogels' equilibrium mass swelling ratio is the hydrophilic gel, which is then dissolved in PBS to produce the swollen network structure. The swelling ratio of the PVA hydrogels is 7.89%, whereas that of the co-polymer gels, 60/40 PVA/SF = 17.56%, is noticeably greater. Higher swelling ratios in the gels with more SF and thus wider holes made them weaker and more challenging to handle after swelling. Additionally, SF repels itself in solution by nature because it is a negatively charged molecule. Both of these factors combined account for the increase in swelling ratio as the percentage of SF increases. MTT assay of the HaCaT cells following growth in the SF/PVA hydrogel-based extraction medium. Similar cell growth characteristics could be seen in all of the extract formulations. It was assumed that these hydrogel extracts would be non-toxic as SF and PVA have both been shown to be so.

(Niu et al., 2019) demonstrated the preparation of PVA/SF semi-interpenetrating (semi-IPN) hydrogels using horseradish peroxidase (HRP) and hydrogen peroxide (H_2O_2). Raw silk fibers were treated three times in a 0.05 wt% Na_2CO_3 solution and dissolved in the ternary solvent $CaCl_2$: CH_3CH_2OH : H_2O at a molar ratio of 1:2:8. The combined solution was then dialyzed, centrifuged, and finally freeze-dried. PVA (4–16% w/v) and SF (8% w/v) solutions were combined in equal volumes to create PVA/SF hydrogels. The hydrogen bonds between the hydroxyl groups of PVA and the amide groups of SF are primarily responsible for the intermolecular interactions. When phenolic radicals develop between SF macromers, the precursor hydrogel solutions go through polymerization with HRP and H_2O_2, which are essential for gel formation. SEM images of several hydrogels show that there was no identifiable phase separation and that each sample had a unique three-dimensional porous structure. The porous structure and uniform dispersion of the hydrogels had a connection. The mass loss rate of hydrogel was between 12.63 to 58.45%, but the mass loss rates of PVA/SF hydrogels differed with the PVA/SF mix ratio. With the addition of more PVA/SF, the compressive modulus of the hydrogels decreased from 3.012 to 0.592 kPa. The trend for compression stress at 30% strain was identical. The primary supporting skeleton in this kind of gelation system is fibroin, which is crosslinked by HRP and H_2O_2. As a result, the

amount of fibroin in PVA/SF gels determines their mechanical characteristics. The cytotoxicity of PVA/SF semi-IPN hydrogel was carried out using L929 cells stained with live and dead cells. With the passage of time, each group's cell-normalized vitality marginally declined but remained over 75%. These hydrogel extracts would also be non-toxic because SF and PVA have been demonstrated to be non-toxic and because enzymatic crosslinking does not use toxic substances.

มหาวิทยาลัยเทคโนโลยีสุรนารี

CHAPTER III

RESEARCH METHODOLOGY

3.1 Materials

Raw silk cocoons from the mulberry silkworm *Bombix mori cocoons* were obtained from the Queen Sirikit Department of Sericulture Center, Nakhon Ratchasima, Thailand. Poly (vinyl alcohol) (PVA) (M_w 13,000-23,000, 87-89% hydrolyzed), Glycidyl methacrylate (GMA, 97 %), N,N,N',N'-Tetramethyl-ethylenediamine (TEMED, 99%) and Lithium phenyl(2,4,6- trimethylbenzoyl) phosphinate (LAP) were purchased from Sigma-Aldrich (USA). Anhydrous sodium carbonate (Na_2CO_3) and Ethanol (EtOH) absolute anhydrous were purchased from Carlo Erba Reagenti, Anhydrous calcium chloride ($CaCl_2$) were purchased from ANaPURE. Calcium Nitrate 4-Hydrate ($Ca(NO_3)_2$) was purchased from Kemaus. Dimethylsulfoxide (DMSO) and Acetone were purchased from RCI Labscan Limited. Deuterium Oxide (D_2O, 99.9%) and Dimethyl Sulfoxide-d6 (d, 99.9%) were purchased from Cambridge Isotope Laboratories (DMSO-d_6, Sigma-Aldrich). SnakeSkin dialysis tubing (molecular weight cut-off, 10 kDa) was purchased from Thermo Scientific.

มหาวิทยาลัยเทคโนโลยีสุรนารี

3.2 Experimental

3.2.1 Preparation of glycidyl methacrylate (GMA) grafted onto silk fibroin (SF-g-GMA)

Raw silk cocoons were cut into small pieces and degummed with 1% (w/v) Na_2CO_3 at a weight ratio of 1:50, boiled at 98±2°C for 30 minutes to remove sericin, and then washed with deionized water several times. Subsequently, the degummed silk was dried overnight at 60°C in a hot air oven. 5 g. of degummed silk was dissolved in a mixture of $CaCl_2$:$Ca(NO_3)_2$:H_2O:EtOH (30:5:45:20 weight ratio) in a microwave (Samsung, MS23K3513AW, 800 W.) as shown in Figure 1. GMA was added to the SF

solution in the grafting process, SF/GMA molar ratio of 1/0.070, 1/0.210, 1/0.350, and 1/0.490 were prepared. GMA in SF solution was stirred at 300 rpm at 60±2°C for 1 hour.

The solution was called SF-g-GMA. The SF-g-GMA solutions were then filtrated through a filter paper (20–25) and dialyzed with deionized water using SnakeSkin dialysis tubing with a molecular weight cutoff of 10 kDa for 3 days, and deionized water was replaced every 4 hours to remove salts and non-reactions. After completion of the dialyze, the undissolved impurities were removed by centrifugation at 10,000 rpm at 4°C for 20 minutes to remove silk aggregates as well as debris from the original cocoons. The SF-g-GMA solutions were frozen at -60 °C for 12 h. and freeze-dried at -70°C for 48 h. The freeze-dried SF-g-GMA was stored at room temperature in a desiccator until further use.

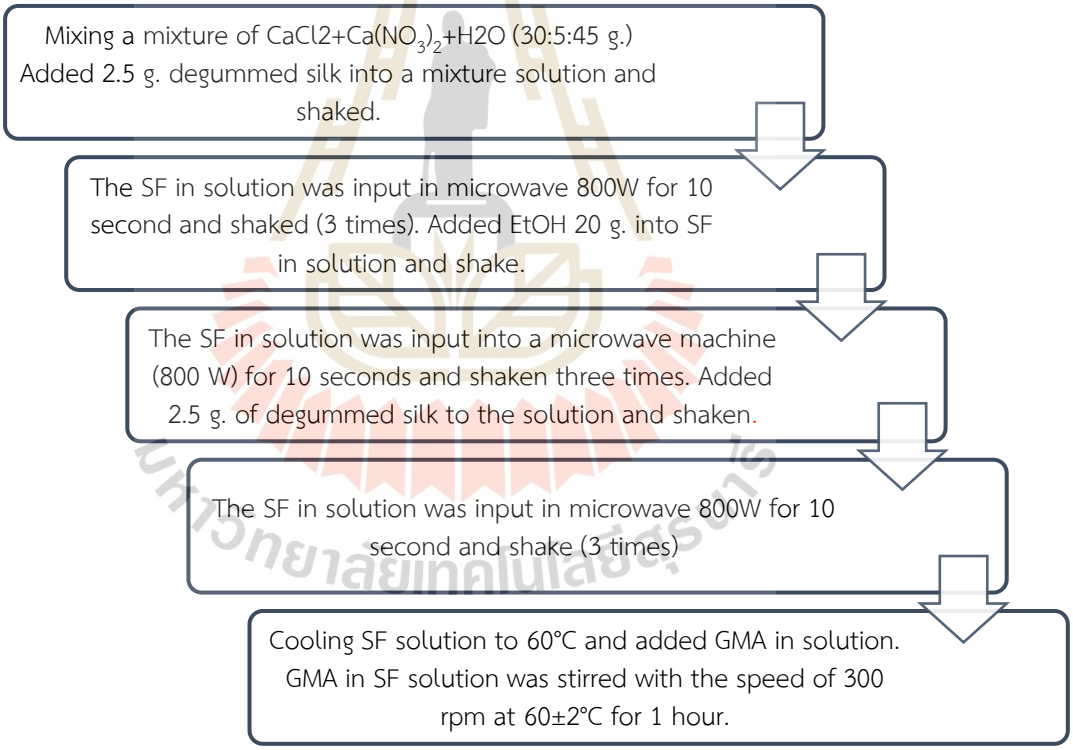

Figure 3.1 Scheme of protocols used to extraction the silk fibroin and GMA grafting onto SF

3.2.2 Preparation of glycidyl methacrylate grafted onto PVA (PVA-g-GMA)

PVA was dissolved in DMSO to obtain a 5% (w/v) solution at 60 °C. As the solution was clear, a definite amount of GMA was added to the PVA solution with

stirring. The PVA-g-GMA solution contained 50, 100, 150, 200, 250, and 300 mM of GMA. 0.17 ml of TEMED was added as a catalyst. The reaction was stirred at 60 °C for 6 hours. The PVA-g-GMA solution was allowed to cool to room temperature and precipitate with an excess of acetone. The precipitate was air dried at room temperature in a fume hood for 24 hours, then dried in a hot air oven at 60 °C for 48 hours, and dried in a vacuum oven at 45 °C for 24 hours.

3.2.3 Characterization for SF-g-GMA and PVA-g-GMA

3.2.3.1 Nuclear Magnetic Resonance (^{1}H-NMR)

The ^{1}H-NMR spectra of PVA, PVA-g-GMA, GMA, SF, and SF-g-GMA were characterized by Nuclear Magnetic Resonance (NMR) (Bruker AVANCE III 500 MHz). The ^{1}H-NMR spectra of PVA, PVA-g-GMA, and GMA were dissolved in 500 μL of dimethyl sulfoxide-d_6 (DMSO-d_6) as the solvent per 7 mg sample. Subsequently, 7 mg of SF-g-GMA, SF, and GMA were dissolved in 500 μL of deuterium oxide (D_2O).

The degree of methacrylate substitution (DS%) of GMA grafted onto PVA was determined with ^{1}H-NMR analysis. It was determined by calculating the relative area of the characteristic peaks of PVA, PVA-g-GMA, and GMA. Its value was examined using an equation. (1) [(Crispim et al., 2006)].

$$DS\% = \frac{(GMA\ (CH_2)/2)}{PVA\ (OH) + (GMA\ (CH_2)/2)} \times 100 \qquad (1).$$

The degree of methacrylate substitution (DM%) of GMA grafted onto SF-g-GMA was determined using the area of the proton peak of the aromatic ring in the tyrosine of SF (= 6.7–7.3 ppm) and the proton peak of the vinyl group in GMA (= 5.9–6.2 ppm), as follows in equation (2) (Bae, Kim, & Park, 2020).

$$DM\% = \frac{(GMA\ (CH_2)/2)}{(Tyrosine/4) \times (\frac{100}{11.11})} \times \frac{100}{mole\%\ of\ reactive\ group} \times 100 \qquad (2).$$

Tyrosine was discovered to contain 11.11 mol% of the amino acids in SF after their composition was analyzed using an amino acid analyzer (Bae et al., 2020).

3.2.3.2 Fourier Transform Infrared Spectroscopy (FTIR)

A Bruker Tensor Fourier-transform infrared spectroscometer (FTIR, Bruker, Billerica, MA, USA) was used to characterize the functional groups of the PVA, SF, GMA, PVA-g-GMA, and SF-g-GMA. The spectra were obtained in the wavenumber range of 4000 and 400 cm^{-1}. At a resolution of 4 cm^{-1}, each run contained 64 background scans and 64 sample scans. Each sample was measured three times, with each run taking place on a different section or side of the same sponge/hydrogel. To eliminate any residue from the previous sample, the ATR diamond crystal (TYPE A225/QL) was cleaned between samples using ethanol.

3.2.3.3 Determination of Molecular weight (MW)

The gel permeation chromatography analysis (GPC) analysis was used to determine the weight average molecular weight (Mw), the number average molecular weight (Mn), and the polymer dispersity index (PDI). SF pure and SF-g-GMA were dissolved in deionized water, and the sample solutions were filtered through a hydrophilic 45-l syringe filter.

Silk fibroin protein electrophoretic mobility was visualized with sodium dodecyl sulfate polyacrylamide gel electrophoresis (SDS-PAGE) and a 13% gradient gel for electrophoresis (Bio-Rad, Mini-PROTEAN® Tetra Cell). A molecular marker of 5-250 kDa (Precision Plus Potein Dual Xtra Standard) was used to determine molecular weight (MW). The SF freeze-dried was dissolved in ultrapure deionized water and mixed with an equivalent amount of loading buffer (created by 4X Solubilizing Buffer (SB) and 2-Mercaptoethanol) and boiled for 5 min. Electrophoresis was performed for about 1 h. with an electric current of 150 V. After electrophoresis, the gel was immersed in 0.1% Coomassie Brilliant Blue R-250 staining solution for 30–60 min, washed with destaining solution for 1 h. and washed with deionized water for 1 h.

3.2.4 Preparation of PVA-g-GMA/SF-g-GMA injectable hydrogel

The 100 mM PVA-g-GMA was dissolved in 10% v/v DMSO in deionized water to obtain a 10% (w/v) solution and stirred at 60 °C until a homogenous solution

was obtained. The 490 mM SF-g-GMA was dissolved in deionized water at 50% w/v at room temperature. The mixture solutions of PVA-g-GMA and SF-g-GMA were thoroughly mixed at different ratios of PVA-g-GMA to SF-g-GMA: 100/0, 75/25, 50/50, 25/75, and 0/100 (w/w), followed by the addition of 0.3% (w/v) LAP. All gels were polymerized with UV light (365 nm) for 10 minutes at an intensity of 6 mW/cm^2. The molds were used to create a 96-well plate with a well diameter of 6.72 mm.

3.2.5 Characterization for PVA-g-GMA/SF-g-GMA injectable hydrogel

3.2.5.1 Gel fraction and Swelling ratio

Gel fraction can be assumed to be the degree of crosslinking. The PVA-g-GMA hydrogels were dried in a hot air oven at 40°C for 24 h. to a constant weight and weighed (W_o). The PVA-g-GMA hydrogels were immersed in deionized water for 24 h at 37 °C, then dried in a hot air oven at 40°C for 24 h to a constant weight and weighed (W_f). The gel fraction was calculated according to the following equation: (3)

$$\text{Gel fraction} = \frac{Wf}{Wo} \times 100 \qquad (3)$$

The PVA-g-GMA hydrogels were dried in a hot air oven to a constant weight at 40°C for 24 h. After that, it was immersed in deionized water at 37°C for 24 h. and weighed (Wd). The PVA-g-GMA hydrogels were dried in a hot air oven to a constant weight at 40°C for 24 h. and weighed (W0). The swelling ratio was calculated according to the following equation: (4)

$$\text{Swelling ratio} = \frac{Ws - Wo}{Wo} \times 100 \qquad (4).$$

3.2.5.2 Compression test

The PVA-g-GMA solutions were injected into a 96-well plate (6.72 mm in diameter and 2 mm in thickness) and crosslinked by UV light. then immersed in PBS overnight. The compression test of the PVA-g-GMA hydrogels was performed using a TA-XT plus texture analyzer (Stable Micro Systems, TA.XT plus C, UK) in compression mode with a load cell of 1 kg. The PVA-g-GMA hydrogels were

compressed at a constant rate of 5 mm/min. Three samples were tested for each group.

3.2.5.3 Rheological and viscosity measurements

The dynamic oscillatory rheology was performed on an MCR52 rheometer (Anton Paar MCR52, Austria) at 25 °C. The solution samples (PVA-g-GMA, SF-g-GMA, and PVA-g-GMA/SF-g-GMA) and the hydrogel samples (PVA-g-GMA/SF-g-GMA ratio at 100/0, 75/25, 50/50, 25/75, and 0/100) were characterized using conical plate geometry (50 mm diameter and 1-degree cone angle) with frequency sweeps from 0.1 to 100 s^{-1} and shear rate of 5%.

3.2.5.4 Morphological structure measurement

The PVA-g-GMA/SF-g-GMA biphasic injectable hydrogels were frozen at -60 °C for 12 h. and then freeze-dried at -70°C for 48 h. The cross-sectional morphologies of the freeze-dried PVA-g-GMA/SF-g-GMA biphasic injectable hydrogels were examined using a Field Emission Scanning Electron Microscope (FESEM; Carl Zeiss, Auriga, Oberkochen, Germany) at an operating voltage of 3 keV. Segments of cross-sectional surfaces were prepared by the slicing method and then sputtered with gold before FESEM measurements. The pore sizes were determined by measuring 100 random pores from FESEM images of the same sample using ImageJ software. (Wayne Rasband NIH, Washington DC, USA).

3.2.5.5 In vitro degradation

The biphasic injectable hydrogel with dimensions of 8 mm in diameter and 2 mm in thickness (n = 3) was dried in a hot air oven at 40 °C for 24 h. After that, biphasic injectable hydrogels were immersed in phosphate buffered saline (PBS, pH = 7.4) and incubated at 37 °C for 1, 2, 3, 4, 8, 12, 16, 20, and 24 weeks. The PBS solution was exchanged with freshly prepared solution every 3 days. The biphasic injectable hydrogels were washed with deionized water, dried, and weighed. The degradation rate was calculated by Equation (5) (Promnil, Ruksakulpiwat, Numpaisal, & Ruksakulpiwat, 2022):

$$\% \text{ Residual weight} = 100 - [(\frac{W_i - W_f}{W_i}) \times 100] \quad (5)$$

Where W_i is the initial dry weight of the sample, while W_f is the weight of the sample after immersing it in PBS.

3.2.5.6 Cell viability and Live/Dead cell in 3D cell culture

Human chondrocyte cell lines (CSPCs) at 5 x 10^5 cells/ml were centrifuged in medium. PVA-g-GMA/SF-g-GMA solutions (LAP 0.3% w/v) were prepared at a ratio of 100:0, 75:25, 50:50, 25:75, and 0:100. Cells were added in a different solution ratio of PVA-g-GMA/SF-g-GMA to a density of 5 x 10^5 cells/ml. 30 μL were injected into a 96-well plate, UV photocrosslinking was performed on the hydrogel for 10 min, and 100 μL of fresh medium were added. The cell culture was incubated for 1, 3, and 7 days in 37 °C with a 5% CO_2 humidified incubator.; the medium was exchanged every 3 days. The cell viability and live/dead cells in a biphasic injectable hydrogel were measured by a Live/Dead assay kit (Calcein AM, 7-AAD, ab270789) Live cell-Calcein-AM (Cat.206700) , Dead cell-Ethidium homodimer (ab145323) under a confocal microscope (Nikon ECLIPSE Ti). A green fluorescence signaled the presence of living cells, whereas a red fluorescence signaled the presence of dead cells. After 1, 3, and 7 days, cells were stained with live/dead cell stain and incubated for 10 min in a dark room at 37°C. Cell morphology was investigated by the confocal microscope. The cell viability was calculated as the survival rate of cells in the encapsulated biphasic injectable hydrogel by counting with ImageJ software.

3.2.5.7 Quantitative analysis for gene expression

A 20 μL biphasic solution composed of PVA-g-GMA/SF-g-GMA solutions and cells at a density of 5 x 105 cells/mL were injected into a 96-well plate, and the biphasic injectable hydrogel was fabricated by UV photocrosslinking for 10 min. A biphasic injectable hydrogel was cultured at 7, 14, and 28 days. The total RNA was extracted from the HCPCs in a biphasic injectable hydrogel with TRIzol reagent and the RNeasy mini kit (Qiagen, Hilden, Germany). Quantitative real-time polymerase chain reaction (qRT-PCR) was complete with Fluorescein Kit (BIOLINE, London, UK) and

the SYBR Green kit (Thermo Fisher Scientific, Waltham, MA, USA). The primer sequences for the qRT-PCR test are listed in Table

Table 3.1 Sequences of primer sets for RT-qPCR ((Numpaisal et al., 2017))

Gene		Primer sequence (5' to 3')
Type I collagen (COL1A1)	Sense	GGA GGA GAG TCA GGA AGG
	Antisense	GCA ACA CAG TTA CAC AAG G
Type II collagen (COL2A1)	Sense	GGC AGA GGT ATA ATG ATA AG
	Antisense	ATG TCG TCG CAG AGG
Aggrecan (ACAN)	Sense	ATA CCG TCG TAG TTC C
	Antisense	TCC TTG TCT CCA TAG C

3.2.5.8 Statistical analysis

For each the experiments were repeated three times with each specimen. Data were reported as mean ± standard deviation (SD.). The data were analyzes using one-way analysis of variance (ANOVA) and Tukey test was used to determine statistically significant difference with Minitab® 19 software (version 19.1.1). The level of significance was set of 95% (p = 0.05)

มหาวิทยาลัยเทคโนโลยีสุรนารี

CHAPTER IV

RESULTS AND DISCUSSION

4.1 Weight average molecular weight (Mw) of SF unmodified and SF-g-GMA

The molecular weight was determined by SDS-PAGE; weight average molecular weight (Mw), number average molecular weight (Mn), and polymer dispersion index (PDI) were used by GPC. Results are shown in Figures 4.1-4.2, and Table 4.1. The MW of SF-g-GMA was measured by SDS-page and GPC at various times during GMA grafting at 1, 2, and 3 h. According to the original silk fibroin molecule characterized by SDS-PAGE, that was degraded into a variety of polypeptides of various sizes, which were then extracted using a salt solution.

Natural SF in *B. mori cocoon* is a mainly molecular complex composed of heavy chain (H-chain), light chain (L-chain), and glycoprotein P25 proteins of 350 kDa, 26 kDa, and 30 kDa molecular weights, respectively (Um, Kweon, Lee, & Park, 2003). The average MW of SF-g-GMA at various times during GMA grafting at 1, 2, and 3 h shows no difference in a weight molecular, that shows a smear band at heavy chains of about more than 250 kDa and two proteins with smaller molecular masses: the light chains of about 25 kDa and the smear band at roughly 30 kDa glycoprotein P25.

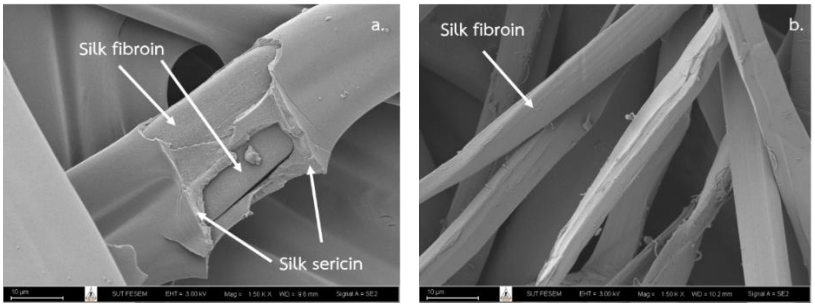

Figure 4.1 (a.) Raw silk cocoon consist of silk fibroin and silk sericin and (b.) silk fibroin degummed by Na_2CO_3 solution

Table 4.1 shows the weight average molecular weight (Mw), number average molecular weight (Mn), and polymerdispersity index (PDI) of SF unmodified and SF-g-GMA at various grafting times at 1, 2, and 3 h. by gel permeation chromatography (GPC). A comparison of grafting times showed the Mw, Mn, and PDI of SF-g-GMA at the same SF concentration. The Mw and Mn decrease with the increasing time of grafting GMA into PVA, from 1 to 3 h. Due to the degradation or denature of amino chains, the use of temperature and long periods of time shortened the amino chains (Zengkai Wang et al., 2020). As grafting time increased, molecular weight distribution changed along with the drop in Mw. The PDI slightly increased, showing that the molecular weight distribution broadened a little bit throughout the course of the grafting process. This could be attributed to an increase in the number of smaller MW chains (Kavda, Micheluz, Elsasser, & Pamplona, 2021).

Therefore, the low molecular weight and thus the optimal 1 h. grafting condition are used to graft GMA onto silk fibroin chains.

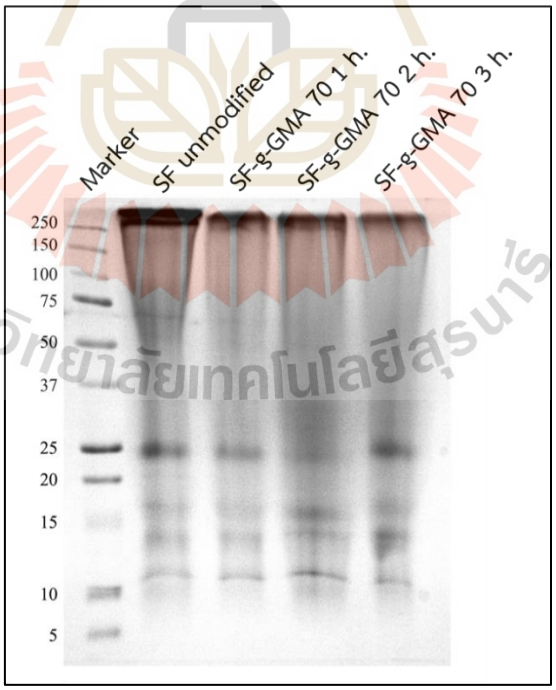

Figure 4.2 SDS-page analysis of SF-g-GMA prepared with time various at 1, 2, and 3 h.

Table 4.1 Weight average molecular weight (Mw), number average molecular weight (Mn), and polymer dispersion index (PDI) of SF unmodified and SF-g-GMA at various grafting times.

Sample	Mn	Mw	PDI
SF unmodified	359,610	444,592	1.24
SF-g-GMA 1h.	201,895	396,517	1.96
SF-g-GMA 2h.	113,664	352,535	3.10
SF-g-GMA 3h.	106,240	342,854	3.23

4.2 Effect of the grafting conditions of GMA onto PVA (PVA-g-GMA) and SF (SF-g-GMA)

4.2.1 ^{1}H-NMR characteristic of PVA-g-GMA and SF-g-GMA

^{1}H-NMR technique was used for determining the amount of methacrylate groups in PVA-g-GMA as well as for identifying the reaction mechanism of transesterification and epoxy ring open are report in Figure 4.3, 4.4, 4.5. The ^{1}H-NMR spectra of unmodified PVA, GMA monomer, and PVA-g-GMA 100 mM are presented in Figure 4.3. The solvents of DMSO-d_6 present in the polymer structures gave sharp peaks at chemical shifts (δ) of 3.3 ppm. In the spectrum of unmodified PVA, the characteristic proton peaks of (CH_2-CH-O**H**) were at δ =4.3-4.7 ppm (H2), (CH_2-C**H**-OH) at δ =3.7-4.0 ppm (H3) and (C**H$_2$**-CH-OH) at δ = 1.4 ppm (H5). In the spectrum of GMA monomer, the characteristic proton peaks of (-C=C**H$_2$**) at δ = 6.1, 5.8 ppm (H1), (-C**H$_2$**-CH-) at δ = 4.1, 4.5 ppm (H2), (-CH_2-C**H**-) at δ = 3.2 ppm (H3), (-O-C**H$_2$**) at δ = 2.7, 2.8 ppm (H4), and (-C-C**H$_3$**) at δ = 1.9 ppm (H5) (Shah et al., 2015). In the spectrum of PVA-g-GMA, in addition to the peaks of unmodified PVA, new peaks appeared belonging to the protons of the vinyl group (-C=C**H$_2$**), which appeared at δ = 5.6 and 6.0 ppm (H1) and were attributed to the distinctive double bond of the methacrylate group, proving the methacrylate group was effectively grafted onto the pendant hydroxyl groups of unmodified PVA, the CH group of GMA (-C**H**- of O- methacrylate group) at δ =5.2 ppm

(H2) and the methyl group (C**H**$_3$-C=C) of GMA unit appeared at δ =1.9 ppm (H6) (Crispim et al., 2006) (Erdoğan, Akdemir, Hamitbeyli, & Karakışla, 2019). In addition, without the peak (-C**H**$_2$-CH-) at δ = 4.1, 4.5 ppm (H2) and (-CH$_2$-C**H**-) at δ = 3.2 ppm (H3), the epoxy ring made by GMA It is obvious that the way GMA and PVA interacted was through transesterification and epoxy ring opening.

The ^{1}H-NMR spectra of unmodified PVA, GMA monomer, and PVA-g-GMA various GMA contents at 50, 100, 150, 200, 250, and 300 mM are shown in Figure 4.6. The results obtained showed that as the amount of GMA was increased throughout the chemical modification process, the intensity of vinyl group at δ = 5.6 and 6.0 ppm (H1) increased as well. Meanwhile, the intensity of PVA decreases with the amount of GMA was increased due to GMA molecule is reactions onto the OH (CH$_2$-CH-O**H**) at δ =3.7-4.0 ppm (H4) of PVA structure occurs by way of the transesterification and epoxy ring opening mechanism.

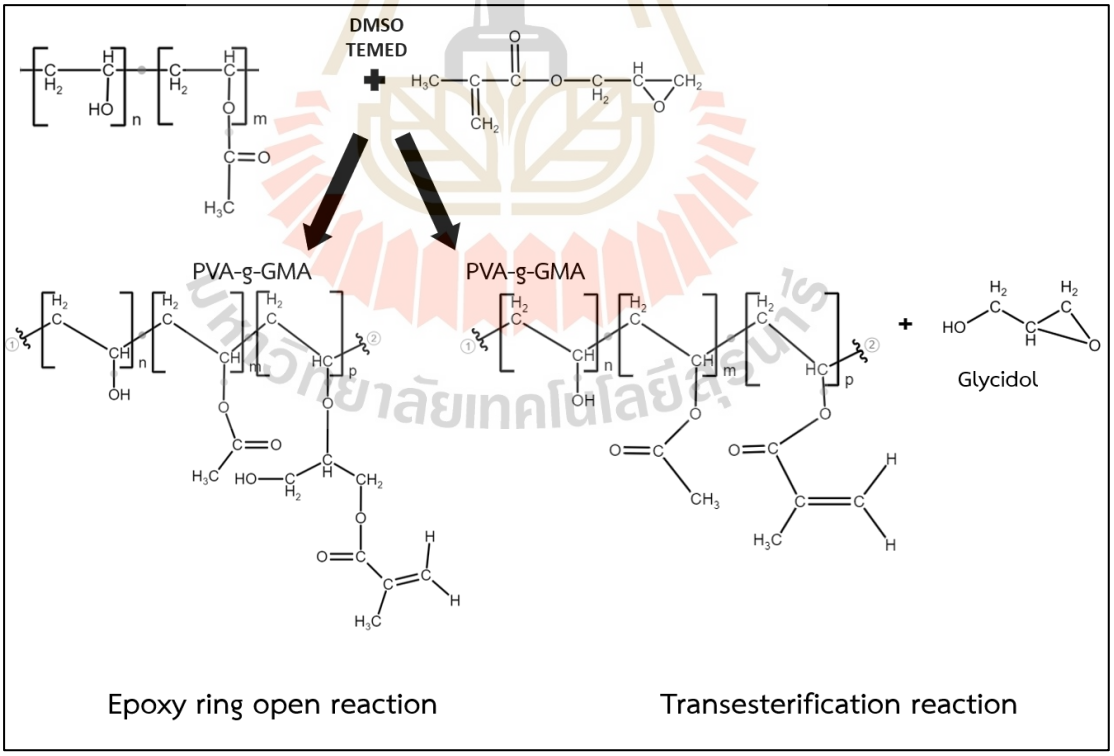

Figure 4.3 Purpose of a mechanism for GMA grafting onto PVA: (1) by epoxy ring opening; (2) by transesterification

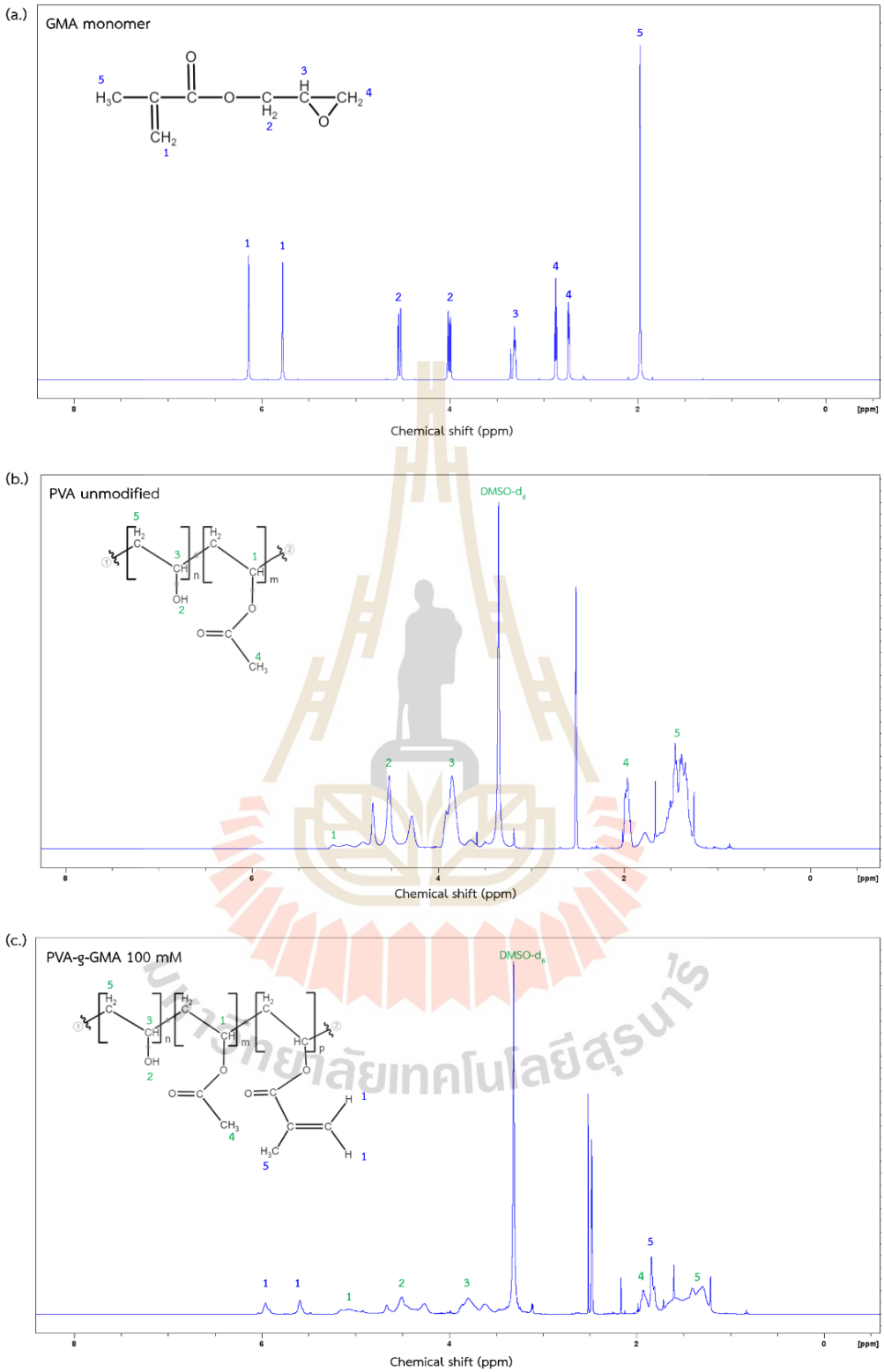

Figure 4.4 The ^{1}H-NMR spectra and molecular structure of (a.) GMA monomer, (b.) PVA unmodified, and (c.) PVA-g-GMA 100 mM

The GMA functional group percentage, or degree of substitution methacrylate, DS% of the PVA-g-GMA are show in Table 4.2 was also calculated with Eq.1. The DS% of PVA-g-GMA an increased from 5.78% to 26.67%, respectively, when GMA concentration increased from 50 mM to 300 mM, as shown by a decrease in the hydroxyl group (Table 4.2).

Table 4.2 Degree of methacrylate substitution, DS% of the PVA-g-GMA

Condition	GMA (CH_2)	PVA (OH)	Degree of substitution (%DS)
PVA-g-GMA 50 mM	0.1225	2.0277	5.78
PVA-g-GMA 100 mM	0.2395	1.7476	12.06
PVA-g-GMA 150 mM	0.2918	1.4790	16.77
PVA-g-GMA 200 mM	0.2326	0.9886	19.34
PVA-g-GMA 250 mM	0.2615	0.8622	23.82
PVA-g-GMA 300 mM	0.4438	1.2650	26.67

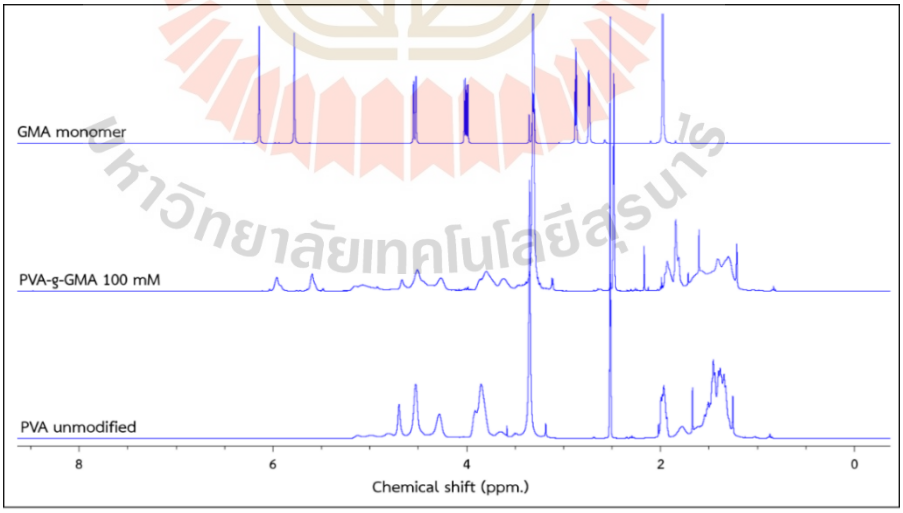

Figure 4.5 Comparison the ^{1}H-NMR spectra of GMA monomer, PVA unmodified and PVA-g-GMA 100 mM

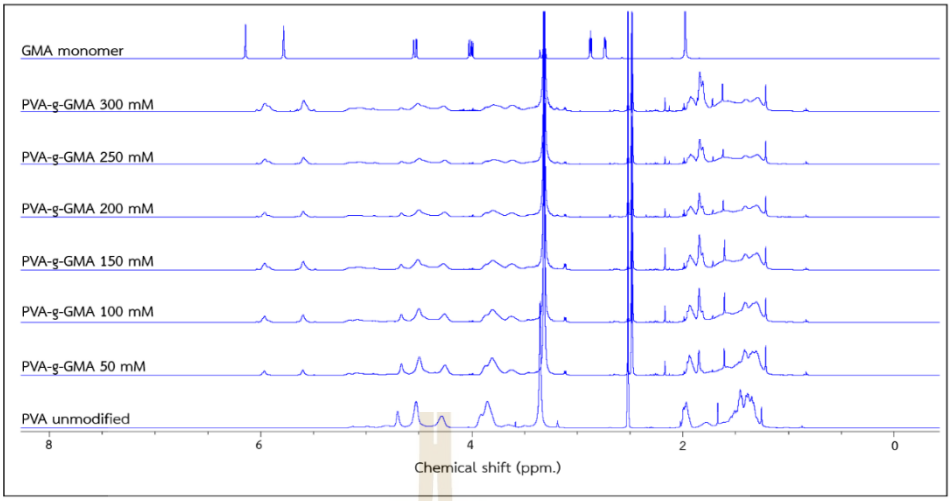

Figure 4.6 The ^{1}H-NMR spectra of GMA monomer, PVA unmodified and PVA-g-GMA various GMA contents at 50, 100, 150, 200, 250, and 300 mM

The GMA modified SF to increase water solubility and determined the optimal %DM to improve water solubility without losing the properties of SF. In the SF-g-GMA synthesis, the amount of GMA added to the SF solution varied from 70 mM to 490 mM, and hence GMA was able to react with amino groups (-NH_2), hydroxyl groups (-OH), and carboxylic groups (-COOH). The SF-g-GMA was synthesized by the ring-open epoxy group at GMA (Figure 4.7). The SF side chain was modified by GMA to increase water soluble, and the ^{1}H-NMR spectra of the GMA monomer, SF unmodified, and SF-g-GMA are shown in Figure 4.8, 4.9. The solvent of deuterium oxide (D_2O) shows a peak at δ = 4.7 ppm. From the ^{1}H-NMR spectrum of SF unmodified, the characteristic proton peak of the aromatic ring in the tyrosine is at δ = 6.7–7.3 ppm (H1), and the lysine methylene is at δ = 2.65-3.05 ppm. In addition, the spectra of SF-g-GMA showed a gentle decrease of the aromatic ring in the tyrosine. Specifically, the new peaks showed that the characteristic resonance of the methacrylate vinyl group at δ = 5.6-5.8 and 6.0-6.2 ppm (H1) has been created by the inclusion of the GMA, and the integration of these peaks grew as more GMA was added, and the degree of methacrylate substitution (DM%) of GMA grafted onto SF-g-GMA increased with increasing GMA content. Tyrosine is an amino acid that has reactive groups that GMA may modify, and it makes up roughly 11.11 mol% of all amino acids (Bae et al., 2020).

As the GMA content increased from 70 to 490 mM, the %DM of SF-GMA increased from 1.86 to 9.92 (Table 4.3). The greatest %DM was found in SF-g-GMA 490 mM (%DM, 9.92 %), maybe as a result of the side reactions that the excessive addition of GMA generated between the GMA molecules.

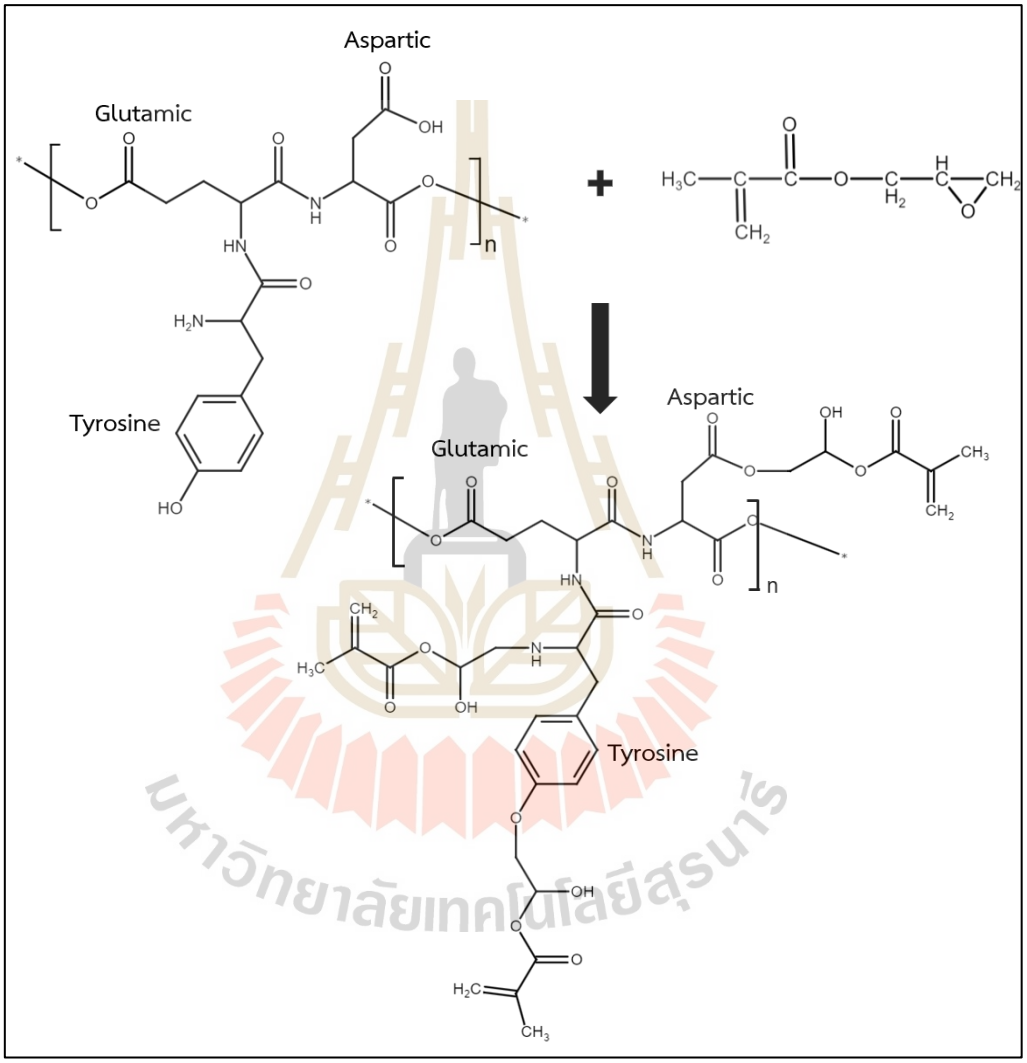

Figure 4.7 Purpose of a mechanism for GMA grafting onto SF by epoxy ring opening

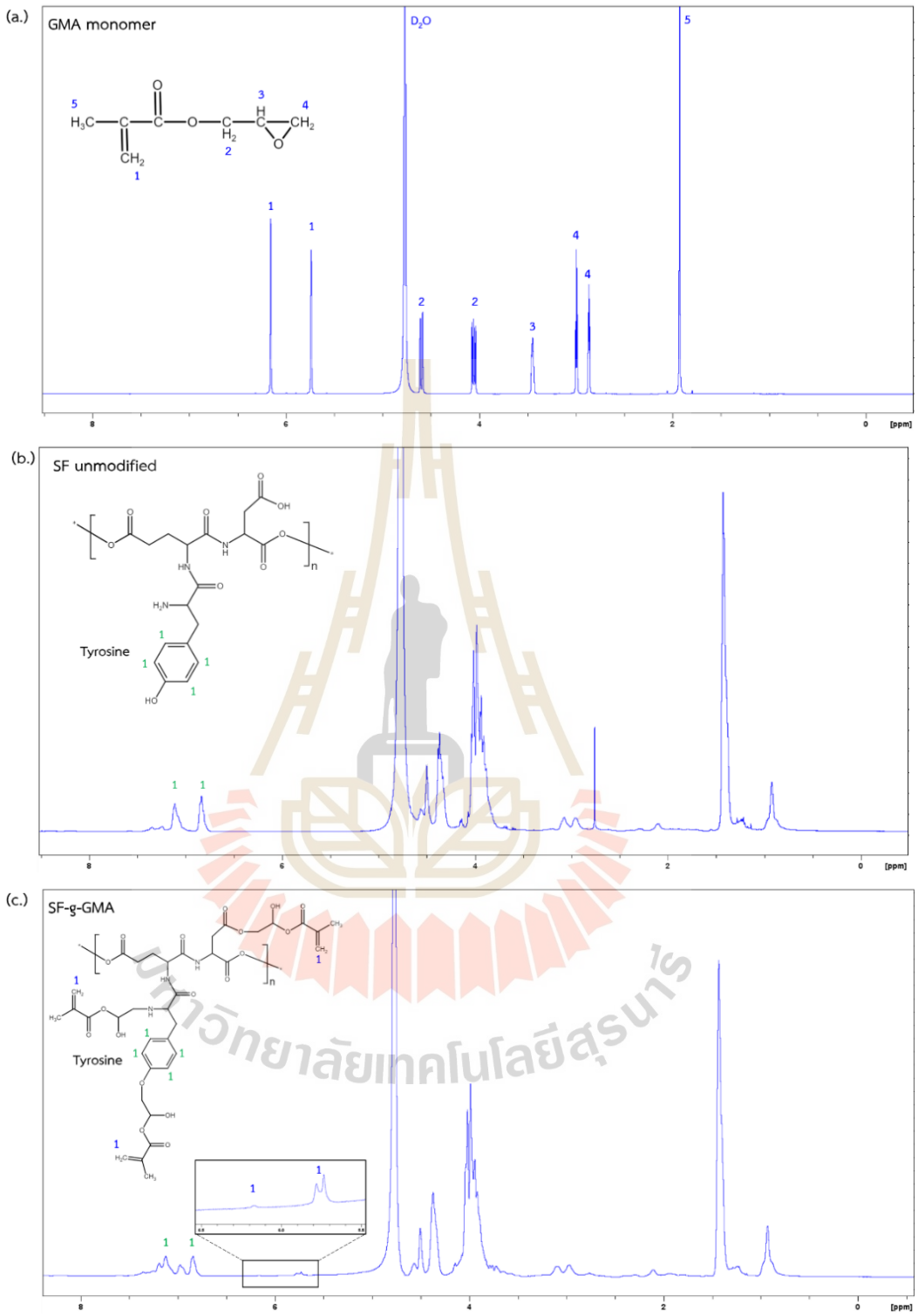

Figure 4.8 The ^{1}H-NMR spectra and molecular structure of (a.) GMA monomer, (b.) SF unmodified, and (c.) SF-g-GMA 490 mM

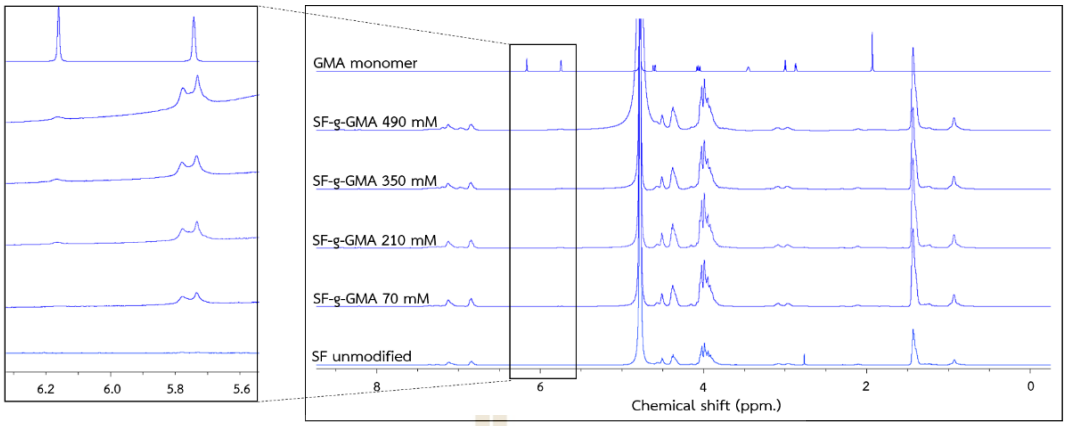

Figure 4.9 The ^{1}H-NMR spectra of GMA monomer, SF unmodified and SF-g-
various contents at 70, 210, 350, and 490 mM

Table 4.3 Degree of methacrylate substitution, DM% of the SF-g-GMA

Condition	GMA (CH_2)	Tyrosine	Degree of methacrylate (%DS)
SF-g-GMA 70 mM	0.0130	0.6817	1.86
SF-g-GMA 210 mM	0.0325	0.6771	4.57
SF-g-GMA 350 mM	0.0400	0.6789	5.56
SF-g-GMA 490 mM	0.0629	0.5710	9.92

4.2.2 FTIR characteristic of PVA-g-GMA and SF-g-GMA

The Fourier-transform infrared spectroscopy (FTIR) of PVA unmodified, GMA monomer, and PVA-g-GMA 100 mM are shown in Figure 4.10. The FTIR spectra of unmodified PVA showed transmittance bands at 842, 1089, 1567, 1731, 2940, 2910, and 3298 cm^{-1}, which corresponded to the characteristic vibrations of =C-H stretching, C-O stretching, C=C stretching, C=O (ester group), CH_2 symmetric stretching, C-H stretching, and O-H stretching, respectively (Xiang et al., 2022) (Erdoğan et al., 2019). GMA monomer showed a peak at 1255 cm^{-1} breathing, 908 cm^{-1} asymmetric deformation, and 843 cm^{-1} symmetrical deformation, which was the characteristic vibration of epoxy groups. A strong peak at 1717 cm^{-1} was attributed to the carbonyl group (C=O), a C=C peak at 1636 cm^{-1} and a strong peak at 1159 cm^{-1} was attributed

to the C-O stretching of the ester group (Erdoğan et al., 2019). The distinctive bands of PVA and GMA on PVA-g-GMA, such as the bending of C=O at 1710 cm^{-1} and C=C at 1634 cm^{-1}, out-of-plan bending vibration of $R_2C=CH_2$ at 949 cm^{-1}, and the stretching vibration of the C-O group at 1175 cm^{-1}, could be found in the spectra of PVA-g-GMA. In addition, without the bands at 1255 cm^{-1} (for breathing), 908 cm^{-1} (for asymmetric deformation), and 843 cm^{-1} (for symmetrical deformation), the epoxy ring of GMA clearly implies that transesterification was the mechanism via which GMA and PVA reacted (S. H. Kim et al., 2018).

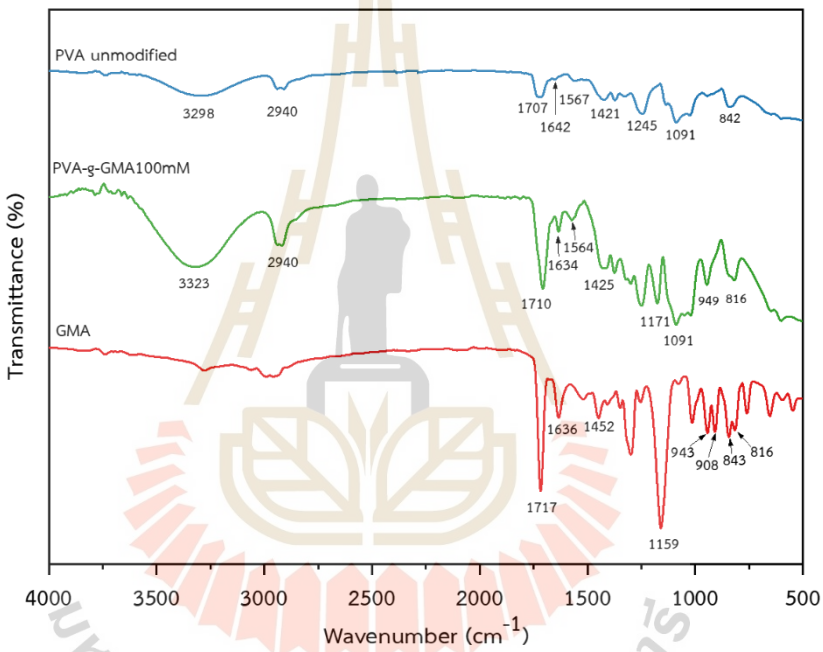

Figure 4.10 Comparison of the FTIR spectra of GMA monomer, PVA-g-GMA 100 mM, and PVA unmodified

The FTIR spectra of PVA-g-GMA synthesized using various GMA contents at 50, 100, 150, 200, 250, and 300 mM are shown in Figure 4.11. The results pointed out that the intensity of these bands was raised by the increasing amount of GMA during the chemical modification process. These can be verified by the increase in the intensity of the FTIR spectra of C-O, C=O, and C=C at 1175 cm^{-1}, 1634 cm^{-1}, and 1710 cm^{-1}, respectively.

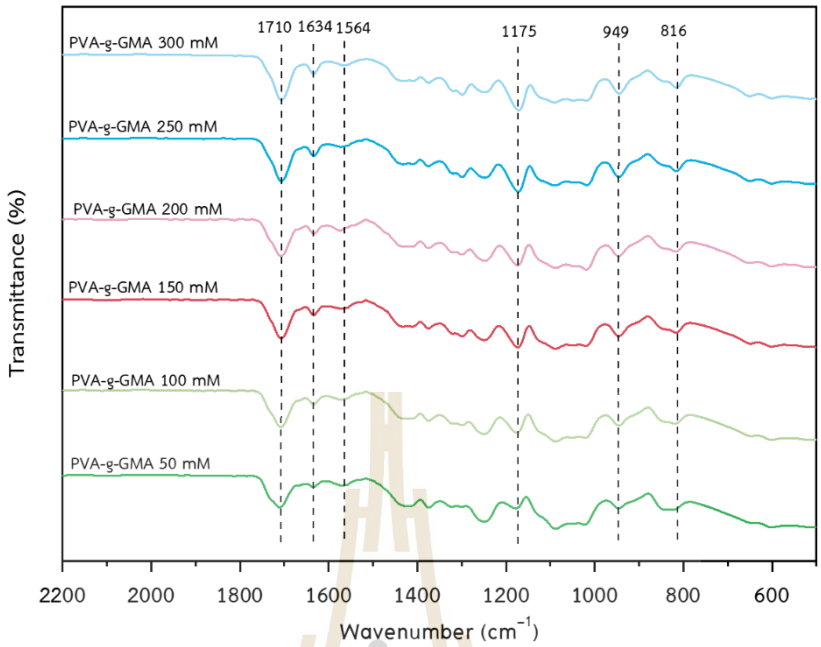

Figure 4.11 PVA-g-GMA 100 mM, and PVA unmodified (A), the FTIR spectra of GMA grafting contents at 50, 100, 150, 200, 250, and 300 mM on PVA

Figure 4.12 shows the FTIR spectra of GMA, SF unmodified, and SF-g-GMA at various GMA contents. The silk fibroin protein has been the most important FTIR spectra region in the amide band, with peaks of 1700–1600 cm^{-1} attributed to the C=O stretching of Amide I, 1600–1500 cm^{-1} attributed to the N-H bending of Amide II, and 1400–1200 cm^{-1} attributed to the C-N stretching of Amide III. There are two types of SF molecular structures: Silk I, consisting of random coil and helix peaks at wavenumber positions 1648–1554 cm^{-1} (amide I) and 1535–1542 cm^{-1}, Silk II, consisting of sheet peaks at wavenumber positions 1610–1630 cm^{-1} (amide I) and 1510–1520 cm^{-1} (amide II). In the spectrum of SF unmodified, it can be seen that the peaks at 1638 cm^{-1} (Amide I), 1517 cm^{-1} (Amide II), and 1234 cm^{-1} (Amide III) were observed and are correlated to the random coil, β-sheet, and ω -helix, respectively. In terms of SF-g-GMA, various GMA contents at 70, 210, 350, and 490 mM demonstrate transmittance bands at 1642 cm^{-1} (Amide I) with the indicated random coil and the bands shifted to 1638 cm^{-1} compared with the SF unmodified; the wavenumber at 1514 cm^{-1} (Amide II) was assigned to β -sheet, and the wavenumber at 1234 cm^{-1} (Amide III) was assigned

to ω-helix, respectively. The small peaks ascertained on SF-g-GMA at 949 and 1168 cm^{-1} were assigned to $R_2C=CH_2$ wagging stretching of the vinyl methacrylate group in the GMA.

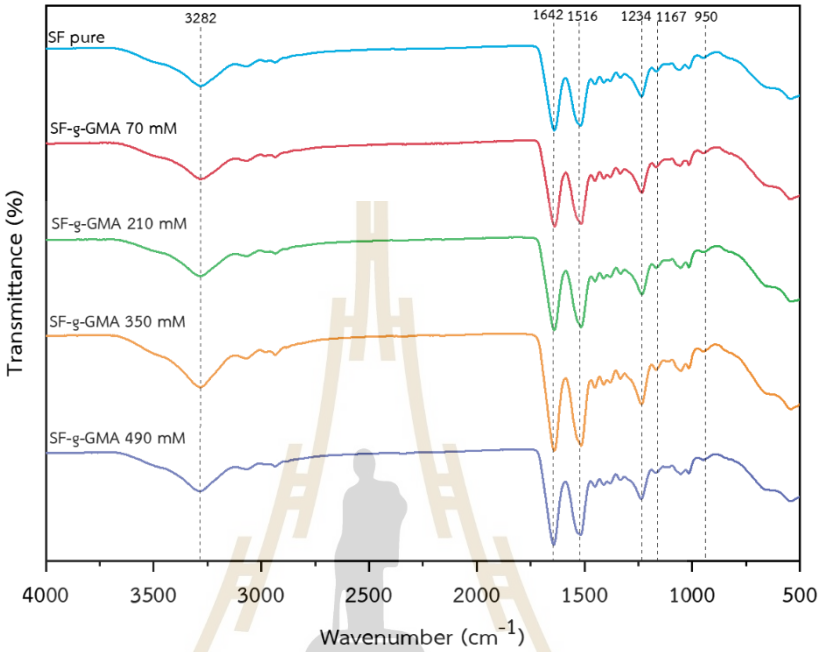

Figure 4.12 The FTIR spectra of SF unmodified, GMA various contents at 70, 210, 350, and 490 mM on SF.

4.3 Effect of PVA-g-GMA/SF-g-GMA ratio on physical properties and mechanical properties of injectable hydrogel

4.3.1 Gel fraction and swelling ratio of injectable hydrogel

Gel fraction was used to determine the insoluble parts of PVA-g-GMA, SF-g-GMA, and PVA-g-GMA/SF-g-GMA injectable hydrogels after immersion in deionized water at 37 °C for 24 h, and the percentage of gel fraction is shown in Figure 4.13. The gel fraction measures the amount of crosslinking created in the hydrogel polymer network. Gel fractions and swelling ratio of PVA-g-GMA injectable hydrogel at various irradiation times at 1, 3, 5, 7, and 10 min are shown in Figure 4.13(a-b). It demonstrated that, the irradiation time not impact to gel fractions and swelling ratio of PVA-g-GMA injectable hydrogel.

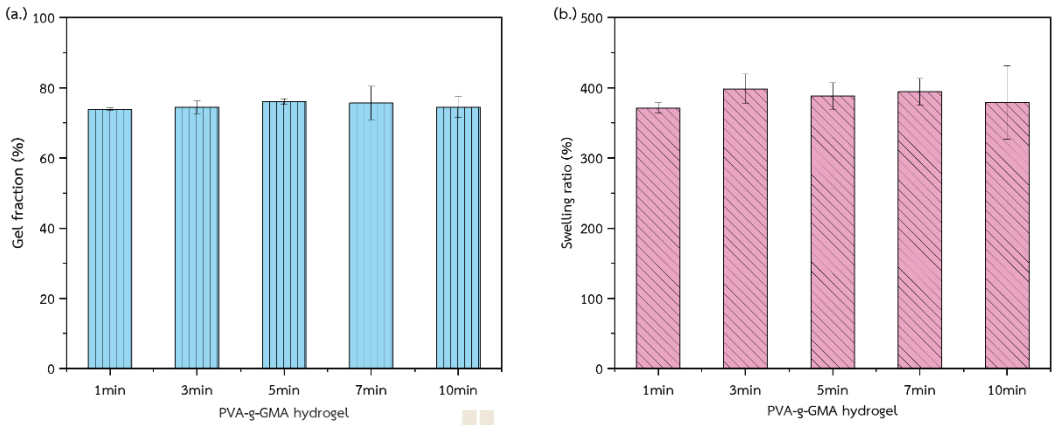

Figure 4.13 (a.) Gel fraction and (b.) swelling ratio of PVA-g-GMA at various irradiation times

The effect of SF-g-GMA concentration on gel fractions and swelling ratio of SF-g-GMA injectable hydrogel, as shown in Figure 4.14(a-b), indicates that the SF-g-GMA concentration at 30% w/v is insufficient to fabricate an injectable hydrogel. The SF-g-GMA concentration increased from 40% w/v to 60% w/v. The percentage of gel fraction slightly increased; however, the swelling ratio evidently decreased. The compressive modulus and the compressive strength increased with increasing SF-g-GMA concentration. We expect that the improved mechanical properties could be associated with physical entanglement of silk fibroin molecules, in addition to the chemical methacrylation of the silk fibroin. The stimuli from this physicochemical entanglement between SF-g-GMA molecules could promote secondary crystalline conformation (β-sheet) more likely, generating added strength and new hydrophobic regions within the Silk fibroin (S. H. Kim et al., 2018).

Moreover, the gel fractions and swelling ratios of PVA-g-GMA/SF-g-GMA injectable hydrogels at different contents. As shown in Figure 4.15 (a-b), the PVA-g-GMA/SF-g-GMA injectable hydrogel at ratios of 100:0, 75:25, 50:50, and 25:75 shows no difference in gel fraction. However, the PVA-g-GMA/SF-g-GMA injectable hydrogel at ratios of 0:100 showed the gel fraction highest (97.60%) than in other condition due to the high crosslink density in the silk fibroin structure from the grafting process. In addition, the swelling ratio decreased from 322.33% to 59.85% with an increasing SF-g-GMA content from 0 to 100% w/w because of the increasing crosslink density in PVA-

g-GMA/SF-g-GMA injectable hydrogel. This outcome showed that a structure with a high crosslink density might support a low amount of water inside a gel structure (Nasution et al., 2022).

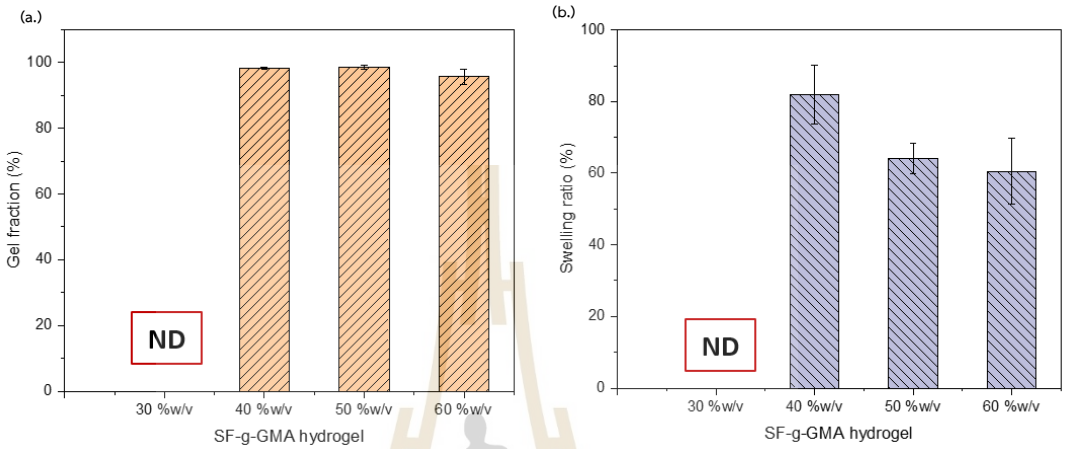

Figure 4.14 (a.) Gel fraction and (b.) swelling ratio of SF-g-GMA at various SF-g-GMA concentration.

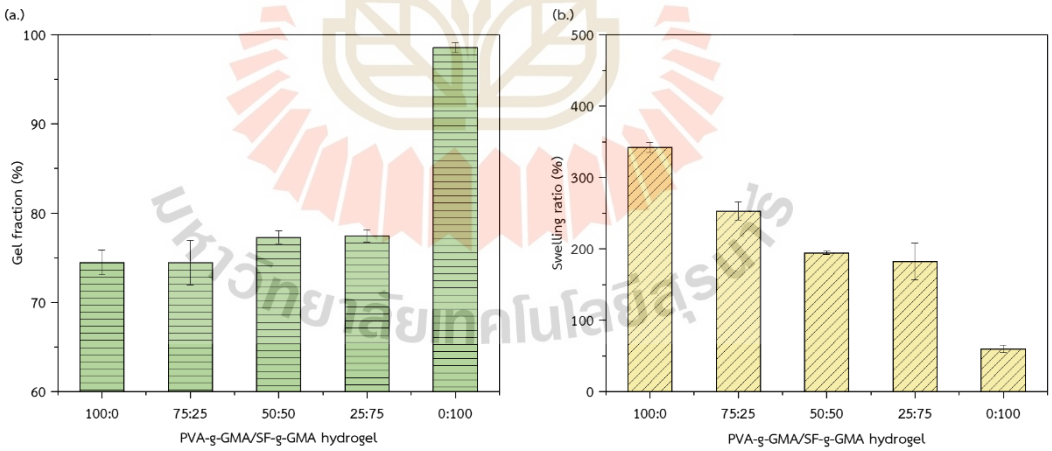

Figure 4.15 (a.) Gel fraction and (b.) swelling ratio of PVA-g-GMA/SF-g-GMA injectable hydrogel at 10 min by photocrosslinked

4.3.2 The FTIR spectra of PVA-g-GMA/SF-g-GMA injectable hydrogel

The FTIR spectra of the different patches were investigated, as shown in Figure 4.16. The main characteristic peaks of PVA-g-GMA were observed at 2915 cm^{-1}, 1725 cm^{-1}, 1660 cm^{-1} corresponding to CH_2 (stretching vibration), C=O (stretching vibration), (C=C), respectively. An intense hydroxyl (OH) band observed at 3000–3600 cm^{-1} and a band peak at 3370 cm^{-1} were attributed to hydrogen bonds. Furthermore, 1246 cm^{-1} corresponds to -C-O-C- stretching, with peaks at 1092 cm^{-1} attributed to CO stretching and OH bending, 947 cm^{-1} attributed to bending $-CH_2$, and 838 cm^{-1} attributed to -CH rock. The main characteristic absorption bands of SF-g-GMA are 1641 cm^{-1} (for amide I, C-O stretching), 1514 cm-1 (for amide II, secondary N-H bonding, due to the β-sheet structure), 1232 cm^{-1} (for amide III, N-H and C-N functionalities) (X. Wang et al., 2015). The amide I peak shifted from 1641 cm^{-1} to 1628 cm^{-1} when increasing SF-g-GMA content in PVA-g-GMA/SF-g-GMA biphasic injectable hydrogel due to the polarity of the alcohol group (-OH) in PVA-g-GMA, leading to a conformational change in the silk fibroin. The alcohol has interacted with SF-g-GMA and induced the random coil/ α-helix to β-sheet conformation. The resulting β-sheet conformation produced a physical crosslink in the PVA-g-GMA/SF-g-GMA biphasic injectable hydrogel (Matsumoto et al., 2006) (Kaewpirom & Boonsang, 2020). The FTIR result showed the PVA-g-GMA/SF-g-GMA injectable hydrogel had more β-sheet structure more than the SF pure sample (PVA-g-GMA/SF-g-GMA ratio at 0/100). The PVA-g-GMA-SF-g-GMA injectable hydrogel ratios at 75:25, 50:50, and 25/:5 have similar peaks (Kaewpirom & Boonsang, 2020). The curves are characterized by the presence of transmission bands typical of both components. Moreover, the width of the OH region (3000–3600 cm^{-1}) was extended by blending PVA and SF, which could characterize the decrease in the intensity of hydrogen bonding. FTIR spectral results implied that SF molecules had interactions with PVA (Raksa, Utke, Ruksakulpiwat, Numpaisal, & Ruksakulpiwat, 2020).

Mechanism of PVA-g-GMA/SF-g-GMA biphasic injectable hydrogel, as shown in Figure 4.17: the crosslinking of PVA-g-GMA and SF-g-GMA occurs when solutions are exposed to UV radiation in the presence of a LAP photoinitiator. The LAP photoinitiator generates free radicals upon absorption of UV light. Then free radical

interaction occurs at the double bond of methacrylate. PVA-g-GMA and SF-g-GMA are subsequently crosslinked to form biphasic injectable hydrogels.

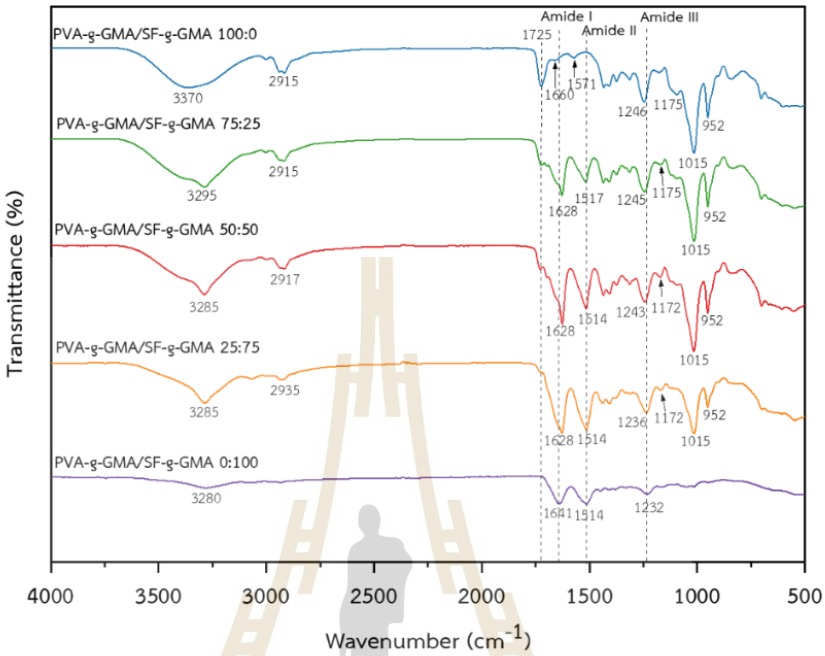

Figure 4.16 FTIR spectra of PVA-g-GMA/SF-g-GMA biphasic injectable hydrogel

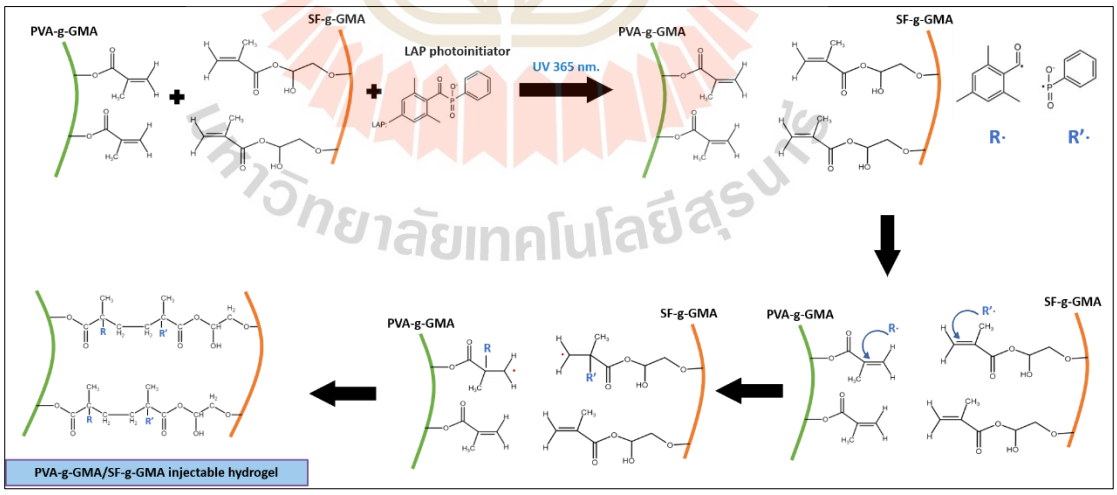

Figure 4.17 Mechanism of PVA-g-GMA/SF-g-GMA biphasic injectable hydrogel

4.3.3 Rheological and viscosity measurements

The rheological behavior of the improved injectable hydrogel was examined to ascertain flow characteristics. In the rheological property analysis, the angular frequency-viscosity (η) of PVA-g-GMA/SF-g-GMA solutions at different blending ratios is shown in Figure 4.18. The curves of viscosity-angular frequency showed the viscosity decreased with increasing angular frequency, and overall, there was shear thinning behavior. This phenomenon is known as shear thinning and is induced by the rising molecular chain alignment that is generated by high shear stress or shear rate. In other words, the fluid system's macroscopic viscosity decreases as a result of the decreased flow resistance between the oriented macromolecules. Shear thinning is another important feature in evaluating the injectability of hydrogels due to the fact that when stressed, the hydrogel should have a lower viscosity, thus making it easier to inject (M. H. Chen et al., 2017).

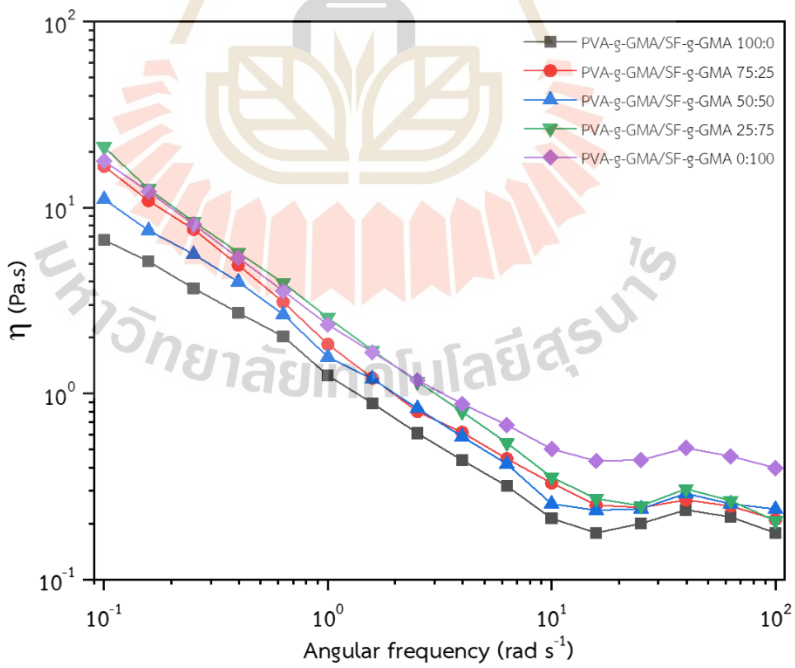

Figure 4.18 The rheological properties of PVA-g-GMA/SF-g-GMA dynamic viscosity measurement of PVA-g-GMA/SF-g-GMA solution at different bending ratio

Dynamic loss modulus (G’’) and dynamic storage modulus (G’) of PVA-g-GMA/SF-g-GMA biphasic injectable hydrogel as shown in Figure 4.19-4.20. The loss modulus (G’’) indicate the viscous of materials and storage modulus (G’) represent the elastic materials. The loss modulus (0.54 to 1.08 kPa) and storage modulus (3.84 to 8.16 kPa) are increased with increasing SF-g-GMA content in PVA-g-GMA/SF-g-GMA biphasic injectable hydrogel due to the polarity of the alcohol group (-OH) in PVA-g-GMA, which caused a conformational shift in the silk fibroin from random coil to β-sheet. (X. Wang et al., 2015). However, the loss modulus and storage modulus of PVA-g-GMA/SF-g-GMA biphasic injectable hydrogel at ratio 0:100 (SF-g-GMA hydrogel) have the lowest values at 0.07 and 0.40 kPa because the SF-g-GMA hydrogel indicated the highest elasticity. Over the whole angular frequency range, the storage modulus (G’) values were greater than the loss modulus (G’’) values (G’ > G’’). These findings showed the development of a typical gel structure and crosslinking of injectable hydrogel (Yan et al., 2023).

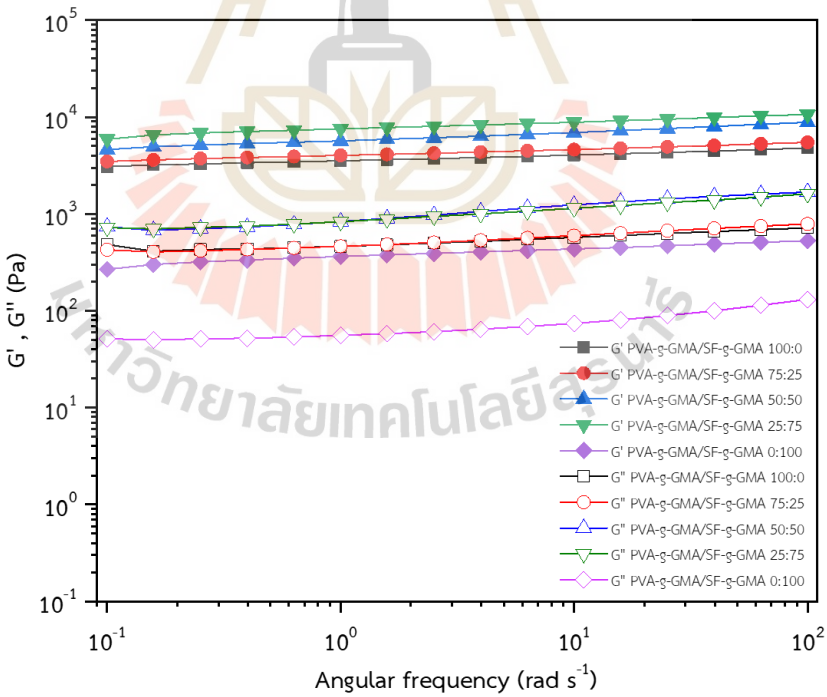

Figure 4.19 Comparison of dynamic loss modulus (G’) and dynamic storage modulus (G’’) of PVA-g-GMA/SF-g-GMA biphasic injectable hydrogel

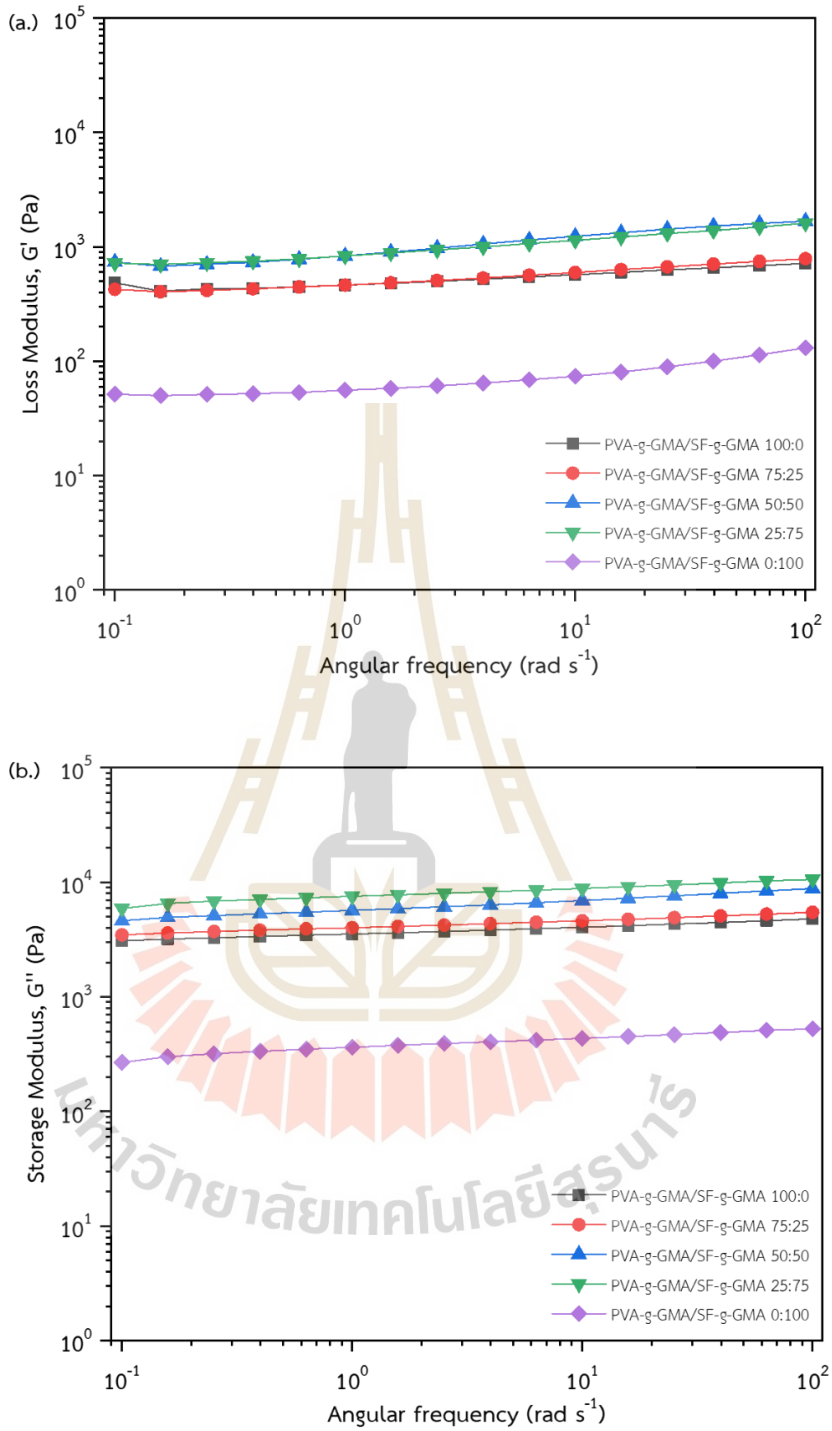

Figure 4.20 (a.) The dynamic loss modulus (G’) and (b.) dynamic storage modulus (G’’) of PVA-g-GMA/SF-g-GMA biphasic injectable hydrogel

4.3.4 Mechanical properties of PVA-g-GMA/SF-g-GMA injectable hydrogel

The mechanical properties of hydrogel play an important role in mimicking meniscus tissue (De Rosa, Filippone, Best, Jackson, & Travascio, 2022). As cell adhesion and mechanical properties can influence whether cells respond, the mechanical environment has an important effect on cellular activities (Wolf et al., 2012). As a human meniscus, the characterization by compressive modulus of 0.10-0.15 MPa (Chia & Hull, 2008) (H. Li et al., 2021). In this study, the PVA-g-GMA/SF-g-GMA injectable hydrogel was fabricated by photocrosslinking and demonstrated by compression stimulation. The stress-strain curve and mechanical properties of the PVA-g-GMA/SF-g-GMA injectable hydrogel are shown in Figure 4.21.

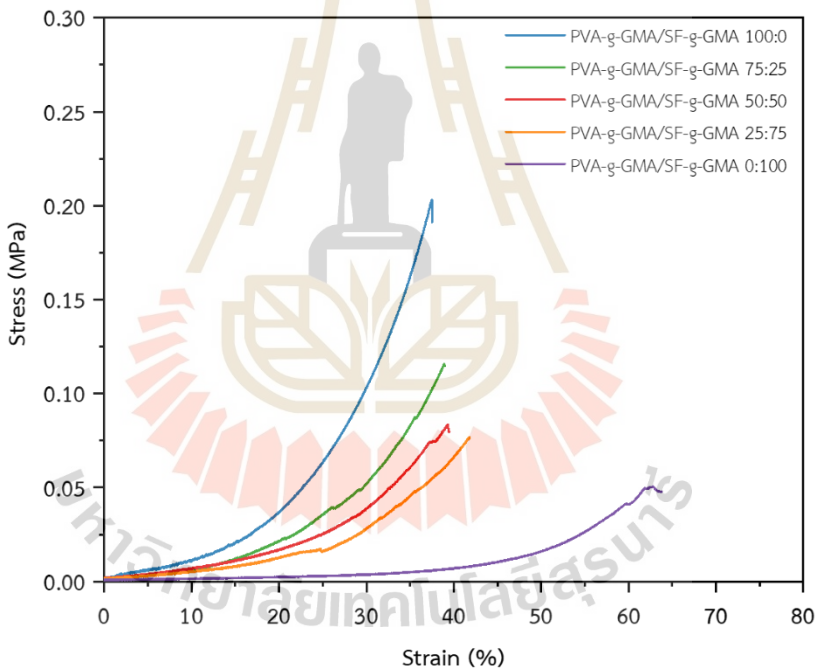

Figure 4.21 Stress-Strain curve of PVA-g-GMA/SF-g-GMA injectable hydrogel

The compressive modulus of PVA-g-GMA/SF-g-GMA injectable hydrogel decreased with increasing SF-g-GMA content. The compressive modulus was 0.17, 0.14, 0.12, 0.09, and 0.01 MPa, respectively, for the injectable hydrogel with SF-g-GMA content of 0, 25, 50, 75, and 100 %w/w. However, when the SF-g-GMA content increased, the compressive modulus of the injectable hydrogel dropped from roughly

0.17 to 0.01 MPa. The compressive modulus, compressive strength, and toughness showed an increasing trend with increasing PVA-g-GMA content blend in PVA-g-GMA/SF-g-GMA injectable hydrogel. In Figure 4.22(a-c)., the compressive modulus of the PVA-g-GMA/SF-g-GMA hydrogel ratio at 100:0 (0.17±0.01 MPa) was significantly higher than those of hydrogel ratio at 75:25 (0.14 ± 0.01 MPa), 50:50 (0.12 ± 0.01 MPa), 25/75(0.09±0.02 MPa), and 0/100 (0.01± MPa). It is dominant that the compressive modulus properties of hydrogel are much closer and higher than the human meniscus (0.10-0.15 MPa) (Sweigart et al., 2004) . The PVA-g-GMA/SF-g-GMA injectable hydrogel promotes the mechanical properties and mimics the mechanical characteristics of meniscus tissue.

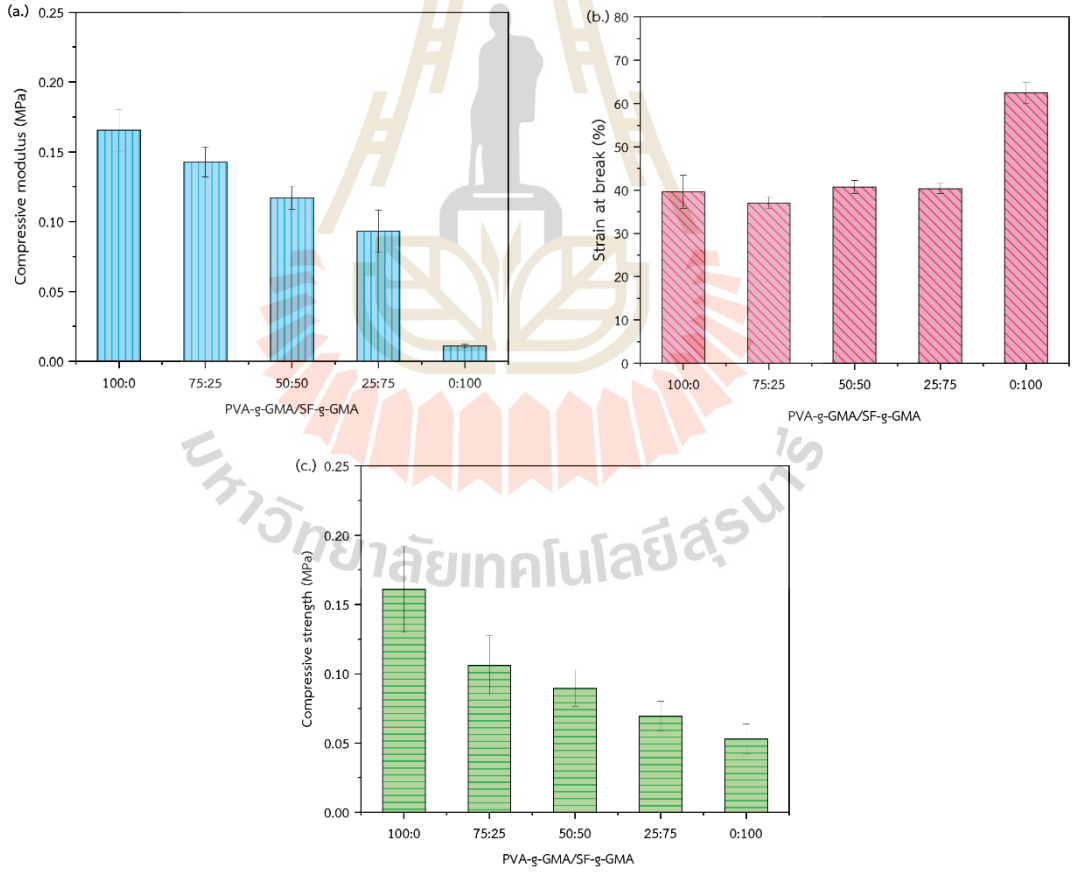

Figure 4.22 Mechanical properties of PVA-g-GMA/SF-g-GMA injectable hydrogel. (a.) Compressive modulus, (b.) Compressive strength and (c.) Compressive strain.

Table 4.4 PVA-g-GMA/SF-g-GMA biphasic injectable hydrogel mechanical properties

PVA-g-GMA/SF-g-GMA	Compressive modulus (MPa)	Compressive strength (MPa)	Compressive strain (%)
100:0	0.17± 0.01	0.16±0.03	39.61±3.81
75:25	0.14 ± 0.01	0.11±0.02	37.08±1.41
50:50	0.12±0.01	0.09±0.01	40.71±1.51
25:75	0.09±0.02	0.07±0.01	40.33±1.17
0:100	0.01±0.00	0.05±0.01	62.54±2.43
Human meniscus	0.10±0.15*	-	19.92±1.36**

(Sweigart et al., 2004) *, (Sandmann et al., 2013) **

4.3.5 The morphology and pore size of biphasic injectable hydrogel

As shown in Figure 4.23, the injectable hydrogel had a cylindrical shape, and the morphology of the cross-section of PVA-g-GMA/SF-g-GMA injectable hydrogel after fully swelling and freezing was examined by FESEM. Clearly, the morphologies of the injectable hydrogel show different pore sizes, which indicates that the three-dimensional homogeneous porous structures of all the samples varied depending on the ratio of PVA-g-GMA and SF-g-GMA. The injectable hydrogels had a homogenous distribution and an interconnected porosity structure without phase separation, as seen in the magnified FESEM image.

The compressive modulus and pore size of PVA-g-GMA/SF-g-GMA biphasic injectable hydrogels are shown in Figure 4.24; all hydrogels do not show significant differences. PVA-g-GMA/SF-g-GMA biphasic injectable hydrogel ratios of 100:0, 75:25, and 50:50 show increased pore size but decrease compressive modulus. In addition, the size of a porous material has a significant impact on mechanical properties, and smaller pores improve designed structures compressive properties (Bi et al., 2011). The majority of macroporous hydrogels are weak and rapidly breakable,

greatly limiting their use as scaffolds (Milner et al., 2018) (Heng Li, Li, Li, Wu, & Zhang, 2022).

The PVA-g-GMA/SF-g-GMA at various ratios of 100:0, 75:25, 50:50, 25:75, and 0:100 are shown pore size diameter of 27.11, 40.77, 60.49, 30.20, and 155.74 μm, respectively are shown in Figure 4.25-4.26. The average pore size of the injectable hydrogel increases with an increasing of SF-g-GMA content. The fundamental idea is to alter the volume and size of the porous structure in order to alter the pore size. Swelling molecules often enter the hydrophilic center of the porous structure and extend it, enlarging the pore of the injectable hydrogel (Ahmed, 2015) (Foudazi, Zowada, Manas-Zloczower, & Feke, 2023). Hydrogels with smaller pore sizes exhibit increased compressive strength (Zhao, Li, Ding, Liu, & Ai, 2018). The smaller pores provide a higher density of crosslinking points, resulting in a tighter and more compact network structure. This enhances the overall compressive strength and compressive modulus of the hydrogel (Bashir et al., 2020; Jang et al., 2014).

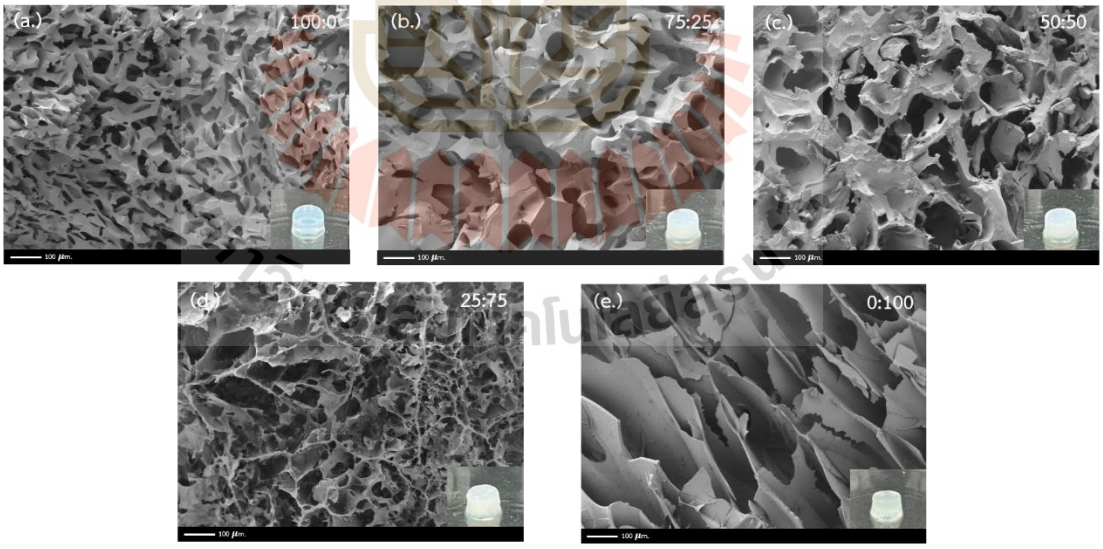

Figure 4.23 The SEM images of PVA-g-GMA/SF-g-GMA hydrogels with different ratios: 100:0, 75:25, 50:50, 25:75, and 0:100. The scale bar measures 100 um.

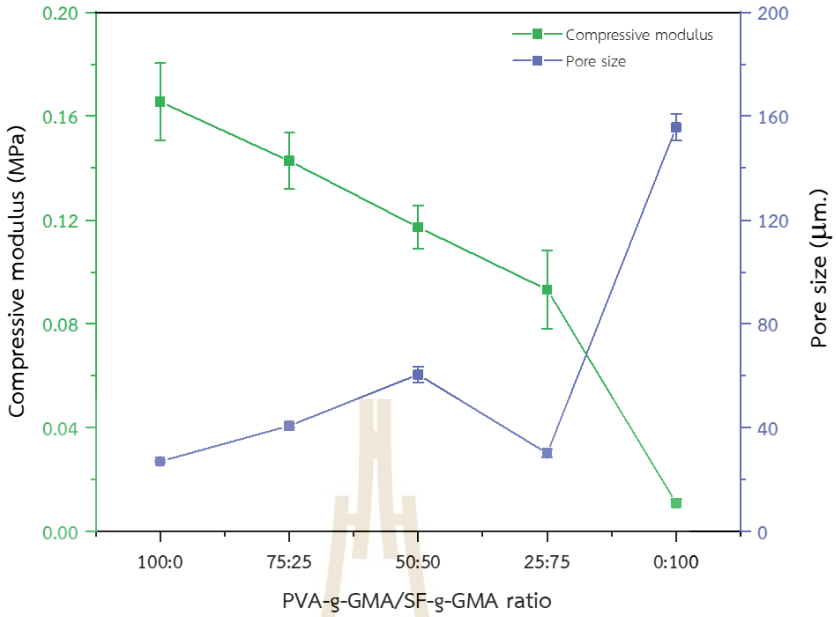

Figure 4.24 Compressive modulus and pore size of PVA-g-GMA/SF-g-GMA biphasic injectable hydrogel

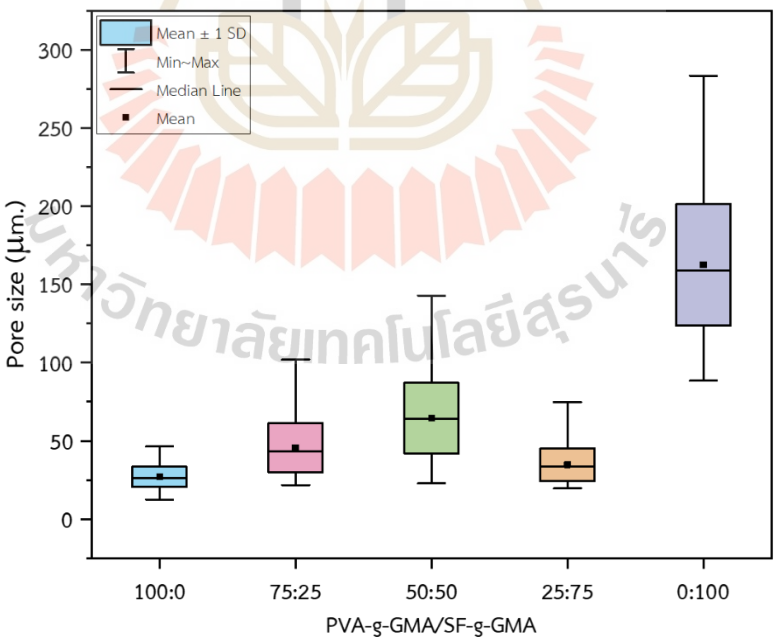

Figure 4.25 Pore size box plot of PVA-g-GMA/SF-g-GMA biphasic injectable hydrogel

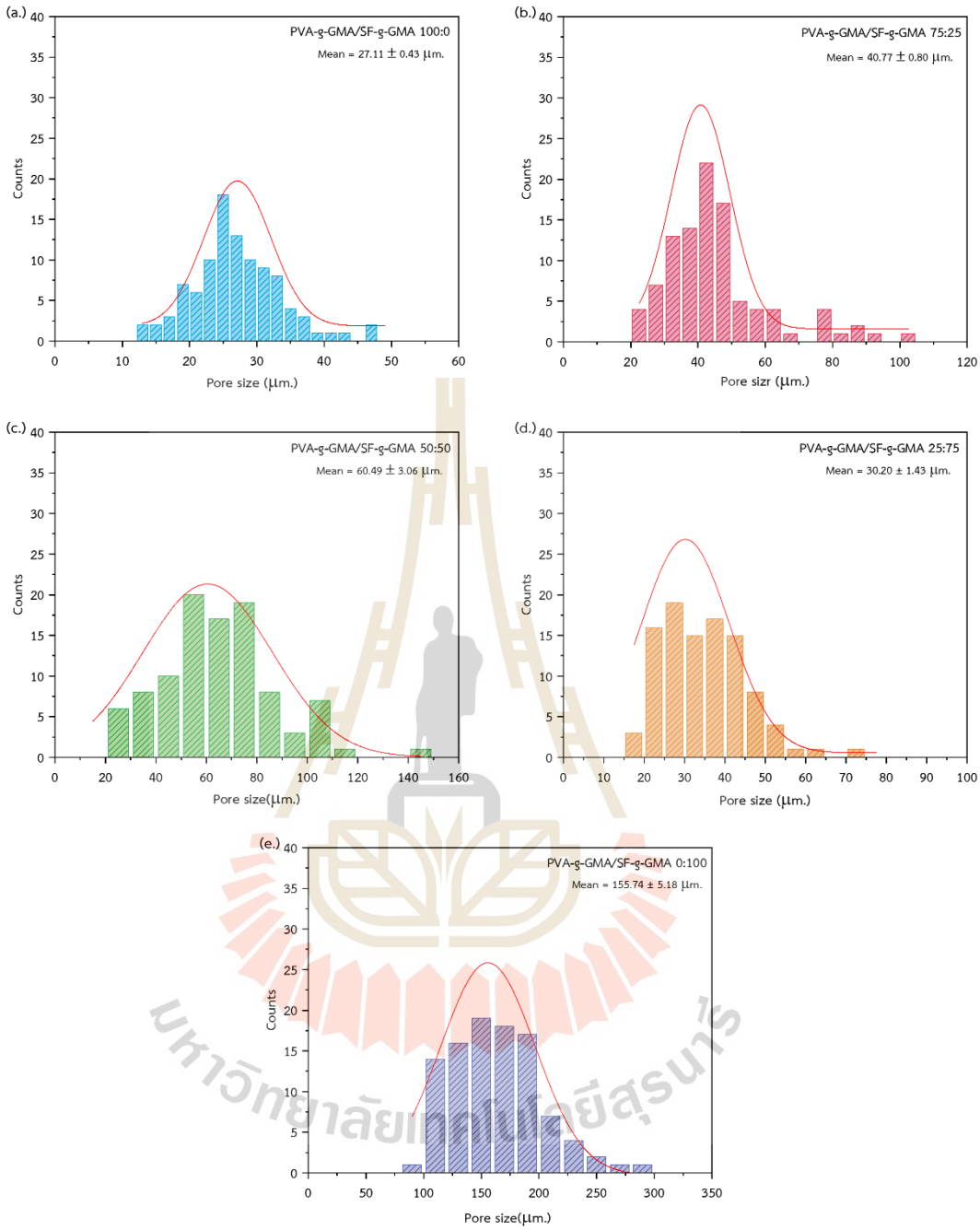

Figure 4.26 Histogram of pore size distribution of PVA-g-GMA/SF-g-GMA injectable hydrogel

4.3.6 In vitro degradation of biphasic injectable hydrogel

Another important consideration for the scaffold is biodegradability. In order to make certain that tissue remodeling or regeneration proceeds properly, the

scaffold must degrade at a suitable rate (Bitar & Zakhem, 2014). All of the in vitro degradation of PVA-g-GMA/SF-g-GMA injectable hydrogel showed relatively little degradation in a period of 4 months, as shown in Figure 4.27. After 1 week of injectable hydrogel incubation, the hydrogel was extremely degraded. As a result, after 2 weeks, it was found that the weight of the hydrogel slightly decreased every week. In 4 months, the degradation rates of PVA-g-GMA/SF-g-GMA 100:0, 75:25, and 50:50 were up to 15.61%, 17.23%, and 18.93%, respectively. PVA-g-GMA/SF-g-GMA 0:100 injectable hydrogel had the lowest degradation rate (4.30%) among hydrogels due to the formed b-sheet structure in hydrogel from dried hydrogel in the oven at 40 C for 24 h. At high temperatures, the conformation change of silk fibroin from a random coil structure to a b-sheet is promoted (G. Li et al., 2001). SF degradation depends on the β-sheet secondary conformation, which is hydrophilic in silk fibroin and is first degraded during the degradation process. (H. Zhang, Xu, Zhang, Li, & Chai, 2022).

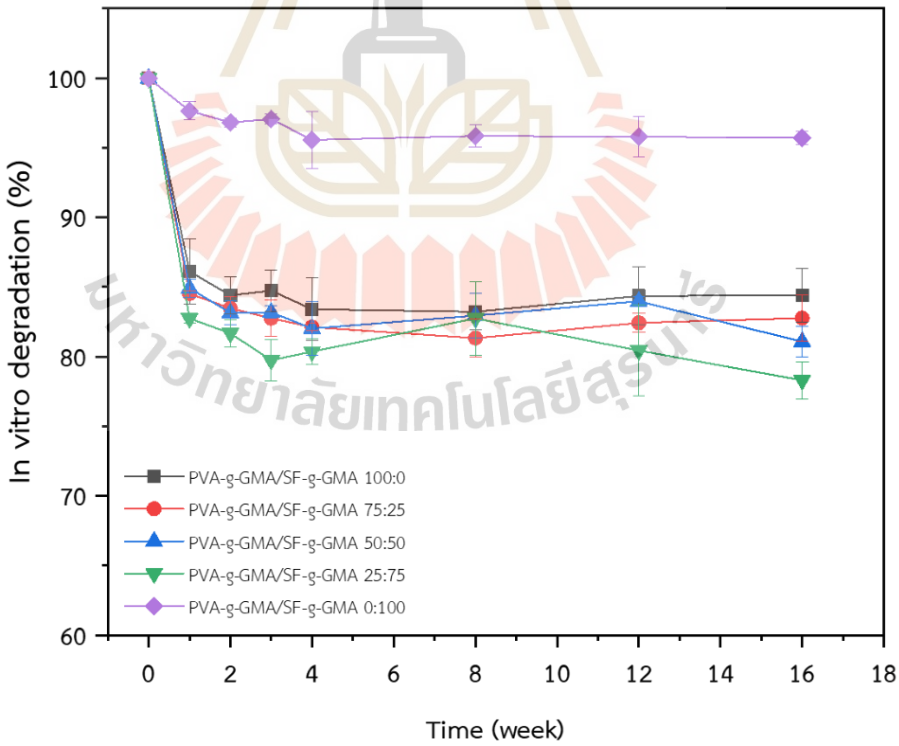

Figure 4.27 In vitro degradation of PVA-g-GMA/SF-g-GMA biphasic injectable hydrogel

4.3.7 Live and dead cell of biphasic injectable hydrogel

Figure 4.28 illustrates the live and dead staining results that demonstrated the cell viability (survival rate) and round-like morphology of the encapsulated human chondrocyte cells in the biphasic injectable hydrogels after 1, 3, and 7 days in culture for potential clinical minimally invasive. Live cells were stained green, whereas dead cells were stained red. After 1, 3, and 7 days of culture, most chondrocytes in each group were alive (green color), with just a small number of dead cells visible (red color).

The cell viability and cell growth of chondrocyte cells in biphasic injectable hydrogel gradually increase from day 1 up to day 7, as shown in Figure 4.29, and significant cell growth was demonstrated at day 1, which clearly increases with increasing SF-g-GMA content. Three days later, the cell density on all samples increased, indicating robust cell growth and proliferation, and the chondrocyte cell survival rate on all samples was not substantially different. The viability of the chondrocyte cells was greater than 80% at all condition periods by days 7 (Chahine, Collette, Thomas, Genetos, & Loots, 2014). The results showed that the chondrocyte cells in the injectable hydrogels exhibited great cell viability even after the photocrosslinking technique, indicating that the biphasic injectable hydrogels promote cell encapsulation for minimally invasive clinical applications (Chahine et al., 2014).

In the PVA-g-GMA/SF-g-GMA biphasic injectable hydrogel ratios of 75:25, 50:50, and 25:75, cell viability was highest when compared to the PVA-g-GMA/SF-g-GMA biphasic injectable hydrogel ratios of 100:0 and 0:100. However, PVA-g-GMA/SF-g-GMA 75:25 and 50:50 biphasic injectable hydrogels have better properties such as compressive modulus, compressive strength, pore size hydrogel, and in vitro degradation. Thus, PVA-g-GMA/SF-g-GMA 75:25 and 50:50 biphasic injectable hydrogels were used to study gene expression.

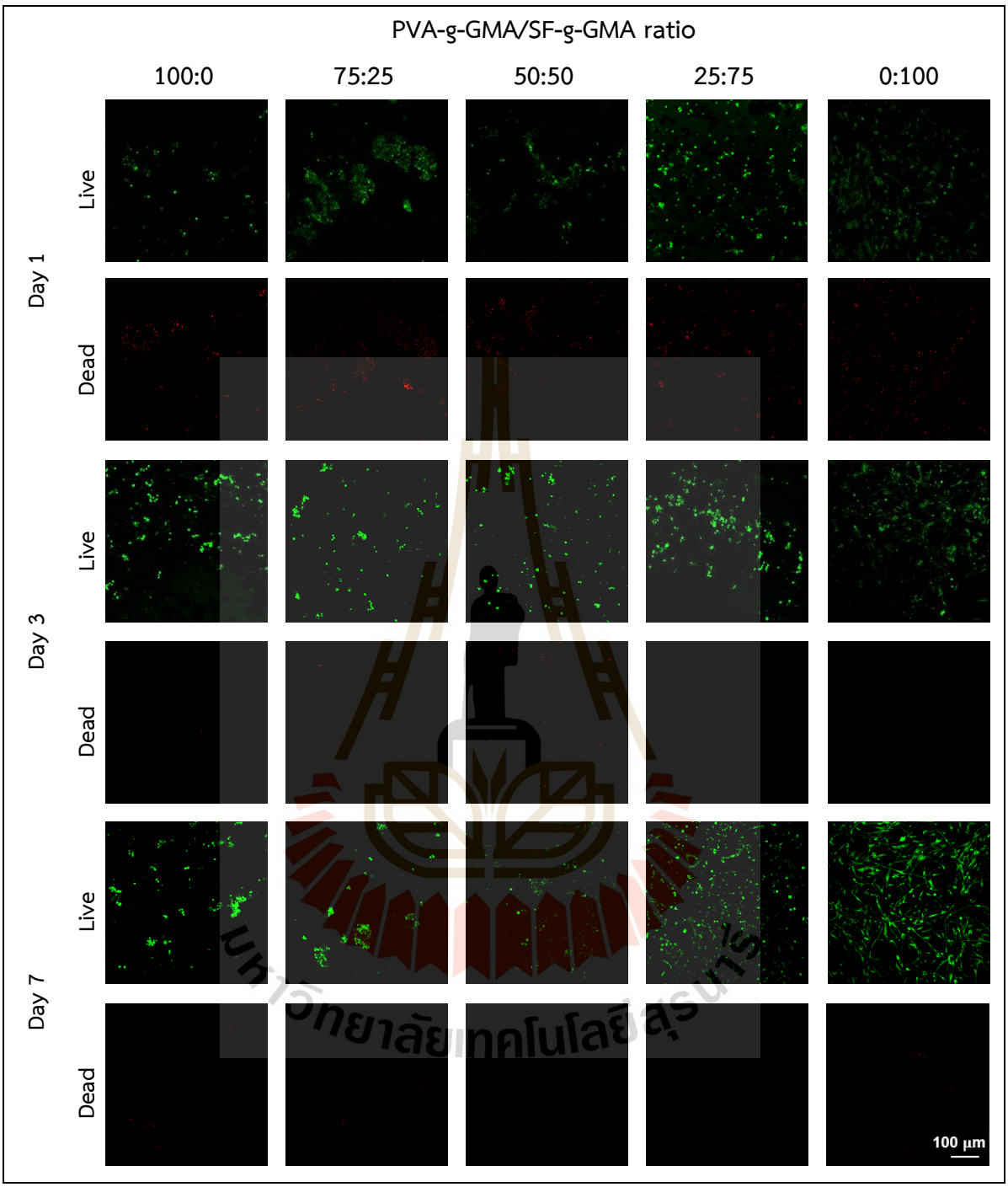

Figure 4.28 Human chondrocyte cell line growth inside the PVA-g-GMA/SF-g-GMA biphasic injectable hydrogel after UV crosslinking. The morphologies of the chondrocytes inside the hydrogel were observed using live and dead staining at day 1, day 3, and day 7.

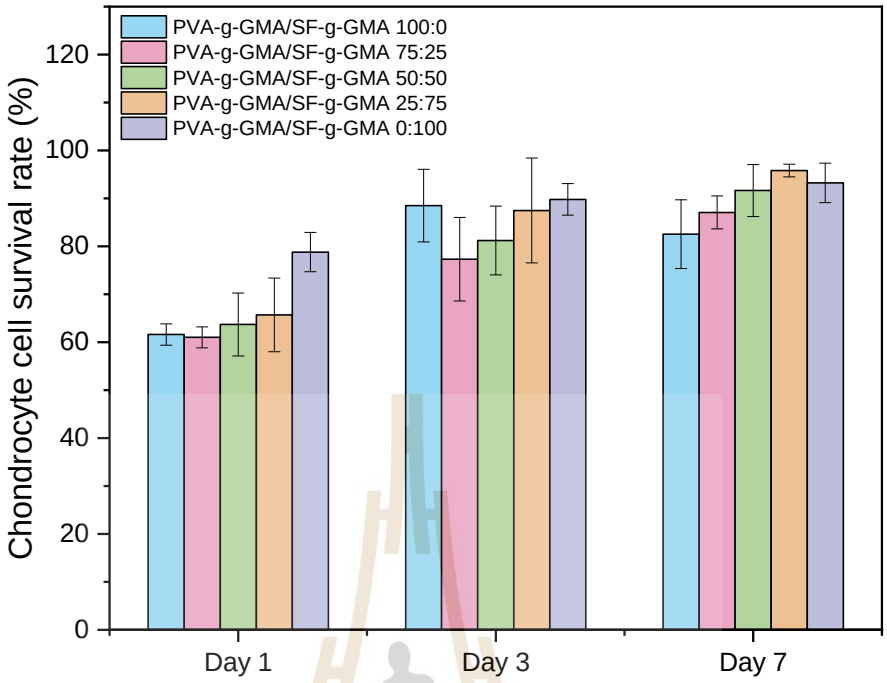

Figure 4.29 The survival rates of human chondrocytes cell inside the PVA-g-GMA/SF-g-GMA biphasic injectable hydrogel

4.3.8 Quantitative analysis of gene expression of biphasic injectable hydrogel

According to live and dead cell and survival rates of human chondrocyte cell results, PVA-g-GMA/SF-g-GMA biphasic injectable hydrogel ratios of 50:50 and 75:25 were used to evaluate gene expression. The gene expression analysis of human chondrocyte cells inside the PVA-g-GMA/SF-g-GMA biphasic injectable hydrogel was investigated to demonstrate cellular phenotypes. Three triplicate sample sets were used for each group of scaffolds. The results were displayed in Figure 4.30.

At day 7, gene expression in both PVA-g-GMA/SF-g-GMA biphasic injectable hydrogel ratios of 75:25 and 50:50 showed expression of COL1A1 higher compared to controls, whereas the expression of COL2A1 in the PVA-g-GMA/SF-g-GMA biphasic injectable hydrogel ratio at 75:25 was higher than 50:50, and there was no difference in expression of COL1A1. At day 14, the expression of both ratios showed higher expression for both COL1A1 and COL2A1 than the control. The PVA-g-GMA/SF-

g-GMA biphasic injectable hydrogel ratio of 50:50 for expression of COL1A1 was higher than 75:25. Conversely, the PVA-g-GMA/SF-g-GMA biphasic injectable hydrogel ratio of 75:25 for expression of COL2A1 was higher than 50:50. At day 28, the expression of COL2A1 in the PVA-g-GMA/SF-g-GMA biphasic injectable hydrogel ratio of 50:50 was higher than 75:25, including both ratios of higher expression than control. As for the expression of COL1A1, there is no difference. On the expression of ACAN for both ratios, there was no difference on days 7, 14, and 28. In our study, we focused on the meniscus repair at the inner zone, the native inner meniscus regions, which carried more COL2A1 (collagen types II) and ACAN (aggrecan) than COL1A1 (collagen types I). The PVA-g-GMA/SF-g-GMA biphasic injectable hydrogel gene expression essentially demonstrated the existence of COL2A1 (Numpaisal et al., 2017) (Numpaisal, Jiang, Hsieh, Chiang, & Chien, 2022).

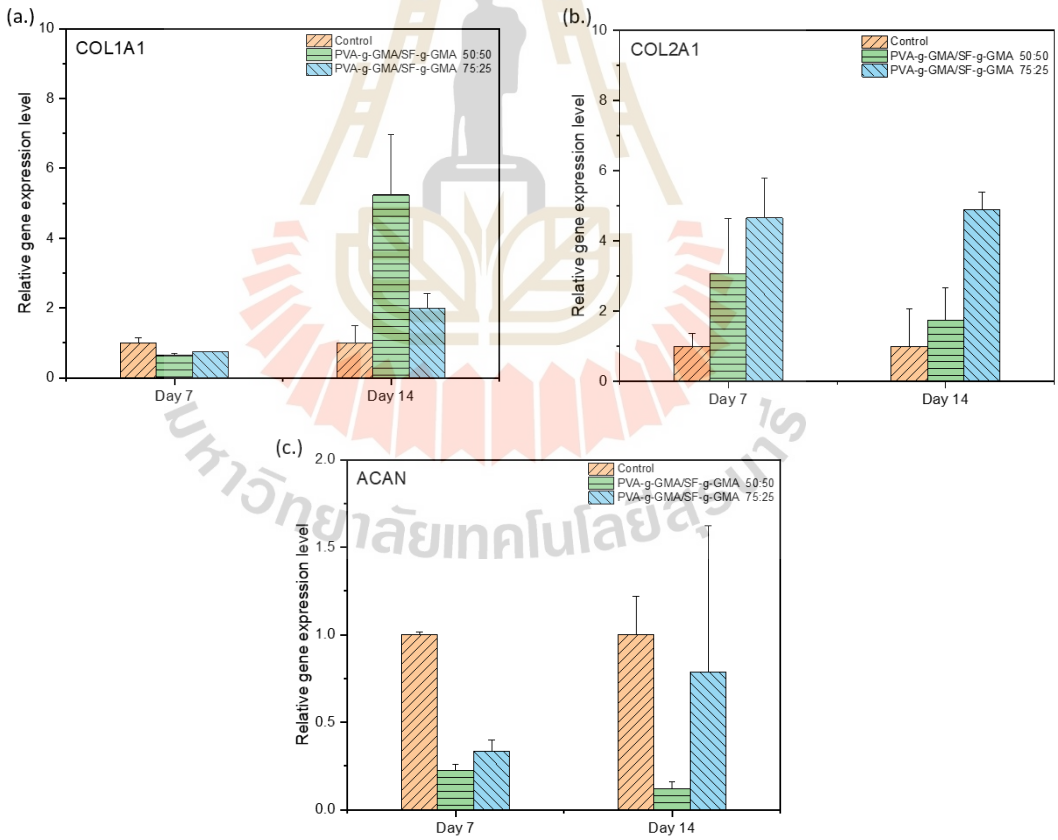

Figure 4.30 Gene expression of human chondrocyte cell inside the PVA-g-GMA/SF-g-GMA biphasic injectable hydrogel analyzed by qRT-PCR of COL1A1, COL2A1, and ACAN at days 7(a.), 14(b.), and 28(c.).

CHAPTER V

CONCLUSION AND RECOMMENDATIONS

5.1 Conclusion

In the present study, the synthesis of PVA-g-GMA and SF-g-GMA were successfully grafted by GMA. The different ratios in biphasic injectable hydrogel formation by mixing PVA-g-GMA/SF-g-GMA were studied in ratios of 100:0, 75:25, 50:50, 25:75, and 0:100. It was found that all the ratios can be fabricated into injectable hydrogels by using UV light with 365 nm, 6 mW/cm^2 intensity, and the action of a LAP photoinitiator. SF-g-GMA changes its chemical structure from random coil to β-sheet conformation, which affects its mechanical properties and morphology. The compressive modulus and pore size were optimal for human chondrocyte cells of the human meniscus. PVA-g-GMA/SF-g-GMA biphasic injectable hydrogels have better degradation properties than unmixed PVA-g-GMA and SF-g-GMA injectable hydrogels. Additionally, injectable hydrogel encapsulation of human chondrocyte cells was also studied. Human chondrocytes were mixed in a mixture of PVA-g-GMA/SF-g-GMA solutions and then injected into a biphasic hydrogel under UV light. PVA-g-GMA/SF-g-GMA biphasic injectable hydrogels, increasing the ratio of SF-g-GMA promoted the viability of human chondrocytes with the *in vitro* cell test.

The PVA-g-GMA/SF-g-GMA 75:25 biphasic injectable hydrogel has the potential to be used as a rapidly photocurable biomimetic biphasic injectable hydrogel for encapsulated augmentation based on mechanical properties, cell encapsulation, cell viability, gene expression, and *in vitro* degradation.

5.2 Recommendations

5.2.1 The mechanical properties of cells encapsulated inside injectable hydrogels

for the bioactive molecule (mechanical stimulation).

5.2.2 In an in vivo study using a mouse or rabbit subcutaneous implantation model to evaluate the injectability and in vivo tissue compatibility of the hydrogel.

มหาวิทยาลัยเทคโนโลยีสุรนารี

REFERENCES

มหาวิทยาลัยเทคโนโลยีสุรนารี

REFERENCES

Ahmed, E. M. (2015). Hydrogel: Preparation, characterization, and applications: A review. *J Adv Res, 6*(2), 105-121. doi:10.1016/j.jare.2013.07.006

Alonso, J. M., Andrade Del Olmo, J., Perez Gonzalez, R., & Saez-Martinez, V. (2021). Injectable Hydrogels: From Laboratory to Industrialization. *Polymers (Basel), 13*(4). doi:10.3390/polym13040650

Awad, H. A., Wickham, M. Q., Leddy, H. A., Gimble, J. M., & Guilak, F. (2004). Chondrogenic differentiation of adipose-derived adult stem cells in agarose, alginate, and gelatin scaffolds. *Biomaterials, 25*(16), 3211-3222. doi:10.1016/j.biomaterials.2003.10.045

Bae, S. B., Kim, M. H., & Park, W. H. (2020). Electrospinning and dual crosslinking of water-soluble silk fibroin modified with glycidyl methacrylate. *Polymer Degradation and Stability, 179*. doi:10.1016/j.polymdegradstab.2020.109304

Baker, M. I., Walsh, S. P., Schwartz, Z., & Boyan, B. D. (2012). A review of polyvinyl alcohol and its uses in cartilage and orthopedic applications. *J Biomed Mater Res B Appl Biomater, 100*(5), 1451-1457. doi:10.1002/jbm.b.32694

Balakrishnan, B., & Banerjee, R. (2011). Biopolymer-based hydrogels for cartilage tissue engineering. *Chem Rev, 111*(8), 4453-4474. doi:10.1021/cr100123h

Bashir, S., Hina, M., Iqbal, J., Rajpar, A. H., Mujtaba, M. A., Alghamdi, N. A., . . . Ramesh, S. (2020). Fundamental Concepts of Hydrogels: Synthesis, Properties, and Their Applications. *Polymers (Basel), 12*(11). doi:10.3390/polym12112702

Bhattacharya, S., & Shunmugam, R. (2020). Polymer based gels and their applications in remediation of dyes from textile effluents. *Journal of Macromolecular Science, Part A, 57*(12), 906-926. doi:10.1080/10601325.2020.1782229

Bi, L., Cao, Z., Hu, Y., Song, Y., Yu, L., Yang, B., . . . Han, Y. (2011). Effects of different cross-linking conditions on the properties of genipin-cross-linked chitosan/collagen scaffolds for cartilage tissue engineering. *J Mater Sci Mater Med, 22*(1), 51-62. doi:10.1007/s10856-010-4177-3

Bitar, K. N., & Zakhem, E. (2014). Design strategies of biodegradable scaffolds for tissue regeneration. *Biomed Eng Comput Biol, 6*, 13-20. doi:10.4137/BECB.S10961

Bonnans, C., Chou, J., & Werb, Z. (2014). Remodelling the extracellular matrix in development and disease. *Nat Rev Mol Cell Biol, 15*(12), 786-801. doi:10.1038/nrm3904

Chahine, N. O., Collette, N. M., Thomas, C. B., Genetos, D. C., & Loots, G. G. (2014). Nanocomposite scaffold for chondrocyte growth and cartilage tissue engineering: effects of carbon nanotube surface functionalization. *Tissue Eng Part A, 20*(17-18), 2305-2315. doi:10.1089/ten.TEA.2013.0328

Chen, M. H., Wang, L. L., Chung, J. J., Kim, Y. H., Atluri, P., & Burdick, J. A. (2017). Methods To Assess Shear-Thinning Hydrogels for Application As Injectable Biomaterials. *ACS Biomater Sci Eng, 3*(12), 3146-3160. doi:10.1021/acsbiomaterials.7b00734

Chen, X., Knight, D. P., Shao, Z., & Vollrath, F. (2001). Regenerated Bombyx silk solutions studied with rheometry and FTIR. *Polymer, 42*(25), 09969-09974. doi:https://doi.org/10.1016/S0032-3861(01)00541-9

Chenga, W., Dingb, Z., Zhengd, X., Lua, Q., Konge, X., Zhoua, X., . . . Kaplanf, D. L. (2021). Injectable Hydrogel Systems with Multiple Biophysical and Biochemical Cues for Bone Regeneration. *Biomater Sci., 8*(9), 2537-2548. doi:10.1039/d0bm00104j

Chia, H. N., & Hull, M. L. (2008). Compressive moduli of the human medial meniscus in the axial and radial directions at equilibrium and at a physiological strain rate. *J Orthop Res, 26*(7), 951-956. doi:10.1002/jor.20573

Chocholata, P., Kulda, V., Dvorakova, J., Kolaja Dobra, J., & Babuska, V. (2020). Biological Evaluation of Polyvinyl Alcohol Hydrogels Enriched by Hyaluronic Acid and Hydroxyapatite. *Int J Mol Sci, 21*(16). doi:10.3390/ijms21165719

Crispim, E. G., Piai, J. F., Schüquel, I. T. A., Rubira, A. F., & Muniz, E. C. (2006). Functionalization of poly(vinyl alcohol) by addition of methacryloyl groups: characterization by FTIR and NMR and optimization of reaction conditions by RSM. *e-Polymers, 6*(1). doi:10.1515/epoly.2006.6.1.793

Das, S., Pati, F., Choi, Y. J., Rijal, G., Shim, J. H., Kim, S. W., . . . Ghosh, S. (2015). Bioprintable, cell-laden silk fibroin-gelatin hydrogel supporting multilineage differentiation of stem cells for fabrication of three-dimensional tissue constructs. *Acta Biomater, 11*, 233-246. doi:10.1016/j.actbio.2014.09.023

de Albornoz, P. M., & Forriol, F. (2012). The meniscal healing process. *Muscles Ligaments Tendons J, 2*(1), 10-18.

De Rosa, M., Filippone, G., Best, T. M., Jackson, A. R., & Travascio, F. (2022). Mechanical properties of meniscal circumferential fibers using an inverse finite element analysis approach. *J Mech Behav Biomed Mater, 126*, 105073. doi:10.1016/j.jmbbm.2022.105073

El-Sherbiny, I. M., & Yacoub, M. H. (2013). Hydrogel scaffolds for tissue engineering: Progress and challenges. *Glob Cardiol Sci Pract, 2013*(3), 316-342. doi:10.5339/gcsp.2013.38

Erdoğan, M. K., Akdemir, Ö., Hamitbeyli, A., & Karakışla, M. (2019). Preparation of hydrophilic woven fabrics: Surface modification of poly(ethylene terephthalate) by grafting of poly(vinyl alcohol) and poly(vinyl alcohol)-g-(N-vinyl-2-pyrrolidone). *Journal of Applied Polymer Science, 137*(16). doi:10.1002/app.48584

fMakris, E. A., Hadidi, P., & Athanasiou, K. A. (2011). The knee meniscus: structure-function, pathophysiology, current repair techniques, and prospects for regeneration. *Biomaterials, 32*(30), 7411-7431. doi:10.1016/j.biomaterials.2011.06.037

Foudazi, R., Zowada, R., Manas-Zloczower, I., & Feke, D. L. (2023). Porous Hydrogels: Present Challenges and Future Opportunities. *Langmuir, 39*(6), 2092-2111. doi:10.1021/acs.langmuir.2c02253

Fox, A. J., Bedi, A., & Rodeo, S. A. (2012). The basic science of human knee menisci: structure, composition, and function. *Sports Health, 4*(4), 340-351. doi:10.1177/1941738111429419

Gaaz, T. S., Sulong, A. B., Akhtar, M. N., Kadhum, A. A., Mohamad, A. B., & Al-Amiery, A. A. (2015). Properties and Applications of Polyvinyl Alcohol, Halloysite Nanotubes and Their Nanocomposites. *Molecules, 20*(12), 22833-22847. doi:10.3390/molecules201219884

Hou, Q., De Bank, P. A., & Shakesheff, K. M. (2004). Injectable scaffolds for tissue regeneration. *Journal of Materials Chemistry, 14*(13). doi:10.1039/b401791a

Howard, D., Buttery, L. D., Shakesheff, K. M., & Roberts, S. J. (2008). Tissue engineering: strategies, stem cells and scaffolds. *J Anat, 213*(1), 66-72. doi:10.1111/j.1469-7580.2008.00878.x

Ikada, Y. (2006). Challenges in tissue engineering. *J R Soc Interface, 3*(10), 589-601. doi:10.1098/rsif.2006.0124

Jang, J., Seol, Y. J., Kim, H. J., Kundu, J., Kim, S. W., & Cho, D. W. (2014). Effects of alginate hydrogel cross-linking density on mechanical and biological behaviors for tissue engineering. *J Mech Behav Biomed Mater, 37*, 69-77. doi:10.1016/j.jmbbm.2014.05.004

Kaewpirom, S., & Boonsang, S. (2020). Influence of alcohol treatments on properties of silk-fibroin-based films for highly optically transparent coating applications. *RSC Adv, 10*(27), 15913-15923. doi:10.1039/d0ra02634d

Kaith, B. S., Singh, A., Sharma, A. K., & Sud, D. (2021). Hydrogels: Synthesis, Classification, Properties and Potential Applications—A Brief Review. *Journal of Polymers and the Environment, 29*(12), 3827-3841. doi:10.1007/s10924-021-02184-5

Kamoun, E. A., Omer, A. M., Khattab, S. N., Ahmed, H. M., & Elbardan, A. A. (2018). In-Situ UV-Photopolymerized PVA-g-GMA Hydrogels for Biomedical Applications: I. Synthesis, Characterizations and Grafting Optimization. *Journal of Applied Pharmaceutical Science*. doi:10.7324/japs.2018.8106

Kavda, S., Micheluz, A., Elsasser, C., & Pamplona, M. (2021). Development of a gel permeation chromatography method for analysing cellulose nitrate in museums. *J Sep Sci, 44*(9), 1795-1804. doi:10.1002/jssc.202001018

Ketabat, F., Khorshidi, S., & Karkhaneh, A. (2018). Application of minimally invasive injectable conductive hydrogels as stimulating scaffolds for myocardial tissue engineering. *Polymer International, 67*(8), 975-982. doi:10.1002/pi.5599

Kim, M. H., & Park, W. H. (2016). Chemically cross-linked silk fibroin hydrogel with enhanced elastic properties, biodegradability, and biocompatibility. *Int J Nanomedicine, 11*, 2967-2978. doi:10.2147/IJN.S106467

Kim, S. H., Lee, Y. J., Chao, J. R., Kim, D. Y., Sultan, M. T., Lee, H. J., . . . Park, C. H. (2020). Rapidly photocurable silk fibroin sealant for clinical applications. *NPG Asia Materials, 12*(1). doi:10.1038/s41427-020-0227-6

Kim, S. H., Yeon, Y. K., Lee, J. M., Chao, J. R., Lee, Y. J., Seo, Y. B., . . . Park, C. H. (2018). Precisely printable and biocompatible silk fibroin bioink for digital light processing 3D printing. *Nat Commun, 9*(1), 1620. doi:10.1038/s41467-018-03759-y

Kundu, J., Poole-Warren, L. A., Martens, P., & Kundu, S. C. (2012). Silk fibroin/poly(vinyl alcohol) photocrosslinked hydrogels for delivery of macromolecular drugs. *Acta Biomater, 8*(5), 1720-1729. doi:10.1016/j.actbio.2012.01.004

Li, G., Zhou, P., Shao, Z., Xie, X., Chen, X., Wang, H., . . . Yu, T. (2001). The natural silk spinning process. A nucleation-dependent aggregation mechanism? *Eur J Biochem, 268*(24), 6600-6606. doi:10.1046/j.0014-2956.2001.02614.x

Li, H., Li, J., Li, T., Wu, C., & Zhang, W. (2022). Macroporous polyvinyl alcohol-tannic acid hydrogel with high strength and toughness for cartilage replacement. *Journal of Materials Science, 57*(17), 8262-8275. doi:10.1007/s10853-022-07209-5

Li, H., Li, P., Yang, Z., Gao, C., Fu, L., Liao, Z., . . . Guo, Q. (2021). Meniscal Regenerative Scaffolds Based on Biopolymers and Polymers: Recent Status and Applications. *Front Cell Dev Biol, 9*, 661802. doi:10.3389/fcell.2021.661802

Li, S., Chen, C., Zhang, D., Zhang, X., Sun, B., & Lv, S. (2018). Microwave-assisted fast and efficient dissolution of silkworm silk for constructing fibroin-based

biomaterials. *Chemical Engineering Science, 189*, 286-295. doi:10.1016/j.ces.2018.06.003

Li, X., Fan, Q., Zhang, Q., Yan, S., & You, R. (2020). Freezing-induced silk I crystallization of silk fibroin. *CrystEngComm, 22*(22), 3884-3890. doi:10.1039/d0ce00360c

Li, X., Sun, Q., Li, Q., Kawazoe, N., & Chen, G. (2018). Functional Hydrogels With Tunable Structures and Properties for Tissue Engineering Applications. *Front Chem, 6*, 499. doi:10.3389/fchem.2018.00499

Lim, D. J. (2022). Cross-Linking Agents for Electrospinning-Based Bone Tissue Engineering. *Int J Mol Sci, 23*(10). doi:10.3390/ijms23105444

Liu, M., Zeng, X., Ma, C., Yi, H., Ali, Z., Mou, X., . . . He, N. (2017). Injectable hydrogels for cartilage and bone tissue engineering. *Bone Res, 5*, 17014. doi:10.1038/boneres.2017.14

Martens, P., & Anseth, K. S. (2000). Characterization of hydrogels formed from acrylate modified poly(vinyl alcohol) macromers. *Polymer, 41*(21), 7715-7722. doi:https://doi.org/10.1016/S0032-3861(00)00123-3

Matsumoto, A., Chen, J., Collette, A. L., Kim, U.-J., Altman, G. H., Cebe, P., & Kaplan, D. L. (2006). Mechanisms of Silk Fibroin Sol–Gel Transitions. *The Journal of Physical Chemistry B, 110*(43), 21630-21638. doi:10.1021/jp056350v

Milner, P. E., Parkes, M., Puetzer, J. L., Chapman, R., Stevens, M. M., Cann, P., & Jeffers, J. R. T. (2018). A low friction, biphasic and boundary lubricating hydrogel for cartilage replacement. *Acta Biomater, 65*, 102-111. doi:10.1016/j.actbio.2017.11.002

Miyaguchi, Y., & Hu, J. (2005). Physicochemical Properties of Silk Fibroin after Solubilization Using Calcium Chloride with or without Ethanol. *Food Science and Technology Research, 11*(1), 37-42. doi:10.3136/fstr.11.37

Mu, X., Sahoo, J. K., Cebe, P., & Kaplan, D. L. (2020). Photo-Crosslinked Silk Fibroin for 3D Printing. *Polymers, 12*(12). doi:10.3390/polym12122936

Murphy, A. R., & Kaplan, D. L. (2009). Biomedical applications of chemically-modified silk fibroin. *J Mater Chem, 19*(36), 6443-6450. doi:10.1039/b905802h

Murphy, C. M., O'Brien, F. J., Little, D. G., & Schindeler, A. (2013). Cell-scaffold interactions in the bone tissue engineering triad. *Eur Cell Mater, 26*, 120-132. doi:10.22203/ecm.v026a09

Naeem, F., Khan, S., Jalil, A., Ranjha, N. M., Riaz, A., Haider, M. S., . . . Afzal, S. (2017). pH responsive cross-linked polymeric matrices based on natural polymers: effect of process variables on swelling characterization and drug delivery properties. *Bioimpacts, 7*(3), 177-192. doi:10.15171/bi.2017.21

Nasution, H., Harahap, H., Dalimunthe, N. F., Ginting, M. H. S., Jaafar, M., Tan, O. O. H., . . . Herfananda, A. L. (2022). Hydrogel and Effects of Crosslinking Agent on Cellulose-Based Hydrogels: A Review. *Gels, 8*(9). doi:10.3390/gels8090568

Nguyen, Q. V., Huynh, D. P., Park, J. H., & Lee, D. S. (2015). Injectable polymeric hydrogels for the delivery of therapeutic agents: A review. *European Polymer Journal, 72*, 602-619. doi:10.1016/j.eurpolymj.2015.03.016

Nicodemus, G. D., & Bryant, S. J. (2008). Cell encapsulation in biodegradable hydrogels for tissue engineering applications. *Tissue Eng Part B Rev, 14*(2), 149-165. doi:10.1089/ten.teb.2007.0332

Niu, C., Li, X., Wang, Y., Liu, X., Shi, J., & Wang, X. (2019). Design and performance of a poly(vinyl alcohol)/silk fibroin enzymatically crosslinked semi-interpenetrating hydrogel for a potential hydrophobic drug delivery. *RSC Advances, 9*(70), 41074-41082. doi:10.1039/c9ra09344c

Numpaisal, P. O., Jiang, C. C., Hsieh, C. H., Chiang, H., & Chien, C. L. (2022). Prospective Application of Partially Digested Autologous Chondrocyte for Meniscus Tissue Engineering. *Pharmaceutics, 14*(3). doi:10.3390/pharmaceutics14030605

Numpaisal, P. O., Rothrauff, B. B., Gottardi, R., Chien, C. L., & Tuan, R. S. (2017). Rapidly dissociated autologous meniscus tissue enhances meniscus healing: An in vitro study. *Connect Tissue Res, 58*(3-4), 355-365. doi:10.1080/03008207.2016.1245727

Pamplona, R., Gonzalez-Lana, S., Romero, P., Ochoa, I., Martin-Rapun, R., & Sanchez-Somolinos, C. (2023). Tuning of Mechanical Properties in Photopolymerizable Gelatin-Based Hydrogels for In Vitro Cell Culture Systems. *ACS Appl Polym Mater, 5*(2), 1487-1498. doi:10.1021/acsapm.2c01980

Parhi, R. (2017). Cross-Linked Hydrogel for Pharmaceutical Applications: A Review. *Adv Pharm Bull, 7*(4), 515-530. doi:10.15171/apb.2017.064

Parivatphun, T., Sangkert, S., Kokoo, R., Khangkhamano, M., & Meesane, J. (2022). Biphasic scaffolds of polyvinyl alcohol with silk fibroin for oral and maxillofacial surgery based on mimicking materials design: fabrication, characterization, properties. *Journal of Materials Science, 57*(3), 2131-2148. doi:10.1007/s10853-021-06718-z

Peretti, G. M., Campo-Ruiz, V., Gonzalez, S., Randolph, M. A., Wei Xu, J., Morse, K. R., . . . Yaremchuk, M. J. (2006). Tissue engineered cartilage integration to live and devitalized cartilage: a study by reflectance mode confocal microscopy and standard histology. *Connect Tissue Res, 47*(4), 190-199. doi:10.1080/03008200600809935

Pham, D. T., & Tiyaboonchai, W. (2020). Fibroin nanoparticles: a promising drug delivery system. *Drug Deliv, 27*(1), 431-448. doi:10.1080/10717544.2020.1736208

Piantanida, E., Alonci, G., Bertucci, A., & De Cola, L. (2019). Design of Nanocomposite Injectable Hydrogels for Minimally Invasive Surgery. *Acc Chem Res, 52*(8), 2101-2112. doi:10.1021/acs.accounts.9b00114

Promnil, S., Ruksakulpiwat, C., Numpaisal, P. O., & Ruksakulpiwat, Y. (2022). Electrospun Poly(lactic acid) and Silk Fibroin Based Nanofibrous Scaffold for Meniscus Tissue Engineering. *Polymers (Basel), 14*(12). doi:10.3390/polym14122435

Pyarasani, R. D., Jayaramudu, T., & John, A. (2018). Polyaniline-based conducting hydrogels. *Journal of Materials Science, 54*(2), 974-996. doi:10.1007/s10853-018-2977-x

Raksa, A., Utke, R., Ruksakulpiwat, C., Numpaisal, P.-o., & Ruksakulpiwat, Y. (2020). *Morphological and chemical characterization of electrospun silk fibroin/polyvinyl alcohol nanofibers*. Paper presented at the The Second Materials Research Society of Thailand International Conference.

Samadian, H., Maleki, H., Allahyari, Z., & Jaymand, M. (2020). Natural polymers-based light-induced hydrogels: Promising biomaterials for biomedical applications. *Coordination Chemistry Reviews, 420*. doi:10.1016/j.ccr.2020.213432

Sandmann, G. H., Adamczyk, C., Grande Garcia, E., Doebele, S., Buettner, A., Milz, S., . . . Tischer, T. (2013). Biomechanical comparison of menisci from different species and artificial constructs. *BMC Musculoskelet Disord, 14*, 324. doi:10.1186/1471-2474-14-324

Shah, P. N., Kim, N., Huang, Z., Jayamanna, M., Kokil, A., Pine, A., . . . Lee, Y. (2015). Environmentally benign synthesis of vinyl ester resin from biowaste glycerin. *RSC Advances, 5*(48), 38673-38679. doi:10.1039/c5ra03254g

Sinna, J., Numpaisal, P. O., Ruksakulpiwat, C., & Ruksakulpiwat, Y. (2021). *Extraction of silk fibroin and glycidyl methacrylate grafting on silk fibroin optimization of SF-g-GMA for meniscus tissue engineering.* Paper presented at the Materials Today: Proceedings.

Sun, A. X., Numpaisal, P.-o., Gottardi, R., Shen, H., Yang, G., & Tuan, R. S. (2016). Cell and Biomimetic Scaffold-Based Approaches for Cartilage Regeneration. *Operative Techniques in Orthopaedics, 26*(3), 135-146. doi:10.1053/j.oto.2016.06.003

Sun, W., Gregory, D. A., Tomeh, M. A., & Zhao, X. (2021). Silk Fibroin as a Functional Biomaterial for Tissue Engineering. *Int J Mol Sci, 22*(3). doi:10.3390/ijms22031499

Svensson, F. (2019). *Epidemiology of meniscus position: associations with knee symptoms and osteoarthritis*.

Sweigart, M. A., Zhu, C. F., Burt, D. M., DeHoll, P. D., Agrawal, C. M., Clanton, T. O., & Athanasiou, K. A. (2004). Intraspecies and interspecies comparison of the compressive properties of the medial meniscus. *Ann Biomed Eng, 32*(11), 1569-1579. doi:10.1114/b:abme.0000049040.70767.5c

Szliszka, E., Czuba, Z. P., Domino, M., Mazur, B., Zydowicz, G., & Krol, W. (2009). Ethanolic extract of propolis (EEP) enhances the apoptosis- inducing potential of TRAIL in cancer cells. *Molecules, 14*(2), 738-754. doi:10.3390/molecules

Tan, H., & Marra, K. G. (2010). Injectable, Biodegradable Hydrogels for Tissue Engineering Applications. *Materials, 3*(3), 1746-1767. doi:10.3390/ma3031746

Teh, T. K. H., & Goh, J. C. H. (2017). 6.12 Tissue Engineering Approaches to Regeneration of Anterior Cruciate Ligament ☆. In *Comprehensive Biomaterials II* (pp. 194-215).

Treuting, R. (2000). Minimally invasive orthopedic surgery: arthroscopy. *Ochsner J, 2*(3), 158-163.

Um, I. C., Kweon, H. Y., Lee, K. G., & Park, Y. H. (2003). The role of formic acid in solution stability and crystallization of silk protein polymer. *Int J Biol Macromol, 33*(4-5), 203-213. doi:10.1016/j.ijbiomac.2003.08.004

Vaquero, J., & Forriol, F. (2016). Meniscus tear surgery and meniscus replacement. *Muscles Ligaments Tendons J, 6*(1), 71-89. doi:10.11138/mltj/2016.6.1.071

Wang, H. Y., Zhang, Y. Q., & Wei, Z. G. (2021). Dissolution and processing of silk fibroin for materials science. *Crit Rev Biotechnol, 41*(3), 406-424. doi:10.1080/07388551.2020.1853030

Wang, X., Partlow, B., Liu, J., Zheng, Z., Su, B., Wang, Y., & Kaplan, D. L. (2015). Injectable silk-polyethylene glycol hydrogels. *Acta Biomater, 12*, 51-61. doi:10.1016/j.actbio.2014.10.027

Wang, Z., Li, X., Cui, Y., Cheng, K., Dong, M., & Liu, L. (2020). Effect of molecular weight of regenerated silk fibroin on silk-based spheres for drug delivery. *Korean Journal of Chemical Engineering, 37*(10), 1732-1742. doi:10.1007/s11814-020-0591-5

Wang, Z., Xiong, Y., Tang, X., Li, Q., Zhang, Z., Li, J., & Chen, G. (2019). An arthroscopic repair technique for meniscal tear using a needle and suture: outside-in transfer all-inside repair. *BMC Musculoskelet Disord, 20*(1), 614. doi:10.1186/s12891-019-2984-3

Wang, Z., Yang, H., Li, W., & Li, C. (2018). Effect of silk degumming on the structure and properties of silk fibroin. *The Journal of The Textile Institute, 110*(1), 134-140. doi:10.1080/00405000.2018.1473074

Wehland, M., Steinwerth, P., Aleshcheva, G., Sahana, J., Hemmersbach, R., Lutzenberg, R., . . . Grimm, D. (2020). Tissue Engineering of Cartilage Using a Random Positioning Machine. *Int J Mol Sci, 21*(24). doi:10.3390/ijms21249596

Wolf, M. T., Daly, K. A., Brennan-Pierce, E. P., Johnson, S. A., Carruthers, C. A., D'Amore, A., . . . Badylak, S. F. (2012). A hydrogel derived from decellularized dermal extracellular matrix. *Biomaterials, 33*(29), 7028-7038. doi:10.1016/j.biomaterials.2012.06.051

Woltje, M., Kolbel, A., Aibibu, D., & Cherif, C. (2021). A Fast and Reliable Process to Fabricate Regenerated Silk Fibroin Solution from Degummed Silk in 4 Hours. *Int J Mol Sci, 22*(19). doi:10.3390/ijms221910565

Wu, J., Chen, Q., Deng, C., Xu, B., Zhang, Z., Yang, Y., & Lu, T. (2020). Exquisite design of injectable Hydrogels in Cartilage Repair. *Theranostics, 10*(21), 9843-9864. doi:10.7150/thno.46450

Wu, J., Ding, Q., Dutta, A., Wang, Y., Huang, Y.-h., Weng, H., . . . Hong, Y. (2015). An injectable extracellular matrix derived hydrogel for meniscus repair and regeneration. *Acta Biomaterialia, 16*, 49-59. doi:https://doi.org/10.1016/j.actbio.2015.01.027

Xiang, C., Zhang, X., Zhang, J., Chen, W., Li, X., Wei, X., & Li, P. (2022). A Porous Hydrogel with High Mechanical Strength and Biocompatibility for Bone Tissue Engineering. *J Funct Biomater, 13*(3). doi:10.3390/jfb13030140

Xue, X., Hu, Y., Wang, S., Chen, X., Jiang, Y., & Su, J. (2022). Fabrication of physical and chemical crosslinked hydrogels for bone tissue engineering. *Bioact Mater, 12*, 327-339. doi:10.1016/j.bioactmat.2021.10.029

Yan, K., Zhang, X., Liu, Y., Cheng, J., Zhai, C., Shen, K., . . . Fan, W. (2023). 3D-bioprinted silk fibroin-hydroxypropyl cellulose methacrylate porous scaffold with optimized performance for repairing articular cartilage defects. *Materials & Design, 225*, 111531. doi:https://doi.org/10.1016/j.matdes.2022.111531

Yang, C. M., Lee, J., Lee, S. Y., Lee, H., Chathuranga, K., Lee, J., & Park, W. (2022). Silk Fibroin/Tannin/ZnO Nanocomposite Hydrogel with Hemostatic Activities. *Gels, 8*(10). doi:10.3390/gels8100650

Yang, H., Wang, Z., Wang, M., & Li, C. (2020). Structure and properties of silk fibroin aerogels prepared by non-alkali degumming process. *Polymer, 192*. doi:10.1016/j.polymer.2020.122298

Ye, B., Wu, B., Su, Y., Sun, T., & Guo, X. (2022). Recent Advances in the Application of Natural and Synthetic Polymer-Based Scaffolds in Musculoskeletal Regeneration. *Polymers (Basel), 14*(21). doi:10.3390/polym14214566

Zhang, H., Xu, D., Zhang, Y., Li, M., & Chai, R. (2022). Silk fibroin hydrogels for biomedical applications. *Smart Medicine, 1*(1). doi:10.1002/smmd.20220011

Zhang, Y., & Habibovic, P. (2022). Delivering Mechanical Stimulation to Cells: State of the Art in Materials and Devices Design. *Adv Mater, 34*(32), e2110267. doi:10.1002/adma.202110267

Zhao, H., Li, L., Ding, S., Liu, C., & Ai, J. (2018). Effect of porous structure and pore size on mechanical strength of 3D-printed comby scaffolds. *Materials Letters, 223*, 21-24. doi:10.1016/j.matlet.2018.03.205

มหาวิทยาลัยเทคโนโลยีสุรนารี

APPENDIX

PUBLICATIONS

มหาวิทยาลัยเทคโนโลยีสุรนารี

List of publications

Jiraporn Sinna, Chaiwat Ruksakulphiwat, Piya-on Numpaisal, and Yupaporn Ruksakulphiwat. (2021). Extraction of silk fibroin and glycidyl methacrylate grafting on silk fibroin optimization of SF-g-GMA for meniscus tissue engineering. **Materials Today: Proceedings** 47: 3476-3479.

Jiraporn Sinna, Chaiwat Ruksakulphiwat, Piya-on Numpaisal, and Yupaporn Ruksakulphiwat. (2023). Injectable Hydrogel from Glycidyl Methacrylate Grafted Poly (Vinyl Alcohol) for Meniscus Tissue Engineering. **AIP Conference Proceedings.**

Jiraporn Sinna, Piya-on Numpaisal, and Yupaporn Ruksakulphiwat. Photocrosslinked biphasic injectable hydrogel from synthetic glycidyl methacrylate grafted onto poly (vinyl alcohol) and silk fibroin for meniscus tissue engineering. **Patent pending:** 2201005505

มหาวิทยาลัยเทคโนโลยีสุรนารี

ARTICLE IN PRESS

Materials Today: Proceedings xxx (xxxx) xxx

Contents lists available at ScienceDirect

Materials Today: Proceedings

journal homepage: www.elsevier.com/locate/matpr

Extraction of silk fibroin and glycidyl methacrylate grafting on silk fibroin optimization of SF-g-GMA for meniscus tissue engineering

Jiraporn Sinna [a,b,c], Piya-on Numpaisal [c,d,*], Chaiwat Ruksakulpiwat [a,b,c], Yupaporn Ruksakulpiwat [a,b,c,*]

[a] School of Polymer Engineering, Institute of Engineering, Suranaree University of Technology, Nakhon Ratchasima 30000, Thailand
[b] Center of Excellence on Petrochemical and Materials Technology, Chulalongkorn University, Bangkok 10330, Thailand
[c] Research Center for Biocomposite Materials for Medical Industry and Agricultural and Food Industry, Nakhon Ratchasima 30000, Thailand
[d] School of Orthopedics, Institute of Medicine, Suranaree University of Technology, Nakhon Ratchasima 30000, Thailand

ARTICLE INFO

Article history:
Available online xxxx

Keywords:
Poly (vinyl alcohol)
PVA
Glycidyl methacrylate
Silk fibroin
Meniscus Tissue engineering

ABSTRACT

In this work, silk fibroin (SF) fibers were dissolved in calcium chloride ($CaCl_2$) solution. Effects of $CaCl_2$ concentration (40, 50 and 60%wt) and ratio between silk fibroin and $CaCl_2$ (1:5, 1:10, 1:15, 1:20 and 1:25 wt/wt) on silk fibroin solubility were studied. Dialysis method was used to remove salt and purify the dissolved silk fibroin. Effect of dialysis time on the efficiency of removing salt was studied. Glycidyl methacrylate was grafted onto SF by the *trans*-esterification reaction. The grafting reaction was confirmed by FTIR.

© 2021 Elsevier Ltd. All rights reserved.

Selection and peer-review under responsibility of the scientific committee of the 5th International Conference on Smart Materials and Nanotechnology.

1. Introduction

Silk cocoon is a natural polymer, composed of two main parts, silk fibroin (SF) and silk sericin (SS). There is 72–81% of silk fibroin and 20–30% of sericin [1]. Silk fibroin (SF) has a high mechanical strength, flexibility, light weight and excellent biocompatibility such as adherence and proliferation of various cells [2–4]. Recently, the application of silk fibroin in biomedical materials has received a great attention [5], especially in the application of tissue engineering [6]. Silk fibroin can be processed into different forms and structures such as solution, gel, film, powder, and porous sponges. It can be dissolved with neutral solutions of calcium chloride ($CaCl_2$). In this work, silk fibroin was obtained from silk cocoon by degumming and extraction process using $CaCl_2$ solution. Effect of GMA content on grafting to silk fibroin was examined. Structural characterization of SF and GMA grafted SF (SF-g-GMA) was determined by FTIR.Fig. 1.

2. Preparation of SF-g-GMA powder

Silk cocoons (The Queen Sirikit Department of Sericulture Center, Nakhon Ratchasima in Thailand) were cut into small pieces, washed and dried at 40 °C for 8 h. in hot air oven. Silk was degummed by adding silk in 1 wt% Na_2CO_3 (Erba Reagenti) at the ratio of 1:20 and boiled until 100 °C, last for 30 min. After degumming process, the degummed silk fiber was dried overnight at 40 °C in hot air oven. To determined proper condition for silk fibroin (SF) extraction, different concentration of $CaCl_2$ (ANaPure); 40,50 and 60 wt% and various ratios between degummed silk and $CaCl_2$ were studied. Glycidyl methacrylate (GMA, 99%, Sigma-Aldrich) was added into SF/$CaCl_2$ solution.

In grafting process SF/GMA molar ratio at 1/0.5, 1/0.10 and 1/0.15 were prepared. GMA in SF/$CaCl_2$ solution was stirred with the speed of 500 rpm at 70 °C for 6 h. The solutions were then filtrated and dialyzed with distilled water using cellophane paper for 5–6 days. Silk-g-GMA solution was stored at 4 °C for further use.

3. Characterizations

3.1. Fourier transform infrared spectroscopy (FTIR)

Bruker Tensor 27 spectrometer using attenuated total reflectance (ATR) equipped with a platinum diamond crystal (TYPE

* Corresponding authors at: School of Orthopedics, Institute of Medicine, Suranaree University of Technology, Nakhon Ratchasima 30000, Thailand.

E-mail addresses: piya-on@sut.ac.th (P.-o. Numpaisal), yupa@sut.ac.th (Y. Ruksakulpiwat).

https://doi.org/10.1016/j.matpr.2021.03.464
2214-7853/© 2021 Elsevier Ltd. All rights reserved.
Selection and peer-review under responsibility of the scientific committee of the 5th International Conference on Smart Materials and Nanotechnology.

Please cite this article as: J. Sinna, Piya-on Numpaisal, C. Ruksakulpiwat et al., Extraction of silk fibroin and glycidyl methacrylate grafting on silk fibroin optimization of SF-g-GMA for meniscus tissue engineering, Materials Today: Proceedings, https://doi.org/10.1016/j.matpr.2021.03.464

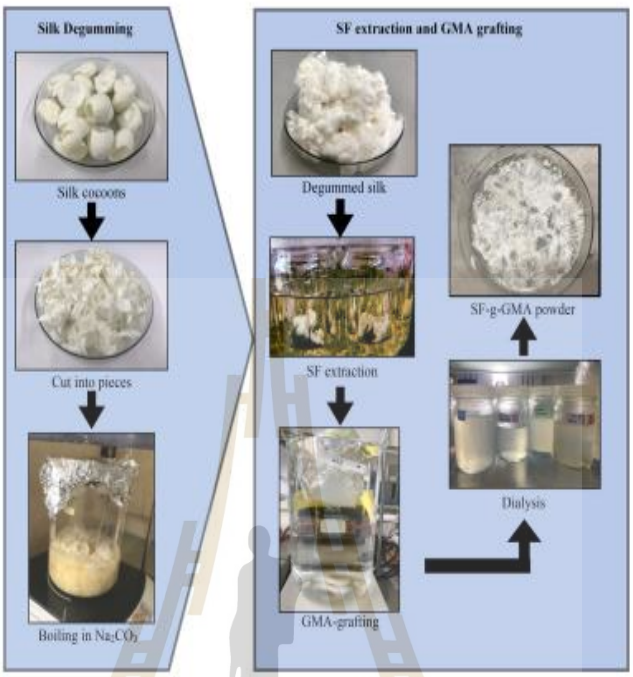

Fig. 1. Schematic diagram preparation of SF-g-GMA powder.

A225/QL) was used to study structural characterization of SF and SF-g-GMA. Spectra were obtained at 1 cm^{-1} resolution and 64 scan rates in the wavenumber range from 4000 to 400 cm^{-1}. All samples were dried in a vacuum oven at 60 °C for 24 h before testing.

3.2. Conductivity measurements

The SF-g-GMA solution was dialyzed using a cellophane paper against deionized water. The deionized water was renewal 3 different patterns; every 4 h, every 8 h and at 4,8,12 h. From 4,8,12 h. pattern, 1st day dialysis water was replaced every 4 h., 2nd –3rd day; dialysis water was replaced every 8 h. After that, dialysis water was replaced every 12 h. until the conductivity value equal to the conductivity of deionized water. The efficiency of salt extraction was evaluated through conductivity measurement using an edge® Dedicated Conductivity/TDS/Salinity Meter - HI2003.

4. Results and discussion

Silk fibroin fiber can be dissolved with LiBr solution, ternary solvent of $CaCl_2$/ethanol/H_2O (1:2:8 in molar ratio) and $CaCl_2$ solution. From the previous studied, the $CaCl_2$ solution has better solubility compared to other solutions such as LiBr solution [7]. As seen in Table 1, it also shows increase in solubility of degummed silk by increasing concentration of $CaCl_2$.

Fig. 2 shows extraction time of degummed silk solution at various SF: $CaCl_2$ ratio at concentration 60%w/v $CaCl_2$ solution. Extraction time dramatically decreased at SF: $CaCl_2$ ratio of 1:15, and slowly decreased afterward.

Table 2 shows the dissolving rate of degummed silk at various SF: $CaCl_2$ ratio. It can be seen by increasing SF: $CaCl_2$ ratio up to 1:15; dissolving rate was significantly increased. After that dissolving rate was slowly increased.

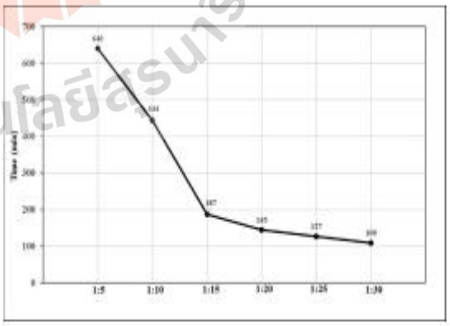

Fig. 2. Extraction time of degummed silk form solution at various SF: $CaCl_2$ ratio.

Table 1
Effect of solubility of degummed silk solution at 1:5 SF: $CaCl_2$ ratio at 60%w/v $CaCl_2$, 70 °C for 1 h.

$CaCl_2$ concentration	40% w/v	50% w/v	60% w/v
Solubility (g/100 g)	5.5365 ± 0.90	10.7851 ± 2.11	24.8389 ± 4.82

Table 2
The dissolving rate of degummed silk solution at various SF: $CaCl_2$ ratio at 60%w/v $CaCl_2$, 70 °C for 3 h.

SF: $CaCl_2$ ratio	1:5	1:10	1:15	1:20	1:25	1:30
Dissolving rate (g/h)	1.12	1.62	3.84	4.94	5.64	6.61

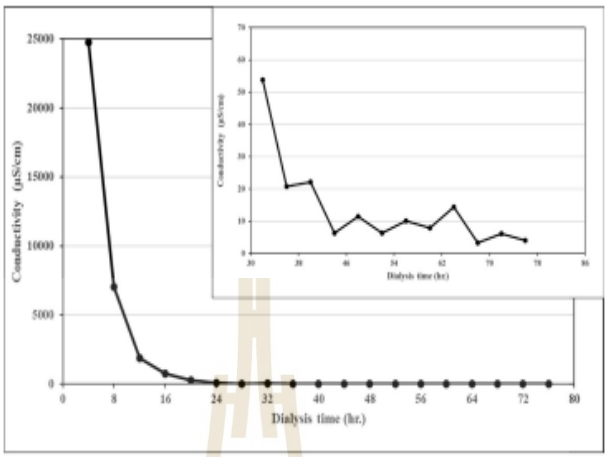

(a)

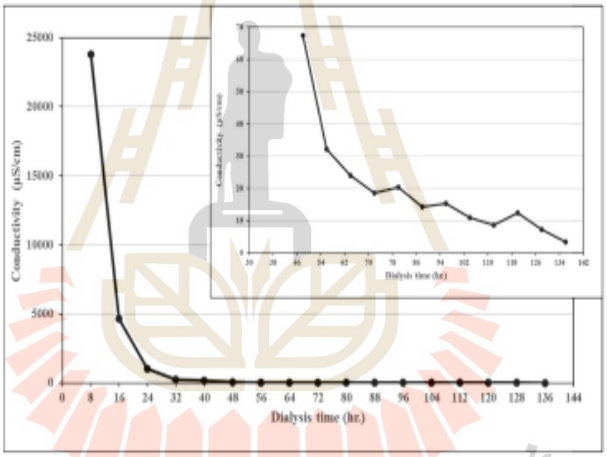

(b)

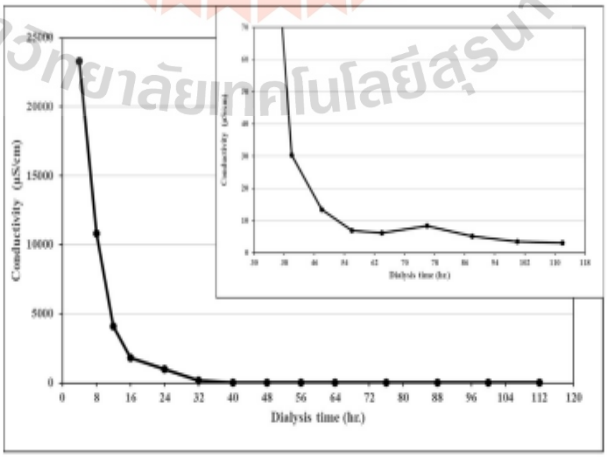

(c)

Fig. 3. Conductivity at different dialysis time and deionized water renewal, every 4 h(a), every 8 h(b) and at 4,8,12 h(c).

มหาวิทยาลัยเทคโนโลยีสุรนารี

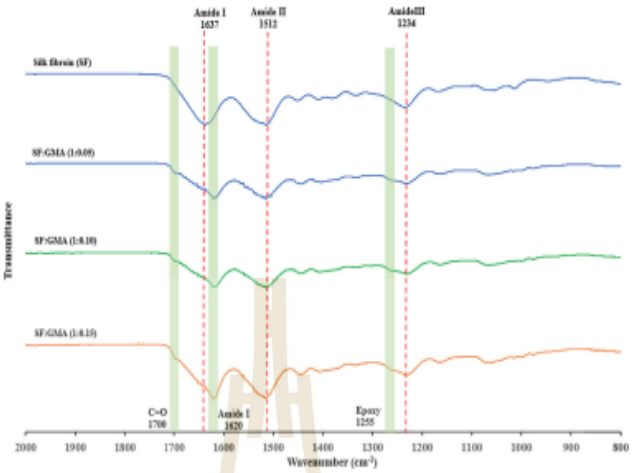

Fig. 4. FTIR spectra of SF and SF-g-GMA using the following feed solution molar ratios of SF/GMA: 1/0.5, 1/0.10 and 1/0.15.

From Fig. 2 and Table 2, the optimum SF: $CaCl_2$ ratio for silk fibroin was obtained at 1:15. Therefore, SF: $CaCl_2$ at 1:15 ratio was used to graft GMA onto silk fibroin solution during extraction process.

The effect of deionized water renewal pattern reported by the difference in conductivity before and after dialysis was shown in Fig. 3. In Fig. 3 (a)-(c), the conductivity of SF solution was very high at the beginning and decreased by time. It could be from dispersibility of SF solution. The conductivity changed from different dialysate concentration. Various dialysis time and the deionized water were renewed every 4 h(a), every 8 h(b), and at 4–8-12 h. Total dialysis time of each pattern was 3, 6 and 5 days, respectively.

Fourier-transform infrared spectroscopy (FTIR) was shown in Fig. 4. The FTIR spectra of SF and SF-g-GMA, both SF and SF-g-GMA demonstrate transmittance bands at 1620, 1512 and 1234 cm^{-1}, which were associated with amide I, amide II and amide III, respectively [8]. In the spectrum of SF-g-GMA, some characteristic bands can be assigned to the respective groups: stretching of C = O due to methacryloyl groups at 1700 cm^{-1} and of C = C due to vinyl groups at 1637 cm^{-1}, breathing of the epoxy ring at 1255 cm^{-1} [9]. The GMA functional groups were only slightly detectable or hidden by SF peaks because the molecular weight of GMA is much smaller than that of the SF.

5. Summary

The dissolution rate of silk increased with increasing $CaCl_2$ concentration. The homogeneous of SF solution was obtained by using concentration 60%w/v of $CaCl_2$ solution of SF: $CaCl_2$ ratio of 1:15 for 3 h. Dialysis process was significantly removed salts which presented in the silk fibroin solution. The suitable dialysis time of silk fibroin solution was about 3 days with changing deionized water every 4 h. Finally, it was shown that GMA can be successfully grafted onto SF.

Acknowledgement

The authors wish to acknowledge Suranaree University of Technology and the Center of Excellence on Petrochemical and Materials Technology for their financial support.

References

[1] Q. Zhang, S. Yan, M. Li, Materials. 2 (2009) 2276–2295.
[2] W. Huang, S. Ling, C. Li, F.G. Omenetto, D.L. Kaplan, Chem Soc Rev. 47 (2018) 6486–6504.
[3] L.-D. Koh, Y. Cheng, C.-P. Teng, Y.-W. Khin, X.-J. Loh, S.-Y. Tee, M.-Y. Han, et al., Prog. Polym. Sci. 46 (2015) 86–110.
[4] F. Mottaghitalab, H. Hosseinkhani, M.A. Shokrgozar, C. Mao, M. Yang, M. Farokhi, j Control Release. 215 (2015) 112–128.
[5] C. Vepari, D.L. Kaplan, Prog Polym Sci. 32 (2007) 991–1007.
[6] H.J. Park, O.J. Lee, M.C. Lee, B.M. Moon, H.W. Ju, J. Lee, C. Park, Int J Biol Macromol. 78 (2015) 215–223.
[7] Q. Wang, Q. Chen, Y. Yang, Z. Shao, Biomacromolecules 14 (1) (2013) 285–289.
[8] H. Liu, J. Wei, L.J. Zheng, Y.P. Zhao, Adv Mat Res 788 (2013) 174–177.
[9] Crispim, E. G., Piai, J. F., Schüquel, I. T. A., Rubira, A. F., & Muniz, E. C., e-Polymers, 6 (2006) 1-18.

BIOGRAPHY

Miss Jiraporn Sinna was born on January 16, 1997, in Nakhon Ratchasima, Thailand. She finished high school from Phimai Wittaya School in 2014. She received her Bachelor's Degree in Engineering (Polymer Engineering) from Suranaree University of Technology in 2018. During her bachelor's degree, she gave poster in the topic of "Thermal properties of Polyvinyl alcohol (PVA) composite based on silk fibroin and silk sericin prepared from Bombyx Mori silk" in the Second Materials Research Society of Thailand International Conference (MRS) in Pattaya, Thailand and published in the AIP Conference Proceedings. In 2019, she continued her Master's degree in Materials Engineering Program at School of Polymer Engineering, Institute of Engineering, Suranaree University of Technology. During her master's degree, she gave poster and oral presentations, the first on the topic "Extraction of silk fibroin and glycidyl methacrylate grafting on silk fibroin optimization of SF-g-GMA for meniscus tissue engineering" at the 5th International Conference on Smart Materials and Nanotechnology (SmartMat@2020) in Pattaya, Thailand, and published in the Materials Today Proceedings. The second in the topic of "Injectable hydrogel from glycidyl methacrylate grafted poly (vinyl alcohol) for meniscus tissue engineering" in the 37th International Conference of the Polymer Processing Society (PPS-37) in Fukuoka, Japan, and accepted in the AIP Conference Proceedings and "Rapidly Poly (vinyl alcohol) Grafted Glycidyl Methacrylate Injectable Hydrogel by Photo Crosslinking for Meniscus Tissue Engineering" in the Combined Meeting of TOSSM & APKASS 2022, Pattaya City, Thailand and certificate of attendance from Center for Continuing Medical Education (CCME), Thailand. Her research article in the topic of "Development of poly (vinyl alcohol)/silk fibroin injectable hydrogels by photo crosslinking for meniscus tissue engineering" which was under the supervision of Assoc. Prof. Dr. Yupaporn Ruksakulpiwat, Assoc. Prof. Dr. Chaiwat Ruksakulpiwat and Assist. Prof. Dr. Piya-on Nompaisal (M.D.). Her master's degree was supported by Suranaree University of Technology, the Center of Excellence on Petrochemical and Materials Technology, and

the Research Center for Biocomposite Materials for Medical Industry and Agricultural and Food Industry.

มหาวิทยาลัยเทคโนโลยีสุรนารี